UNIVERSITY OF CALIFORNIA SAN DIEGO

Connecting Iron-Sulfur Transport at the Cytosol and Mitochondria Interface

A Dissertation submitted in partial satisfaction of the requirements of the degree Doctor of Philosophy

in

Chemistry

by

Jason Thomas Stofleth

Committee in charge:

Professor Patricia A. Jennings, Chair
Professor Joseph A. Adams
Professor Partho Ghosh
Professor Andrew C. Kummel
Professor Stanley J. Opella

2019

The dissertation of Jason Thomas Stofleth is approved, and it is acceptable in quality and form for publication on microfilm and electronically:

_____

_____

_____

_____

_____

Chair

UNIVERSITY OF CALIFORNIA SAN DIEGO

2019

DEDICATION

To my wonderful parents for your love, support, and trust in this most unusual of journeys. Despite your doubts, you have only encouraged me to find my place in the world by giving me “roots and wings”.

To Dave, Mike, and Justin. You have driven me to live my life to the fullest, and you have impacted my decisions more than you will ever know.

EPIGRAPH

“A woodsman was once asked, ‘What would you do if you had just five minutes to chop down a tree?’

He answered, ‘I would spend the first two and a half minutes sharpening my axe.’”

C. R. Jaccard

“‘Hardness,’ I was learning, was the supreme virtue... The greatest compliment one could pay to another was to say he was hard.

Hardness wasn't toughness, nor was it courage, although both were part of it. Hardness was the ability to face an overwhelming situation with aplomb, smile calmly at it, and then triumph through sheer professional pride.”

Nathaniel Fick

TABLE OF CONTENTS

LIST OF FIGURES

LIST OF TABLES

LIST OF ABRREVIATIONS

AP	aldehyde peroxidase
BME	*β*-mercaptoethanol
BSA	bovine serum albumin
C-terminal	carboxyl terminal end of a peptide
CIA	cytosolic iron-sulfur cluster assembly
DIDS	4,4'-Diisothiocyanatostilbene-2,2'-disulfonate
DTT	dithiothreitol
E. coli	*Escherichia coli*
EDTA	ethylenediaminetetraacetic acid
ER	endoplasmic reticulum
Fe-S	iron-sulfur
GRX3	glutaredoxin-3
GSH	reduced glutathione
HDX-MS	hydrogen deuterium exchange mass spectrometry
IPTG	Isopropyl β-D-1-thiogalactopyranoside
ISC	iron-sulfur cluster assembly pathway
kDa	kilodalton
LB	Luria-Bertani medium
mNT	mitoNEET
N-terminal	amino terminal end of a peptide
NAF-1	nutrient-deprivation autophagy factor 1
NTA	nitrilotriacetic acid

OMM	outer-mitochondrial membrane
PDB	Protein Data Bank
ROS	reactive oxygen species
SDS	sodium dodecyl sulfate
SOC	super optimal broth with catabolite repression
TCEP	tris(2-carboxyethyl)phosphine
Tris	tris(hydroxymethyl)aminomethane
TZD	thiazolidinedione
VDAC	voltage-dependent anion channel

ACKNOWLEDGEMENTS

I would like to start by thanking the members of my PhD committee for helping me to progress through my degree, and for the sincere input and advice over the years. It is an honor to have so many highly esteemed scientists guiding a graduate student like myself. I'll be sure to bring coffee to my defense.

Much of the inspiration that lead me to pursue a graduate degree at UC San Diego was the mentorship by Professor S. Saif Hasan (then a lowly grad student as I am now) and Professor William A. Cramer, who spent his post-doc at this university in the lab of Warren L. Butler. Saif was the best grad-student mentor you could ever hope to find, and I model myself in a seemly vain attempt to emulate him. Not that I'm biased, but this department dropped the ball in a big way by not hiring him. Bill's work ethic and proliferative writing has churned out publications from Saif's and my cytochrome b_6f data well into my graduate career. The passion and resolve for discovery those two exhibit helped me fall in love with science. I would be remiss to not thank Dr. Stanislav (Staz) Zakharov for sharing his passion of photosynthesis research ("Run, go centrifuge the chloroplasts now quickly!") and for all the recommended *secret* spots in the mountains, National Parks, and Public Lands; which made for the trip of a lifetime when driving to relocate in San Diego.

Most of my work on glutaredoxin-3 in Chapter 4 would not have been possible without the generous accommodations on behalf of Professor Akif

Tezçan and his lab. Dr. Faith Hefernan, Dr. Lewis Churchfield, Dr. Julian Esselborn, and Dr. Eyal Golub deserve my deepest gratitude for helping me get acquainted with lab equipment and sharing anaerobic glove box time, as well as thoughtful discussions about our respective metalloproteins and fascinating procedural approaches and techniques. Xuemei Huang has been instrumental in helping me, a relative non-expert at NMR, to run HSQCs of my proteins so that I can confirm the folded structures. I'd likely still be trying to set up my first and only experiment, or probably stuck to a magnet without her patience and expert help.

I would also like to thank our NSB 3rd floor neighbors- the labs of Professors Partho Ghosh, Stanley Opella, Neal Devaraj, and Gourisankar Ghosh for use of their specialized lab equipment, and maybe more importantly, the many times planning and participating in happy hours over the years. Cheers to you all.

Much of our labs' work, most notably the VDAC and mitoNEET studies, which appears in the Chapter 3 of this dissertation, was the result of the collaboration with the labs of Professors José Onuchic, Ron Mittler, and Rachel Nechushtai. From their individual wealth of expertise, hard work, keen eyes for editing, and expeditious editing and communication we were able to bring together some exciting new findings from our respective specialties that will contribute greatly to the iron-sulfur protein project story. May you all stay well-funded, well-published, and continue the NEET protein story.

There isn’t space or time enough to express the appreciation I have for my fellow current and former Jennings lab mates I’ve shared time with over the years. Nick Tiee, Kendra Hailey, Josh Chan, Kaitlin Fisher, Colin Lipper, DJ Burban, Ellinor Haglund, Chris Susanto, Dom Capraro, Sulyman Barkho, Melinda Roy, Maria McGlone, and Grace Tao; from morning coffee runs with the *entire* lab, to the famously infamous Lipper Halloween parties, you all have made work feel like my community and it is my sincerest pleasure to call you all my friends. Best wishes for fair winds and following seas to all of you.

The ideas for and success in my investigations would likely have never been realized without the collaborative input, advice, and daily discussions of Professor Mark Paddock and Dr. Colin Lipper in the “Mitopeep” office. Mark has a contagious scientific curiosity and I am excited that he gets to share that with university students and the general public through lots of teaching and outreach. As one of the founders of our project, focused on the biophysical characterization of NEET proteins, I owe quite a bit to the time he spent getting me up and running on this project. We will be Mitopeeps for life.

Lastly, I would like to acknowledge my advisor, Professor Patricia A. Jennings, for bringing me into the lab and guiding me from a fledgling, young scientist to where I am today. Your mentorship has been invaluable to me both as a scientist and as someone who deeply understands the humanity of those you collaborate and work alongside. Thank you.

Chapter 3 is a reprint as it appears in “Stemming the Flow: MitoNEET Redox-Selectively Controls VDAC Gating” by Jason T Stofleth, Lipper CH, Bai

F, Sohn YS, Roy S, Mittler R, Nechushtai R, Onuchic JN, Jennings PA, which has been submitted to the *Proceedings of the National Academy of Sciences* for publication. The dissertation author was a secondary investigator and the primary author of this paper.

Chapter 4, in part, is a preprint as it will appear when submitted for publication, titled “New Connections in Iron-Sulfur Cluster Transport: GRX3 [2Fe-2S] Cluster Transfer is mitoNEET-Specific” by Stofleth JT, Jennings PA; which is being prepared for submission. The dissertation author was the primary investigator and author of this paper.

VITA

2012 B.S., Biochemistry, Purdue University

2014 M.S., Chemistry, University of California San Diego

2019 Ph.D., Chemistry, University of California San Diego

Publications

Stofleth JT, Lipper CH, Paddock ML, Jennings PA (2019). New Connections in Iron-Sulfur Cluster Transport: GRX3 [2Fe-2S] Cluster Transfer is mitoNEET-Specific. Manuscript in preparation.

Stofleth JT, Lipper CH, Bai F, Sohn YS, Roy S, Mittler R, Nechushtai R, Onuchic JN, Jennings PA (2019). Stemming the Flow: MitoNEET Redox-Selectively Controls VDAC Gating. *Proceedings of the National Academy of Sciences*. Submitted for publication.

Tamir S, Paddock ML, Darash-Yahana-Baram M, Holt SH, Sohn YS, Agranat L, Michaeli D, **Stofleth JT**, Lipper CH, Morcos F, Cabantchik IZ, Onuchic JN, Jennings PA, Mittler R, Nechushtai R (2015). Structure-function analysis of NEET proteins uncovers their role as key regulators of iron and ROS homeostasis in health and disease. *Biochimica et Biophysica Acta.* **1853**(6): 1294-1315.

Agarwal R, Hasan SS, Jones LM, **Stofleth JT**, Ryan CM, Whitelegge JP, Kehoe DM, Cramer WA (2015). Role of Domain Swapping in the Hetero-Oligomeric Cytochrome b_6f Lipoprotein Complex. *Biochemistry*. **54**(20): 3151-3163.

Tamir S, Eisenberg-Domovich Y, Conlan AR, **Stofleth JT**, Lipper CH, Paddock ML, Mittler R, Jennings PA, Livnah O, Nechushtai R (2014). A point mutation in the [2Fe-2S] cluster binding region of the NAF-1 protein (H114C) dramatically hinders the cluster donor properties. *Acta Crystallography D Biological Crystallography*. **70**(6): 1572-1578.

Baniulis D, Hasan SS, **Stofleth JT**, Cramer WA (2013). Mechanism of Enhanced Superoxide Production in the Cytochrome b_6f Complex of Oxygenic Photosynthesis. *Biochemistry.* ***52*** (50): 8975–8983.

Baniulis D, **Stofleth JT**, Hasan SS**,** Cramer WA (2013). Increased Superoxide Production in the Cytochrome b_6f Complex: A Function for the Enigmatic Chlorophyll-A. *Biophysical Journal*. **104**(2)*S1*: 488a.

Hasan SS, **Stofleth JT**, Yamashita E, Cramer WA (2013). Lipid-induced Conformation Changes within the Cytochrome b_6f Complex of Oxygenic Photosynthesis. *Biochemistry*. **52**(15): 2649-2654.

Hasan SS, Baniulis D, Yamashita E, Zhalnina MV, Zakharov SD, **Stofleth JT**, Cramer WA (2013). Methods for Studying Interactions of Detergents and Lipids with *α*-Helical and *β*-Barrel Integral Membrane Proteins. *Current Protocols in Protein Science.* **74**(1): 29.7.1-29.7.30.

Stofleth JT (2012). Understanding Free Radicals: Isolating Active Thylakoid Membranes and Purifying the Cytochrome b_6f Complex for Superoxide Generation Studies. *The Journal of Purdue Undergraduate Research*: **2**(11), 64-69.

ABSTRACT OF THE DISSERTATION

Connecting Iron-Sulfur Transport at the Cytosol and Mitochondria Interface

by

Jason Thomas Stofleth

Doctor of Philosophy in Chemistry

University of California, San Diego, 2019

Professor Patricia A. Jennings, Chair

There exist three different NEET family proteins in human cells. Named for their shared characteristic amino acid sequence (Asp-Glu-Glu-Thr), they were first identified as pioglitazone drug targets, one of the thiazolidinedione class of insulin-sensitizing therapeutics for Type 2 diabetes. Although each share similar structural organization and coordinate two [2Fe-2S] clusters with a unique 3Cys:1His coordination chemistry, their cellular localization varies and their functional roles are dissimilar. MitoNEET (mNT, CISD1), was the first characterized and is an outer mitochondrial membrane-anchored dimer with

the C-terminal iron-sulfur cluster domain in the cytosol. Nutrient Deprivation Autophagy Factor 1 (NAF-1, Miner1, CISD2) is anchored to the mitochondrial-associated membranes of the endoplasmic reticulum (ER) with the iron-sulfur cluster domain in the cytosol. The third human NEET family protein is Mitochondrial Inner NEET (MiNT, Miner2, CISD3), is distinguished among the three, as it is the only soluble NEET, exists as a monomer, and is found inside the mitochondrial matrix.

The NEET proteins are critical for cellular iron regulation and reactive oxygen species (ROS) protection, redox sensing, metabolic regulation, and are critical for maintenance of respiratory electron transfer machinery. A missense mutation in NAF-1 causes Wolfram syndrome 2 and other NEET pathologies include neurodegeneration, diabetes, premature aging, as well as play a role in the proliferation of several cancers. Collectively these indicated a crucial underlying cellular role for iron management, redox regulation, and metabolism.

Until recently the role that mNT and NAF-1 play in the cell was unresolved. Though plenty of *in situ* and *in vivo* findings were published, elucidation of the precise cellular role of these proteins proved fruitless to scientific investigation. The major clues to their putative role were that 3Cys:1His iron-sulfur coordination is utilized by other iron-sulfur cluster transfer proteins, and a NEET family protein found in *Arabidopsis thaliana* (At-NEET) transfers iron into the mitochondria. Furthermore, RNAi knockdown of At-NEET caused free iron overload in the cell and led to ROS accumulation.

Both mNT and NAF-1 have recently been identified as key links between the iron-sulfur cluster (ISC) biogenesis pathways in the mitochondria and the cytosol by transferring [2Fe-2S] clusters to human anamorsin, an early key piece of machinery that is responsible for providing [2Fe-2S] to the cytosolic iron-sulfur assembly (CIA) pathway. It has also been shown that mNT can transfer clusters to NAF-1, establishing that these proteins connect the flow of iron-sulfur away from the mitochondria to cytosolic targets.

The method by which iron-sulfur clusters are exported out of the mitochondrion to the cytosol is currently now well characterized. To determine whether human mNT could translocate iron-sulfur clusters into the mitochondrion through the outer membrane voltage dependent anion channel (VDAC), we examined the ability of mNT to control membrane potential across a bilayer embedded with VDAC. We characterized the mNT-VDAC binding with microscale thermophoresis (MST) and hydrogen-deuterium exchange mass spectrometry (HDX-MS) in addition to computational fragment-docking direct-coupling analysis (Fd-DCA) to propose a model for mNT-VDAC binding. Through these data, our model suggests that mNT interacts measurably with the inner VDAC channel in addition to controlling VDAC gating in a redox-dependent manner, while NAF-1 does neither.

To further identify and characterize cytosolic iron-sulfur protein transfer partners, we selected human glutaredoxin-3 (GRX3), a protein recently determined to carry [2Fe-2S] clusters and contribute to the CIA pathway. We identified that GRX3 selectively transfers clusters to mNT, but not NAF-1,

further establishing diverged cellular roles for these two proteins. This is also the only protein reported to date that can transfer [2Fe-2S] clusters to mNT. These findings further solidify the role of the NEET proteins link the ISC and CIA, and demonstrate that there is directionality of iron-sulfur transfer at the interface of the ISC-CIA pathways. This directionality suggests a path for feedback and recycling of cytosolic iron-sulfur.

Chapter 1

Introduction

All life-forms gain a distinct advantage from using metals to drive biological chemistry [1]. Photosynthesis, nitrogen fixation, respiration, and DNA modification, to list a few, absolutely require multiple forms of metals. Cells utilize these metals to drive all cellular processes [2-6]. Common among all kingdoms of life is the use of iron [7]. Iron plays a role in all key cell-viability and proliferation functions, such that its use, transport, and storage has become highly evolved and necessary [8-10]. Most common knowledge of iron might produce thoughts of rust, red blood cells and anemia, red meat, magnets, or the molten core of the earth. However, at the subcellular level, iron can exist in multiple different combinations as important cofactors; namely single irons within protoporphyrins shown in **Figure 1-1,** and iron-sulfur clusters, and in combination with molybdenum, nickel, and copper as demonstrated in **Figure 1-2** [11].

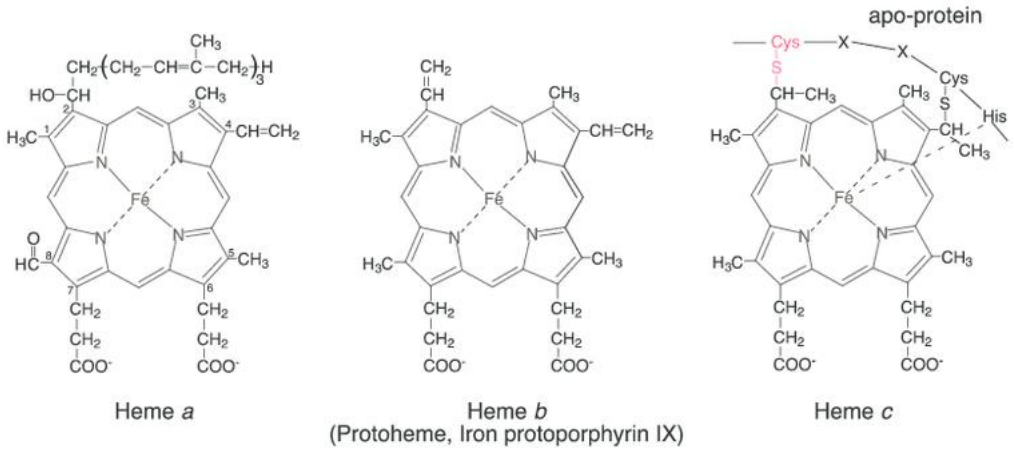

Figure 1-1: Examples of iron-hemes.

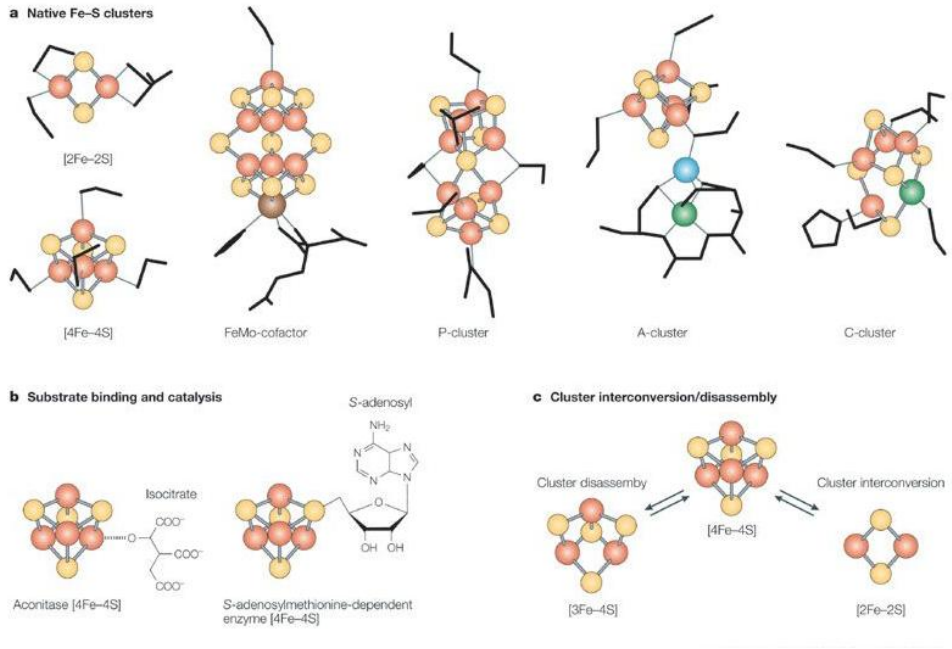

Figure 1-2: Types of iron-sulfur clusters found in biological systems. (a) The Fe–S cluster types that are most common are the [2Fe–2S] and [4Fe–4S] clusters. More complex Fe-S clusters are found in the active site of nitrogenase (the FeMo-cofactor and P-clusters) and in carbon monoxide dehydrogenase (A- and C-clusters), and these are an elaboration of these basic units. The clusters shown are color coded by atom type: iron, red; sulphur, yellow; molybdenum, brown; nickel, green; and copper, blue. Protein ligands are shown in black. **(b)** Examples of substrate binding and catalysis in relation to the iron-based and sulphur-based chemistry of Fe–S clusters. In aconitase, the substrate isocitrate/citrate (isocitrate is shown) is activated when its hydroxyl group becomes ligated to one of the irons of the [4Fe–4S] cluster of aconitase. In *S*-adenosylmethionine-dependent Fe–S enzymes, the adenosylation of a bridging sulphur in a [4Fe–4S] cluster might be directly involved in the mechanism of enzymatic activity (for further information about this process, see Ref. 6). **(c)** Fe–S clusters have a remarkable capability for structure interconversion, ligand-exchange reactions and oxidative degradation [11].

Each of these cofactors, in conjunction with substrate selectivity, can be tuned for one or many extremely important cellular purposes and enzymatic catalysis, in the cell and even through targeted experiemental design of enzymes [12].

Despite iron's role in sustaining human life, many human pathogens and multicellular parasites, like malaria, also require iron for survival and invasion of host organisms [13-17]. Host cells typically control iron tightly, such that iron-starvation is a passive defense mechanism, yet many pathogens are able to find ways around this to utilize iron to proliferate and absence as a way to sense the host's cellular environment [17],[18]. To combat this capability on the part of the pathogen, there has been a push to introduce therapeutics that can actively inhibit the invaders' ability to acquire iron [19]. Most types of cancer cells upregulate iron-based metalloproteins in order to scale up glycolysis in an absence of Krebs/oxidative phosphorylation, termed the Warburg Effect. This enables cancer cells to produce energy rapidly with decreased mitochondrial reliance, and also as a strategy to prevent the cell release free iron from mitochondrial respiratory complexes and follow-on cell-death signals that originate from the mitochondria, that will end cancer proliferation [20-27]. The strategy most cells use as a defense mechanism against undesired cell growth and loss of cell cycle control is to use some form of ROS to combat these negative effects and to self-destruct through cell death pathways [27, 28].

A recent key strategy for therapeutic drug design has been to target metalloproteins, especially those containing iron-sulfur cofactors, due to their vital roles in the cell. When minor functional alterations occur, this can lead to significant cellular strife [29] and seen in **Table 1-1 and Figure 1-3**.

Table 1-1: Iron–sulfur cluster proteins in relation to disease states. Red numbers indicate appearance of Fe-S proteins in Figure 1-2. [29]

Protein	Function	Disease	Most common cause
Frataxin[1]	Iron donor; allosteric effector of NFS1	Friedreich's ataxia (FRDA)	GAA-triplet expansion causing transcriptional silencing
IscU[2]	Fe–S cluster scaffold	IscU myopathy	Splice mutation in intron 4 resulting in decreased protein levels
Fdx2[3]	Electron transport	Fdx2 myopathy	c. 1A > T mutation disrupting the initiation codon
Nfs1[4]	Sulfur donor for cluster assembly	Infantile mitochondrial complex II/III	p. R72Q decreasing transcripts and protein levels
ISD11[5]	Stability factor	Combined oxidative phosphorylation deficiency 19 (COXPD19)	p. R68L resulting in undetectable ISD11 protein levels
Nfu[6]	Late acting [Fe–S] targeting factor	MMDS1	p. G208C resulting in insufficient downstream holo targets
BOLA3[7]	Late acting [Fe–S] targeting factor	MMDS2	Truncation mutation resulting in insufficient downstream holo targets
Iba57[8]	[4Fe–4S] cluster assembly factor	MMDS3	p. Q314P causing protein misfolding and degradation
IscA1/2[9]	[4Fe–4S] cluster assembly	MMDS4	p. G77S resulting in insufficient downstream holo targets
Ind1[10]	Assembly factor for complex I	Complex I deficiency	p. G56R and a c. 815-27T > C branch site mutation leading to aberrant splicing
SDHB[11]	Respiratory complex II	Neurodegeneration and cancer	Mutations at Fe–S cluster ligating cysteines preventing cluster binding
SDHAF1[12]	Assembly factor for complex II	leukoencephalopathy	Mutations that disrupt binding interface for either Hsc20 or SDHB prevent cluster maturation on SDHB
MitoNEET[13] NAF-1	Maintenance of iron homeostasis	Association with cystic fibrosis, Parkinson's disease, and cancer	Related to decrease in mRNA levels

Table 1-1: Iron–sulfur cluster proteins in relation to disease states, continued.

Protein	Function	Disease	Most common cause
FANCJ[15]	Genome maintenance and dbl-strand break repair	Fanconi anemia and breast cancer	p. M299I upregulates helicase activity or p. A349P that impairs DNA–protein interactions
XPD[16]	Nucleotide excision repair and transcription	Xeroderma pigmentosum (XP), Cockayne's syndrome (CS), trichothiodystrophy (TTD), and Cerebro-oculo-facial-skeletal (COFS) syndrome	p. R112H that impairs transcriptional function and inactivates helicase activity
ChlR1[17]	Genome maintenance	Warsaw breakage syndrome	p. R263Q inhibits DNA binding and DNA-dependent hydrolysis
RTEL1[18]	Maintenance of telomeres	Cancer, dyskeratosis congenita (DC), and Hoyeraal-Hreidarsson syndrome (HHS)	Protein mutations that prevent telomere maintenance
POL δ & ε[19]	DNA polymerases	Cancer	Unclear connection
$ABCB_7$[20]	Fe–S cluster export from the mitochondria	X-linked sideroblastic anemia (XLSA)	Protein mutations that result in mitochondrial iron overload
Grx5[21]	[2Fe–2S] cluster carrier	Sideroblastic-like anemia	Aberrant splicing leading to decreased Fe–S cluster transfer and impaired iron homeostasis
IRP[22]	Iron homeostasis	Parkinson's disease	Erroneous regulation generating reactive oxygen species
Grx2[23]	Cluster carrier and redox regulation	Parkinson's disease	Erroneous regulation of GSH levels
FECH[24]	Heme biosynthesis	Erythropoietic protoporphyria	

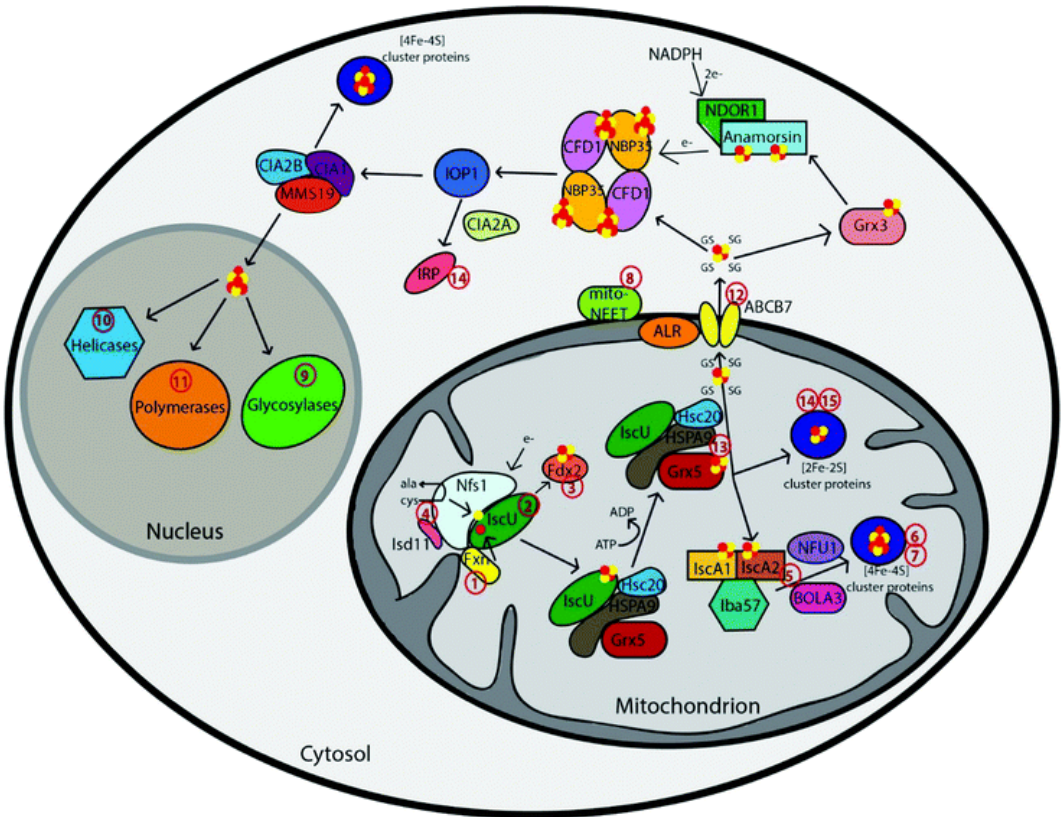

Figure 1-3: Schematic representation summarizing current models of mammalian Fe–S cluster biogenesis based on disease conditions. Nfs1, the cysteine desulfurase, with its cofactor protein Isd11 donates sulfur from L-cysteine for nascent Fe–S cluster assembly. Together, they bind to the primary scaffold protein IscU, the regulator protein frataxin (Fxn), which controls cysteine desulfurase activity and iron delivery, and a source of electrons. The newly formed IscU-bound [2Fe–2S] is subsequently transferred *via* a dedicated chaperone-*co*-chaperone system (Hsc20–HSPA9) to Grx5. From Grx5, the Fe–S clusters are either directly inserted into mitochondrial [2Fe–2S] proteins or transferred *via* specific carrier systems such as the one composed of IscA1, IscA2 and Iba57 to mitochondrial [4Fe–4S] proteins. To date, the presence of another cluster type (such as a glutathione-complexed [2Fe–2S] cluster) under physiological conditions cannot be excluded. For extra-mitochondrial Fe–S cluster, an uncharacterized compound (X) is exported for cytosolic and nuclear cluster trafficking *via* the Fe–S cluster export machinery consisting of ALR, glutathione and $ABCB_7$. Species X has been proposed to be a glutathione-complexed [2Fe–2S] cluster and is depicted as the [2Fe–2S]$(GS)_4$ complex.[17] Cytosolic cluster trafficking has been studied primarily in yeast. Fe–S clusters can be trafficked through Grx3 to anamorsin, which provides electrons to the cytosolic scaffold CFD1–NBP35. From there, [4Fe–4S] clusters are transferred *via* IOP1 to the CIA

proteins and final target proteins, such as IRP. The CIA proteins can complex with MMS19 for cluster delivery to nuclear targets, like polymerases, helicases, and glycosylases. The red numbers in the figure correspond to the disease numbers in the review and in **Table 1-1** [29].

These iron-sulfur targeting drugs also offer an alternative strategy to wreak cellular havoc in various cancers and pathogens through ROS generation, especially in a time when there is an extreme dearth in new antibiotic development, and due to misuse and overuse, bacteria are rapidly becoming resistant to existing antibiotics [30-33]. An alternative therapeutic method of action is to stabilize and inhibit the lability of iron-sulfur clusters, which are vital properties to their cellular function and specific chemistry [34]. Some common examples of iron-sulfur interacting therapeutics are listed in **Table 1-2**.

As seen in **Table 1-2**, mitoNEET and NAF-1 iron-sulfur proteins are prevalent in iron-sulfur therapeutic targeting strategies. MitoNEET (mNT, CISD1) was first identified as a target for pioglitazone, a type-2 diabetes therapeutic [35]. Pioglitazone belongs to the class of insulin-sensitizing compounds known as thiazolidinediones (TZD). TZDs are receptor-agonists of peroxisome proliferator-activated receptor-γ (PPAR-γ), which plays a role in cellular energy storage mediation by enhancing expression of glucose and lipid metabolism genes [36]. TZDs improve insulin resistance by opposing the effect of TNF-α in adipocytes [37]. The discovery of mNT occurred when muscle-specific PPARγ knockout mice fed a high fat diet were still responsive to the action of TZD treatment, ruling out PPARγ as the functional target [38].

Table 1-2: Therapeutic drugs interacting with iron-sulfur clusters [34].

Drug	Therapeutic Property	Therapeutic Indication	Fe-S Protein Target	Mechanism
Hydroxyurea	Anti-proliferative	Sickle cell, leukemia, polycythemia vera, other cancers	Leu1	ROS-mediated
Primaquine	Anti-parasite	Malaria	Rli1, aconitase	Fe-S cluster interaction and ROS-mediated
Cluvenone	Proapoptotic	Acute lymphoblastic leukemia	**MitoNEET, NAF-1**	Fe-S cluster stabilization
MAD-28 (cluvenone derived)	Anti-proliferative	Cancer	**MitoNEET, NAF-1**	Fe-S cluster destabilization
Pioglitazone (TZD)	Anti-diabetes insulin sensitizer	Diabetes	**MitoNEET, NAF-1**	Fe-S cluster stabilization
'882	Antimicrobial	Drug-resistant *Staph. aureus* strains	SUF machinery	Binds to Fe-S cluster biogenesis machinery
Antibiotics	Antimicrobial	Bacterial infections	*unspecified*	ROS-mediated (still debated)
***β*-Phenethyl isothiocyanate (PEITC)**	Anti-proliferative	Leukemia	NADH dehydrogenase3 (respiratory complex I)	ROS-mediated

BC1	Anti-angiogenic, antitumor	Ehrlich carcinoma	*unspecified*	ROS-mediated

It was later discovered that the actual target of pioglitazone was a mitochondrial-associated protein that had been previously uncharacterized [35]. It was named mitoNEET for its localization to the mitochondria and NEET for a unique amino acid motif (asparagine-glutamate-glutamate-threonine) that followed the [2Fe-2S] cluster binding region [35]. Based on the amino acid sequence, mNT was originally thought to be a zinc-finger protein, but additional early studies demonstrated that is was a dimeric [2Fe-2S] that was anchored to the outer mitochondrial membrane by an N-terminal sequence spanned the membrane and the C-terminal [2Fe-2S] cluster-binding domain existed in the cytosol [39]. Two additional NEET proteins were later discovered in humans. The second, named nutrient-deprivation autophagy factor 1 (NAF-1), which was also called Miner1, ERIS, or Noxp70, are expressed from the CISD2 gene. This protein's sequence varies from that of mNT (54% identical and 69% similar), and it localizes to the mitochondrial-associated membranes of the ER [39, 40]. The third homologous NEET protein family member is a monomeric [2Fe-2S] cluster protein that shares much less sequence identity with CISD1 or CISD2, and is a soluble protein found in the mitochondrial matrix [39]. Moreover, these proteins contained a rare 3Cys:1His coordination chemistry of the [2Fe-2S] cluster (Figure 1-4) [40-44].

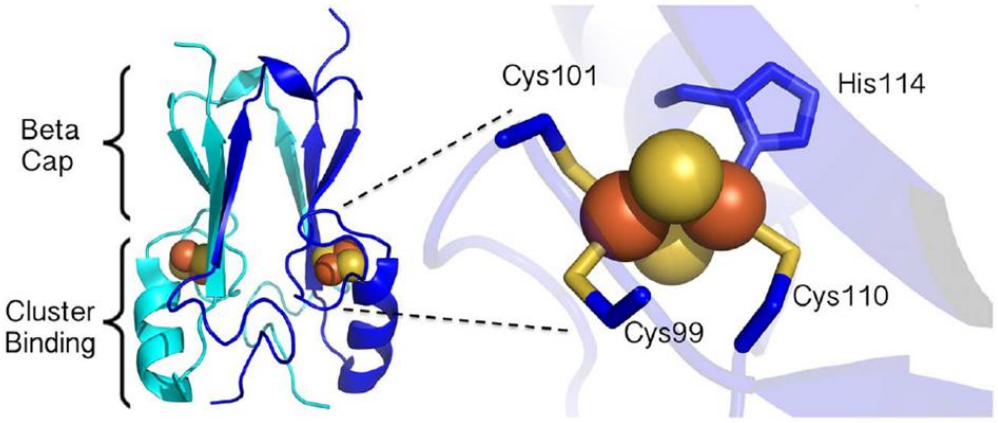

Figure 1-4: The NEET family of proteins bind [2Fe-2S] clusters with 3Cys:1His coordination. To date, all discovered NEET proteins contain this unique coordination, as it is part of their characteristic consensus sequence (NAF-1, PDB: 3FNV) [40].

An ancient role for the CISD proteins was suggested in a recent phylogenetic analysis study, demonstrating that a conserved consensus sequence, [**C**-X-**C**-X2-(S/T)-X3-P-X-**C**-D-G-(S/A/T)-**H**], which includes a characteristic CDGSH sequence followed by the "NEET" motif, and is found across all kingdoms of life [45-47].

After its discovery, mNT and NAF-1 research took two distinctly different primary approaches to attempt to resolve the cellular role of NEET proteins. The first was *in vitro* biophysical characterization and the second was *in vivo* organismal expression-level studies. Much of the organismal studies looked at the effects of knockout/knockdown or overexpression in order to examine systemic effects and draw conclusions from changes in overall phenotype. Much of what was discovered related changes to metabolic alterations, a role in tissue development, shortened lifespan, changes to

autophagy, oxidative stress protection, and iron misregulation [48-53]. Other studies found through shRNA silencing that NEET proteins were upregulated in cancers, and insufficient levels, especially of NAF-1, drastically slowed tumor growth [26]. These biological effects are linked to the protein structure and the [2Fe-2S] cluster coordination site chemistry. The properties of the 3Cys:1His iron-sulfur cluster coordination site is essential to function, such that alteration to a 4Cys coordination site in these proteins has been shown to inhibit cluster lability and also slow cancer growth [54]. This is not surprising, as other proteins involved in iron-sulfur cluster transfer are known to share this unique 3Cys:1His [2Fe-2S] coordination site [55]. While all these studies helped suggest the cellular importance of NEET proteins and suggested a general cellular role, collectively they were not able to pinpoint a specific function.

From the biophysical studies, mNT and NAF-1 were characterized as having pH-sensitive and tunable redox-active [2Fe-2S] clusters [39, 40, 43, 56, 57]. Most notable was that NEET proteins could transfer [2Fe-2S] clusters to an apo-acceptor ferredoxin protein shown in **Figure 1-5** [58]. Of additional significance from this study was that the pioglitazone, the TZD drug which had been shown to bind to mNT and NAF-1 [59], inhibited [2Fe-2S] cluster transfer, even stabilized cluster loss at low pH, and that clusters only transferred in the oxidized $[2Fe\text{-}2S]^{2+}$ and not the reduced $[2Fe\text{-}2S]^{+}$ state [58]. Additional studies demonstrated that the presence of a reducing agent, NADPH, and

mutation of the histidine ligand to create a 4Cys-coordination site abolished transfer to apo-ferredoxin [60, 61].

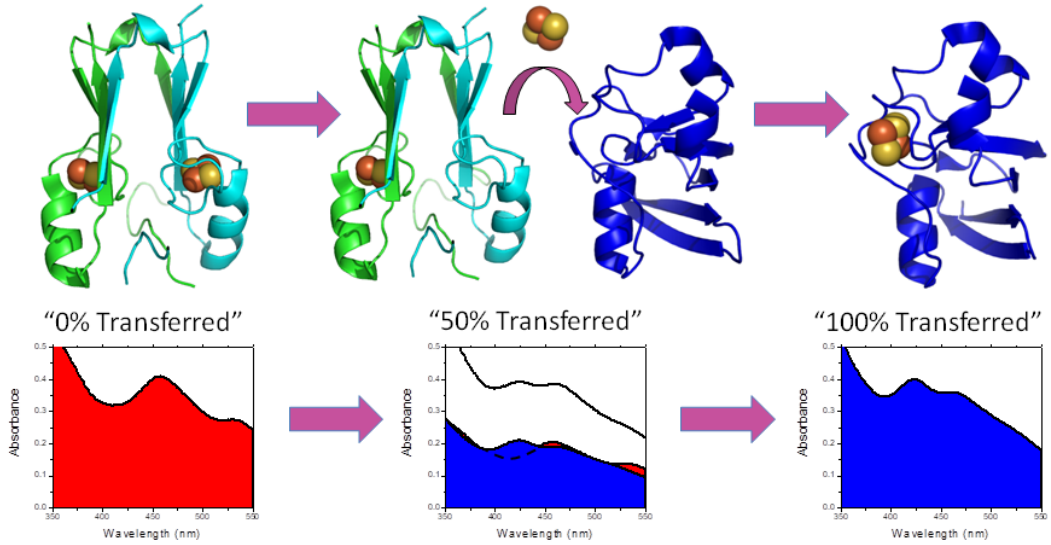

Figure 1-5: Facile transfer of the [2Fe-2S] cluster from mitoNEET (mNT) to apo-ferredoxin (a-Fd). The presence of the [2Fe-2S] cluster in mNT can be observed by UV-Vis spectroscopy with a signature peak at 458 nm and in Fd at 423 nm. Each panel shows the cluster transfer reaction progress. The observed spectra for the combined species are shown as a black line at the top of each frame while the deconvoluted spectra of holo-mNT **(red)** and holo-Fd **(blue)** Upon approaching completion, the visible spectrum resembles that of Fd, as all a-Fd has been converted to the holo form and mNT has been converted to the visible-lacking apo form. [58].

Altogether, these discoveries suggested that investigation of mNT and NAF-1 as iron-sulfur transport proteins would be a promising future direction of research. Follow-on studies confirmed that the lability of the [2Fe-2S] cluster in NEET proteins is critical to function. When breast cancer cells upregulate these proteins, such that when the NAF-1 H114C coordination-site mutant was overexpressed, these cells they experienced increased oxidative stress

through ROS production and exhibited mitochondria with an excess of free iron-pooling [54]. This study also discovered that treatment of breast cancer cells with pioglitazone, which stabilizes 3Cys-1His [2Fe-2S] clusters, also produces the ROS and iron accumulation phenotype. These effects lead to tumors with augmented size and a decrease in tumor aggressiveness. These data, further suggest that mNT and NAF-1 are responsible for mediating iron-sulfur transport from the mitochondrion, in which disruption produces free-iron overload in the mitochondrion and cell-wide uncontrolled ROS generation. Another finding from this study, in conjunction with previous research in breast cancer cell NEET protein expression, was that mNT and NAF-1 were upregulated in breast cancer and had varying effects of NEET protein modification [26, 62].

A fundamental discovery was that both mNT and NAF-1 were able to transfer their iron-sulfur clusters to apo-anamorsin [63], and that a key electron transfer step between mNT and anamorsin was part of the recovery of [2Fe-2S] clusters in anamorsin/CIA machinery [64]. Anamorsin is essential for aspects of cell growth, differentiation, and apoptosis, and also to be essential for cell survival in response [65]. Additionally it is a critical component of the cytosolic iron-sulfur assembly system (CIA) by transferring [2Fe-2S] clusters to cytosolic regulatory protein 1 (IRP1) which supplies iron-sulfur clusters to critical cytosolic iron-sulfur proteins [64].

These data solidified a role of mNT and NAF-1 at the junction of the iron-sulfur assembly pathway of the mitochondrion (ISC) and the cytosolic

iron-sulfur assembly machinery (CIA). For the first time since their discovery, the once enigmatic NEET proteins now had a defined cellular role.

Hence, research aimed at elucidating the differences between mNT and NAF-1 continued, as their localization is not identical and their cellular roles vary, as discussed above. First, molecular dynamics indicate key differences in their secondary and tertiary structure that vary based on the presence and absence of the [2Fe-2S] clusters. These studies explain the variation in their cluster pH-dependent properties, and possibly their different roles in cancer [56, 62, 66]. It was found that directional transfer of [2Fe-2S] clusters occurs from mNT to NAF-1, but not the reverse [67]. This clearly establishes a distinct functional difference, and connects the roles of these two proteins with respect to one another. A summary of these findings in found in **Figure 1-6**, which is modified from the published version [63].

From this point moving forward, our lab had two sub-projects: The first aimed to further resolve the roles of mNT and NAF-1 at the mitochondrion and cytosol interface, and the second aimed to better connect the network between the ISC and CIA pathways. Both aims had the underlying goal to identify and establish a [2Fe-2S] cluster donor for mNT, which was yet undiscovered, and to explore additional iron-sulfur cluster donors to NAF-1. The first approach examined a link between the outer mitochondrial voltage dependent anion channel (VDAC) that despite the name, VDAC can transport a diverse flow of metabolites and ions between the inner mitochondrial space and the cytosol [68-70]. We reasoned that since the mechanism for iron-sulfur

clusters to exit the mitochondria had not been identified, both VDAC and mNT are co-localized on the outer mitochondrial membrane, and the dimensions for mNT made it possible to access the inner-side of VDAC; these two proteins might serve as a method for iron-sulfur entry or exit across the outer mitochondrial membrane (Figure 1-7). Chapter 3 of this dissertation discusses that investigation and the recent results that were submitted for publication.

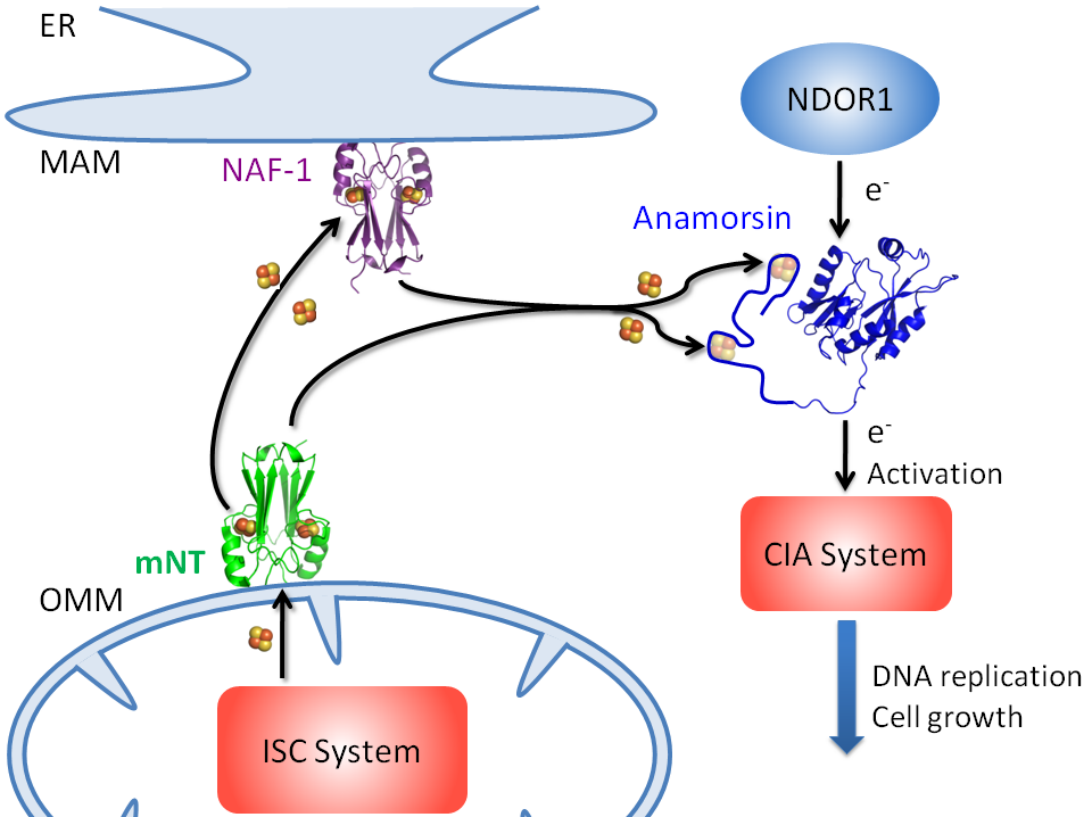

Figure 1-6: Schematic showing mNT and NAF-1 ISC-CIA link and a role as iron-sulfur cluster transfer partners. [63]

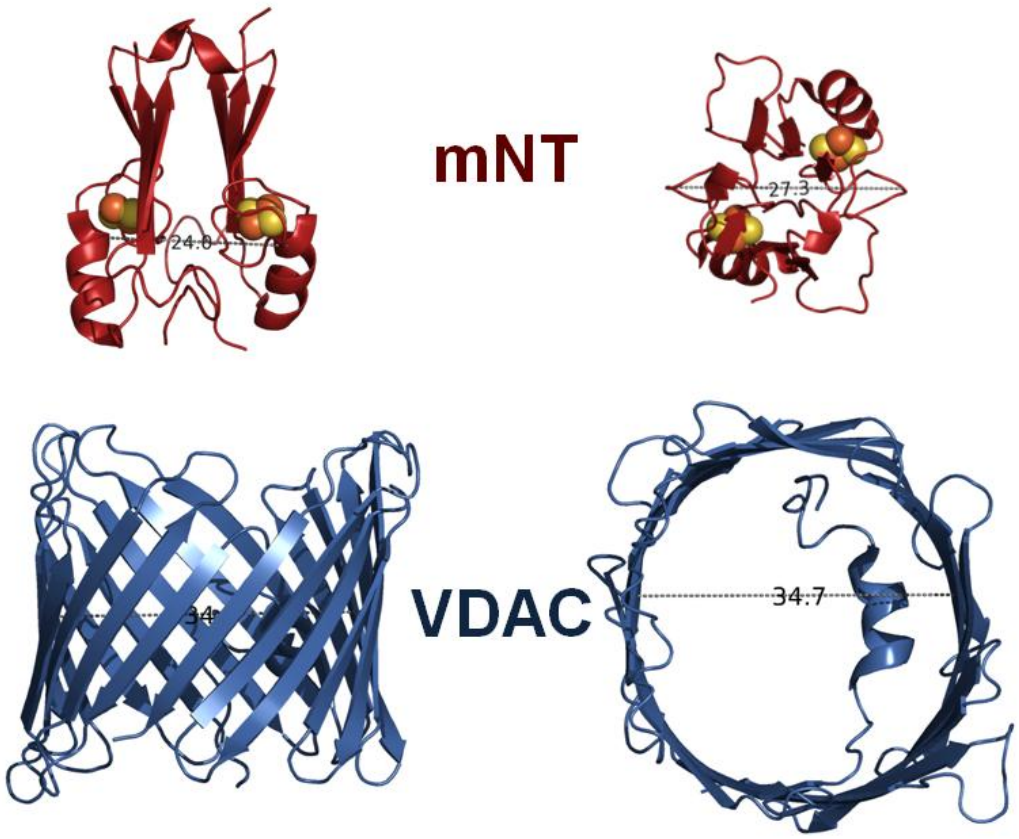

Figure 1-7: A comparison of mNT dimensions to that of VDAC dimensions. (Left) The side-view of each molecule to show width. (Right) The top view, β-cap and cytosol facing side respectively. The VDAC channel structure (PDB: HXDO) has a channel that spans over 30 Å, while mNT has a maximum width in either direction of less than 30 Å.

To examine if mNT or NAF-1 acquired their iron-sulfur cluster from a cytosolic component, or to attempt to identify new iron-sulfur cluster acceptors for the NEET, proteins, we took inventory of the list of potential human cytosolic [2Fe-2S] cluster candidates, shown in **Table 1-3**. This was a short list of three: Glutaredoxin-3 (GRX3), aldehyde oxidase 1 (AOX1), and xanthine dehydrogenase (XDH).

Table 1-3: Inventory of Cytosolic and Nuclear Iron-Sulfur Proteins.

Fe/S protein (human)	Yeast homolog	Fe/S cluster type	Proposed main function
DNA maintenance			
PRIM2	Pri2	[4Fe–4S]	Primase, synthesis of RNA primers for DNA replication
POLA	Pol1	[4Fe–4S]	Catalytic subunit of polymerase α, DNA replication
POLE1	Pol2	[4Fe–4S]	Catalytic subunit of polymerase ε, DNA replication
POLD1	Pol3	[4Fe–4S]	Catalytic subunit of polymerase δ, DNA replication
REV3L	Rev3	[4Fe–4S]	Catalytic subunit of polymerase ζ, DNA repair
FANCJ	absent	[4Fe–4S]	Helicase, DNA repair
NTHL1	Ntg2	[4Fe–4S]	DNA glycosylase, DNA repair
XPD	Rad3	[4Fe–4S]	Helicase, nucleotide excision repair
MUTYH	absent	[4Fe–4S]	DNA glycosylase, DNA repair
RTEL1	absent	[4Fe–4S]	Helicase, telomere stability, anti-recombinase
CHLR1	Chl1	[4Fe–4S]	Helicase, chromosome segregation
DNA2	Dna2	[4Fe–4S]	Helicase/nuclease, DNA repair Okazaki fragment processing,
Amino acid and nucleotide metabolism			
Absent	Leu1	[4Fe–4S]	Isopropylmalate isomerase (leucine biosynthesis)
Absent	Ecm17	[4Fe–4S]	Sulfite reductase, required for biosynthesis of methionine
Absent	Glt1	[4Fe–4S]	Glutamate synthase
→ AOX1	Absent	2× [2Fe–2S]	Aldehyde oxidase (catabolism of xenobiotics)
DPYD	Absent	4× [4Fe–4S]	Dihydropyrimidine dehydrogenase (pyrimidine catabolism)
GPAT	Absent	[4Fe–4S]	Phosphoribosyl pyrophosphate amidotransferase (purine biosynthesis)
→ XDH	Absent	2× [2Fe–2S]	Xanthine dehydrogenase/oxidase
Ribosome function and tRNA modification			
ABCE1	Rli1	2× [4Fe–4S]	Ribosome biogenesis, translation initiation and termination
ELP3	Elp3	2× [4Fe–4S]	Elongator protein 3 (tRNA wobble base modification), SAM
TYW1	Tyw1	2× [4Fe–4S]	tRNA wybutosine biosynthesis, SAM
CDKAL1	Absent	[4Fe–4S]	tRNA modification
CDKRAP1	Absent	[4Fe–4S]	tRNA modification
Other processes			
→ GRX3 (PICOT)	Grx3–Grx4	[2Fe–2S]	Intracellular iron homeostasis
IRP1	Absent	[4Fe–4S]	Intracellular iron regulation
RSAD1 (Viperin)	Absent	[4Fe–4S]	Antiviral activity, SAM
mitoNEET (CISD1)	Absent	[2Fe–2S]	Insulin sensitivity, unknown (located in mitochondrial outer membrane facing cytosol)
MINER1 (NAF1, CISD2)	Absent	[2Fe–2S]	Ca^{2+} metabolism, unknown
MINER2	Absent	[2Fe–2S]	Ca^{2+} metabolism, unknown

My work established that GRX3 plays a unique role in the establishment of [2Fe-2S] cluster homeostasis between mitoNEET and NAF-1 and closes the loop on the mitochondrial-cytosolic iron-sulfur cluster assembly mechanism. The details of the expression, purification, and reconstitution are in Chapter 2, *Materials and Methods*, and the follow-on experiments and results are presented in Chapter 4.

Chapter 2

Materials and Methods

Introduction

A major challenge to *in vitro* experimentation with proteins that contain one or more cofactors is the ability to produce solution-stable constructs that retain the prosthetic group(s) of interest. mNT and NAF-1 are found as novel 2Fe-2S dimeric folds tethered to the outer mitochondrial membrane and endoplasmic reticulum, respectively. In initial studies of the structural and biochemical properties of the functional NEET iron-sulfur cluster containing folds we determined that the cytosolic domains were functional in ferredoxin, anamorsin, and Bcl-2 protein interactions and cluster binding properties [58, 63, 71, 72]. Thus we chose to avoid detergents and lipids in functional experiments, and expressed and purified the soluble regions with the single pass membrane-spanning N-terminal regions removed. Crystal structures determined in our laboratory indicate folding and [2Fe-2S] cluster ligation of the soluble domains. Fortunately, these constructs are now easily overexpressed in *E. coli* with the [2Fe-2S] cluster intact [39, 42]. An additional advantage is that these proteins have very long [2Fe-2S] cluster half-lives in aerobic solutions with a pH above 7.0 [39, 42]. This feature allowed investigation of the [2Fe-2S] cluster transfer capability of these proteins in aerobic conditions at the lab bench for NEET proteins' [2Fe-2S] cluster transfer to the canonical acceptor protein apo-ferredoxin [58] and to the first identified cytosolic iron-sulfur cluster assembly (CIA) factor apo-anamorsin (Figure 2-1) [63].

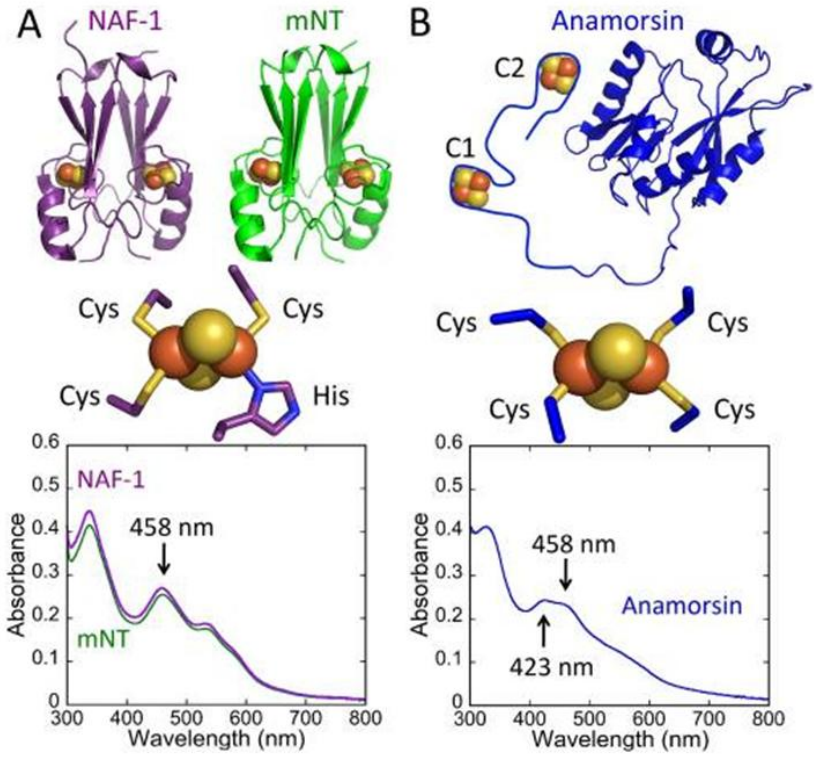

Figure 2-1: Structure and Visible Spectra of NAF-1, mNT, and [2Fe-2S] transfer-partner anamorsin. NAF-1 and mNT are able to transfer [2Fe-2S] clusters to anamorsin, which is tracked by changes in their respective UV-visible absorption peaks, due to a difference in the ligand environment of the [2Fe-2S] cluster. A. (Top) Crystal structures of mNT (PDB code: 2QH7,), NAF-1 (PDB code: 3FNV); (Middle) NEET 2Fe-2S cluster with 3-Cys:1His coordination; (Bottom) Absorption spectra of 25 μM mNT and NAF-1. B. (Top) Crystal structure of the N-terminal domain of Anamorsin (PDB code: 2YUI) with an added schematic of the unstructured 2Fe-2S cluster binding domain; (Middle) Representative Anamorsin 2Fe-2S cluster with 4-Cys coordination (from ferredoxin, PDB code: 1RFK); (Bottom) Absorption spectrum of 43 μM Anamorsin isolated from *E. coli* [63].

In contrast, we identified that GRX3, which connects the mitochondrial and cytosolic iron-sulfur cluster homeostasis pathways, is expressed as a holo-protein in *E. coli*, but rapidly loses its [2Fe-2S] cluster under aerobic environments to yield a monomeric apo-protein that is relatively unstable in

solution without continuous exposure to a reducing agent [73]. GRX3 was only recently characterized as an iron-sulfur protein, and as such the methods to work with a holo-protein were severely undeveloped [73]. To assess the potential [2Fe-2S] cluster transfer from holo-GRX3 to apo-NEET proteins, it was necessary to quantitatively reconstitute a stable holo-construct under anaerobic conditions. Therefore, significant effort was directed towards method development at every step of the procedure and required use of an anaerobic glove-box for 100% of transfer experiment set-up. An additional hurdle to overcome was that the holo-GRX3 protein has a stoichiometry of [2(Grx3):4(GSH):2(2Fe-2S)], and ligation of the GSH (as GS^-) is in reversible equilibrium that required excess GSH to maintain the holo-form of GRX3. My methods were later confirmed with a recent publication that shows GRX3 transfers [2Fe-2S] clusters to anamorsin, a protein our lab had also linked to NEET protein [2Fe-2S] cluster transfer [63, 74]. The procedures indicated in their body of work matched much of what I had developed. The methods involved in optimizations of the GRX3 experiments and modifications to the NEET protein methods described previously, are included in this chapter.

MitoNEET and NAF-1 genes, plasmids, and bacterial strains.

Coding sequences corresponding to the soluble domains of human mNT (amino acids 33-108) and human NAF-1 (amino acids 57-135) were subcloned into a pET28-a(+) vector (EMD Millipore) between NdeI and XhoI restriction endonuclease sites as described previously [42, 60]. The vector

includes an affinity tag of six consecutive histidines separated by a thrombin protease cleavage site to the N-terminal side of the construct and has a kanamycin resistance gene for selection. Expression plasmids were amplified in *E. coli* DH5α cells (EMD Millipore). For protein expression, the mNT and NAF-1 in pET28-a(+) plasmids were transformed into *E. coli* BL-21 (DE3) Codon Plus RIL cells (Agilent) to compensate for rare arginine, isoleucine, and leucine codons found in the native DNA sequence.

Glutaredoxin-3 (GLRX3)gene, plasmid, and bacterial strains.

To determine if the human GRX3 cDNA sequence contained any rare codons for *E. coli* expression, I used the Caltor Rare Codon online tool to assess how many were present (Table 2-1) and how many consecutive rare codons existed (Table 2-2). To avoid cell lines that required multiple antibiotics, such as BL21 (DE3) Rosetta *E. coli* cells, which could lower the protein production yield, the full-length human glutaredoxin-3 gene (*GLRX3*; Accession AAH05289.1) was commercially synthesized with optimized codons for *E. coli* expression and subcloned into the pET28-a(+) plasmid (GenScript). The expression plasmid was amplified in DH5α *E. coli* cells (EMD Millipore). For protein expression the mNT and NAF-1 in pET28-a(+) plasmids were transformed into BL-21 (DE3) *E. coli* cells (EMD Millipore).

Table 2-1: Presence of Rare-Codons in GRX3 cDNA Sequence.

Amino Acid	Rare Codon	Frequency of Occurrence
Arginine	CGA	1
	CGG	1
	AGG	1
	AGA	1
Glycine	GGA	11
	GGG	1
Isoleucine	ATA	5
Leucine	CTA	3
Proline	CCC	2
Threonine	ACG	0

Table 2-2: Rare Codon Repeats in GRX3 cDNA Sequence.

Repeat	Frequency
ATA GGA GGA	1
ATA CTA	1
GGA GGA	1
AGA GGA	1

Escherichia coli transformation.

Competent DH5α and BL-21 cells were transformed by introducing 100-300 ng of DNA (150 ng/μL) per 250 μL of pre-suspended cells that were

thawed on ice and then mixed gently. After a 30 min incubation, the DNA-cell suspensions were heat shocked in a 42 °C water bath for 45 secs and were cooled briefly before 750 µL of SOC medium was added (Mediatech Inc, Corning). The cultures were grown for 1 hr at 37 °C while shaking at 220 rpm, followed by selection and plating on LB-agar medium with 50 µg/mL kanamycin for DH5α and BL-21 (DE3) cells, or 30 µg/mL kanamycin and 30 µg/mL chloramphenicol for BL-21 (DE3) Codon Plus RIL cells.

Expression and purification of MitoNEET and NAF-1.

Both NEET proteins were purified as described previously [58, 75], with the exception that thrombin protease-cleaved proteins were eluted from the nickel-coordinating NTA affinity resin (Qiagen) with a 50 mM Tris (pH 8.0), 20 mM NaCl, and 2 mM $CaCl_2$ buffer in order to eliminate a buffer exchange step prior to an SP-HP (GE Healthcare) cation-exchange chromatography step.

Expression and purification of Glutaredoxin-3.

BL21 (DE3) *E. coli* cells transformed with the GRX3- pET28-a(+) plasmid were grown overnight at 37 °C in 200 mL of LB media containing 50 µg/mL kanamycin, while shaking at 200 rpm. The following day the culture was divided and inoculated into three separate 2 L LB cultures containing a final concentration of 50 µg/mL kanamycin. At an OD_{600} reading between 0.3 – 0.5, $FeCl_3$ was added from a freshly prepared, pre-sterilized stock to a final concentration of 25 µM in the cultures, and the temperature of the cultures

was lowered to 17 °C. At an OD_{600} of 0.6-0.7, protein expression was induced using a final concentration of 1 mM IPTG. The induced cultures were left to grow for 20 h at 17 °C, while shaking at 180 rpm.

The cells were harvested by centrifugation at 6,000 ×*g* at 4 °C for 30 mins, and resuspended to 125 mL final volume in a lysis buffer containing 50 mM Tris (pH 8.0), 500 mM NaCl, and 1 mM PMSF and frozen at -20 °C prior to lysis. Cells were thawed and homogenized by stirring on ice. Cell lysis was performed using two passes through a EmulsiFlex-C5 homogenizer (Avestin), followed immediately by centrifugation at 30,000 ×*g* at 4 °C for 30 min.

The supernatant fraction was applied to ~5 mL of Ni-NTA affinity resin (Qiagen), followed by a 50 mL wash step with lysis buffer with 5 mM imidazole and a 30 mL wash step with 30 mM imidazole. The N-terminal 6x histidine tag was cleaved using 2-3 mg of thrombin in a buffer volume of 45 mL in a 50 mL conical tube. Using bovine thrombin (Thermo-Fisher), the His-tag cleavage reaction was carried out at 4 °C overnight (15-18 hrs) with constant rotating inversion in a buffer of 50 mM Tris (pH 8.0), 150 mM NaCl, and 2 mM $CaCl_2$. The flow-through volume was collected and pooled with an additional 30 mL wash step of 50 mM Tris (pH 8.0), 150 mM NaCl, and 50 mM imidazole. Although the oxygen-sensitive [2Fe-2S] clusters are lost rapidly from GRX3 in air-exposed solution, to further drive the formation of monomeric GRX3 by [2Fe-2S] cluster loss, 100 µM potassium ferricyanide ($K_3[Fe(CN)_6$) was added to protein samples overnight (6-15 h) at 22 °C.

The mixed monomer and dimer GRX3 samples (37 kDa and 74 kDa respectively) were then concentrated to less than 2 mL by centrifugation in 10 kD molecular weight cutoff centrifugal filter units (EMD Millipore) at 3,500 × *g*. PD-10 desalting columns (GE) were pre-equilibrated with 50 mM Tris (pH 8.0), 100 mM NaCl, 5 mM DTT (BioPioneer), and 3 mM GSH, and used to buffer-exchange the protein samples. Samples of < 5 mL were then loaded onto a HiPrep 26/60 Sephacryl S-200 HR size-exclusion chromatography column (GE Healthcare), that had been pre-equilibrated with 50 mM Tris (pH 8.0), 100 mM NaCl, 5 mM TCEP (Thermo-Fisher), and 3 mM GSH (Thermo-Fisher). Since this chromatography step requires the reducing agent and protein to be at room temperature for several hours, TCEP was used instead of DTT due to the significantly longer half-life of the former in aqueous solution. The elution profile yielded two elution peaks from the protein absorption at 280 nm: The dimer at ~155 mL and the monomer fraction at ~250 mL, as shown in the **Figure 2-2** chromatogram. Monomer fractions excluding the peak tails were pooled and re-concentrated by centrifugation as before, to a final concentration of 500 µM, using an extinction coefficient at 280 nm of 34 $mM^{-1}cm^{-1}$ calculated using the ProtParam online tool. Proteins in 500 µL aliquots were flash-frozen in liquid nitrogen and stored at -80 °C until further use.

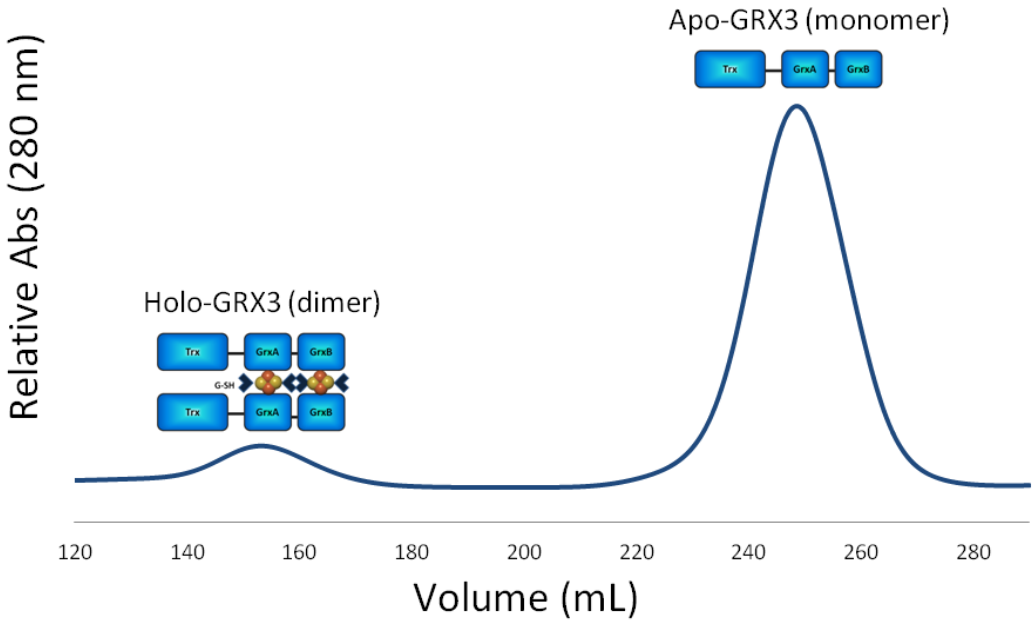

Figure 2-2: Chromatogram for human GRX3 size-exclusion chromatography. A HiPrep 26/60 Sephacryl S-200 HR size-exclusion chromatography column was pre-equilibrated with 350 mL of buffer containing 50 mM Tris (pH 8.0), 150 mM NaCl, 5 mM TCEP, and 3 mM GSH. Protein samples that had been previously purified using Ni-NTA affinity chromatography and subjected to thrombin cleavage were loaded onto the column in a volume less than 10 mL, and eluted at flow-rate of 1.6 mL/min. Elution fractions were collected at 3 mL intervals, and monomer fractions excluding the peak tails were pooled; followed by addition of another 1 mM equivalent of TCEP and concentrated to 500 μM based on the theoretical ε_{280} of 34 $mM^{-1}cm^{-1}$ for monomeric GRX3 (ExPASy ProtParam web-based software, Swiss Institute of Bioinformatics).

Protein characterization and quality analysis.

In order to analyze the approximate size and to qualitatively assess the degree of purity of protein monomers, the purified proteins were separated and analyzed by sodium dodecyl sulfate polyacrylamide gel electrophoresis (SDS-PAGE). The best band separation was displayed using a 10% acrylamide/bis (Bio-Rad) resolving gel for GRX3, and 15% acrylamide/bis for

mNT and NAF-1. In addition to acrylamide/bis, resolving gels contained 500 mM Tris (pH 8.8), 0.1% (w/v) SDS, 0.05% (w/v) ammonium persulfate, and 25 µL of TEMED (Bio-Rad). All stacking gels contained 5% acrylamide/bis, 62 mM Tris (pH 6.8), 0.1% (w/v) SDS, 0.15% ammonium persulfate, and 25 µL of TEMED. The SDS-PAGE running buffer consisted of 25 mM Tris, 192 mM glycine, and 0.1% (w/v) SDS.

Western blotting was used to confirm the identity of the protein band from the SDS-PAGE as GRX3. For the blotting, polyacrylamide gels with protein were transferred to a polyvinylidene fluoride (PVDF) membrane sheet (Bio-Rad) at 60 V (< 300 mA), and incubated with rabbit polyclonal anti–GRX3 antibodies (ProteinTech Group) at a 1:600 dilution in TBT with 5% (w/v) BSA (Sigma), followed by washing and incubation with goat anti-rabbit IgG (heavy + light chains) secondary antibodies conjugated with aldehyde peroxidase (ProteinTech Group) diluted at 1:4000 in TBT with 5% (w/v) BSA. After three washes in TBS-T, GRX3-specific bands were exposed to Western Blue AP detection solution (Promega), which was incubated on the blot for 30 mins until GRX3 protein bands reached the desired colorimetric intensity. Blot images were taken on a InGenius3 imaging and analysis system (Syngene). A image of a sample denaturing (SDS-PAGE) gel and the accompanying western blot are displayed in **Figure 2-3**.

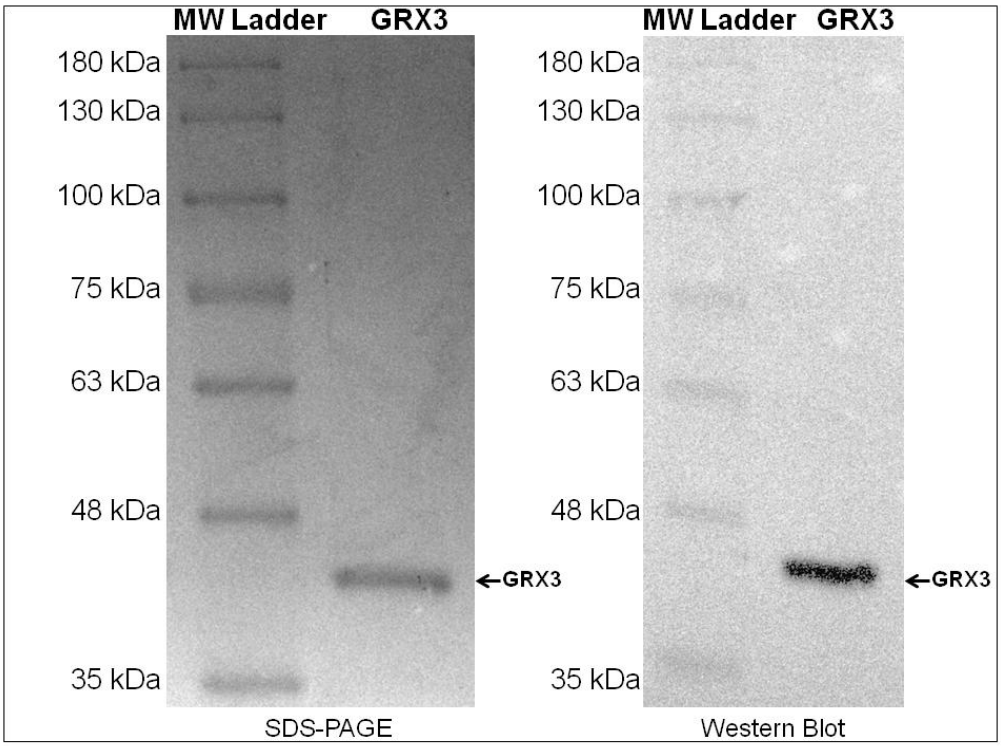

Figure 2-3: SDS-PAGE and western blot of purified GRX3. (Left) A 10% acrylamide gel showing the coomassie-blue stained GRX3 monomer band. Protein fractions were diluted in 1:1 in a loading buffer that contained 0.125 M Tris (pH 6.8), 20% (v/v) glycerol, 4% (w/v) SDS, 0.004% (w/v) bromophenol blue dye, and ~10% BME (Bio-Rad). The band runs at an apparent molecular weight of approximately 40 kDa. The left-most lane contains a molecular weight standard (AccuRuler Prestained Protein Ladder G02101, Lamda Biotech) labeled for apparent molecular weight in Tris-Glycine SDS-PAGE running buffer. **(Right)** A western blot on a PVDF membrane containing the proteins transferred from the SDS-PAGE gel. Rabbit polyclonal anti-GRX3 primary antibodies at a 1:600 dilution were incubated 12-72 hrs at 4 °C, washed, and then incubated with goat anti-rabbit monoclonal antibodies with an aldehyde peroxidase fusion. After washes with TBS to remove excess Tween-20 detergent, the Western Blue AP stabilized substrate solution was incubated until detectable bands appeared at the desired colorimetric intensity. The protein ladder is prestained and serves as a transfer control and sizing reference for western blotting.

UV-Visible spectroscopy was used as an additional method to confirm the identity of GRX3 by its characteristic [2Fe-2S] clusters absorption band at 410

nm, after the initial Ni-NTA affinity chromatography step, shown in **Figure 2-4** [73, 74].

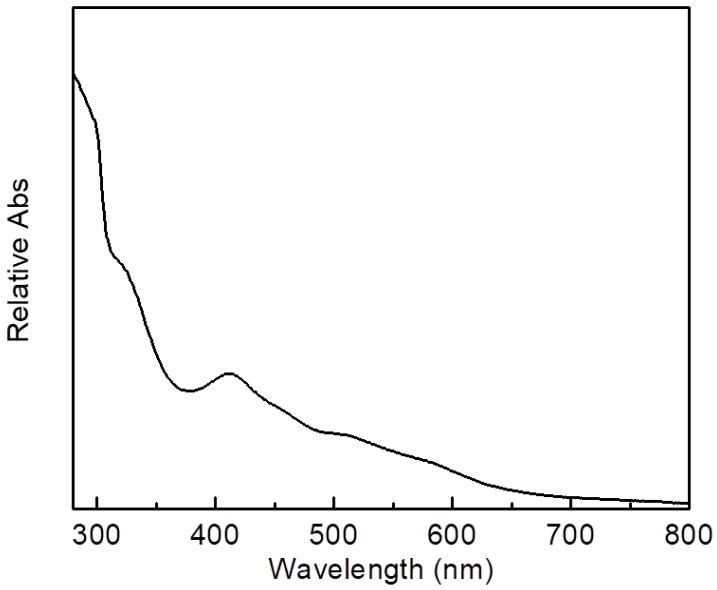

Figure 2-4: Characteristic UV-Visible Spectrum of Purified Holo-GRX3. After elution from Ni-NTA affinity chromatography, DTT (5 mM) was added to GRX3 fractions at 4 °C and the protein was briefly concentrated before taking scans from 250-800 nm in a Cary 50 Spectrophotometer. Samples lost all absorptive properties with ~120 mins.

Removal of [2Fe-2S] clusters to create apo-proteins

Apo-mNT and apo-NAF-1 were produced by taking advantage of the instability of the [2Fe-2S] clusters at acidic pH [76]. Holo-mNT was diluted into acetate buffer (pH 6.0) with 100 mM NaCl and 5 mM DTT at 25 °C for 15 h, until cluster loss was complete, by a total loss of absorbance at 410 nm. Holo-NAF-1 was diluted into acetate buffer (pH 5.0) with 100 mM NaCl and 5 mM TCEP at 37 °C for 48-72 hrs. The reason for utilizing a lower buffer pH for

NAF-1 is due to the [2Fe-2S] cluster of NAF-1 having a decay half-life over four-fold greater than mNT at pH 5.5 [46]. Additionally TCEP has both a greater half-life in aqueous solution and has a [2Fe-2S] cluster destabilizing effect in NEET proteins (unpublished), therefore these conditions optimized creation of the apo-protein to best preserve the biochemical integrity of NAF-1 for follow-up chemical reconstitution and GRX3-[2Fe-2S] cluster transfer assays. Samples were then buffer-exchanged into PD-10 desalting columns (GE Healthcare) pre-equilibrated with 50 mM Tris (pH 8.0), 100 mM NaCl, and 5 mM DTT to separate proteins from free iron and sulfur as well as raise the pH for the assay conditions.

Chemical reconstitution of [2Fe-2S] proteins.

Chemical reconstitutions of [2Fe-2S] clusters into the apo-proteins GRX3, mNT, and NAF-1 were performed anaerobically under argon gas, using a previously established protocol as a starting point for protocol modification [77]. Monomeric apo-proteins at a concentration of ~100 μM were first incubated with fresh 5 mM DTT in Tris buffer (pH 8.0) with 100 mM NaCl for 15 min. GRX3 mixtures contained an additional 3 mM GSH, which is part of the holo-protein [2Fe-2S] cluster ligation and is necessary for reconstitution. $FeCl_3$ and Na_2S were added in steps to each apo-protein solution to a final concentration of up to 500 μM ($\leq$ 5x stoichiometric ratio). The reconstitution mixtures were incubated overnight at 25 °C to maximize yield of this diffusion-dependent process, as described previously [74]. The reconstituted holo-

proteins were then buffer-exchanged using PD-10 desalting columns to give the final concentration of 25 μM dimer (1.4× dilution factor) in order to remove residual free iron, sulfide, and DTT. DTT has been shown to inhibit [2Fe-2S] cluster transfer from mNT and NAF-1 to apo-acceptor proteins and in some cases yield false positives for protein-to-protein Fe-S transfer [58, 78]. Therefore once proteins were sufficiently reduced in the anaerobic argon gas environment, I chose to eliminate DTT as it is inessential and a potentially problematic assay component [63, 78-81]. GRX3 desalting buffer also contained 3 mM GSH to maintain formation of the holo-protein. Reconstituted protein samples to be used for UV-visible spectrophotometric analysis were pipetted into 1 cm path length quartz cuvettes with polytetrafluoroethylene (PTFE) airtight caps, with additional semi-transparent, flexible wax film (Parafilm) wrapping to ensure an anaerobic argon gas environment, despite aerobic transport of the cuvettes.

Protein-to-protein [2Fe-2S] cluster transfer experiments.

Apo-protein samples were first introduced to an anaerobic environment to assess the potential of [2Fe-2S] cluster transfer from either holo-mNT to apo-GRX3 or from holo-NAF-1 to apo-GRX3 to create holo-GRX3 (2 Grx3: 4 GSH : 2 [2Fe-2S]).

Fe-S cluster transfer assays were performed under argon gas at room temperature. Apo-mNT and apo-NAF-1 were diluted to 25-100 μM in 50 mM Tris pH 8.0, and 100 mM NaCl by another PD-10 desalting step to remove any

residual DTT or TCEP reducing agent. Chemically reconstituted GRX3 was then added to the apo-mNT or apo-NAF-1 and the [2Fe-2S] cluster transfer was allowed to occur to completion. Visible changes from brown to red were apparent within less than a minute, and samples did not exhibit further color change progress after 5 min. Although a myriad of incubation times were assayed, from 5 min (time to remove from the glove box without oxygen contamination) up to overnight, additional time did not allow for any advances in reaction progress.

GRX3, mNT, and NAF-1 absorption spectra were collected on a Cary 50 UV-visible spectrophotometer (Varian). Spectra for apo-GRX3, apo/holo-mNT and apo/holo-NAF-1 were obtained under aerobic conditions, while reconstituted holo-GRX3 spectra were taken in a sealed cuvette under anaerobic conditions to prevent rapid [2Fe-2S] cluster release and aggregation.

Stability analysis of MitoNEET with Anion Channel Inhibitor DIDS.

UV-visible absorption spectra were measured within the near-UV to near-IR (from 250-700 nm) on a Varian Cary 50 UV-visible spectrophotometer (Agilent, Santa Clara, CA) at 37 °C. For each assay, 30 μM mNT samples were incubated alone or with 700 μM DIDS (Santa Cruz Biotechnology) in 50 mM phosphate buffer (pH 7.0) and 100 mM NaCl. The [2Fe-2S] cluster stability was determined from monitoring changes in the characteristic absorbance peak at 458 nm as a function of time published previously [42, 60, 76, 82].

Chapter 3

Stemming the Flow: MitoNEET Redox-Selectively Controls VDAC Gating

Abstract

MitoNEET is an outer mitochondrial membrane protein essential for sensing and regulating iron and reactive oxygen species (ROS) homeostasis. It is a key player in multiple human maladies including diabetes, cancer, neurodegeneration and Parkinson's diseases. In healthy cells mitoNEET receives [2Fe-2S] clusters from the mitochondrion and transfers them to acceptor proteins in a process that can be altered by drugs or during illness. Here we report that mitoNEET regulates the outer mitochondrial membrane (OMM) protein voltage-dependent anion channel-1 (VDAC1). VDAC1 is a crucial player in the crosstalk between the mitochondrion and the cytosol. VDAC proteins function to regulate metabolites, ions, ROS and fatty acid transport, as well as function as a "governator" sentry for the transport of metabolites and ions between the cytosol and the mitochondrion [68]. We find that the redox-sensitive [2Fe-2S] cluster protein mitoNEET gates VDAC1 when mitoNEET is oxidized. Addition of the VDAC inhibitor DIDS prevents both mitoNEET binding *in vitro* and mitoNEET-dependent mitochondrial iron accumulation *in situ*. Taken together, our data indicate that mitoNEET regulates VDAC in a redox-dependent manner in cells, closing the pore and likely disrupting VDAC's flow of metabolites.

Introduction

The NEET family of [2Fe-2S] proteins play essential roles in the regulation of mitochondrial iron and reactive oxygen species (ROS)

homeostasis, as well as in the activation of apoptosis, ferroptosis, and autophagy [46, 83, 84]. NEET proteins are associated with several human pathologies including diabetes, cancer, neurodegeneration, Parkinson's disease, Wolfram Syndrome-2 and cystic fibrosis [26, 35, 48, 49, 54, 85]. Many of these pathologies display various degrees of mitochondrial dysfunction, for which mitoNEET (mNT) is a critical regulator against [86, 87]. NEET proteins contain a signature CDGSH domain and are highly conserved from archaea to humans [39, 45, 88]. Each CDGSH domain binds to a redox-active [2Fe-2S] cluster via a characteristic 3Cys-1His coordination motif [42, 43]. There are three human members of the family, mitoNEET (mNT, CISD1), NAF-1 (ERIS, Miner1, CISD2) and MiNT (Miner2, Melanoma nuclear protein 13, CISD3). The founding member of the NEET family, mNT, is a homodimer localized to the cytosolic side of the OMM by a single-pass N-terminal *α*-helix. Each protomer coordinates a single [2Fe-2S] cluster [41, 42, 44]. Interestingly, mNT can repair the [4Fe-4S] cluster of cytosolic iron-regulatory protein-1 (IRP1/aconitase), an important regulator of iron metabolism by either transferring Fe or [2Fe-2S] clusters to it [82]. It also efficiently transfers its [2Fe-2S] clusters to apo-acceptor proteins such as the CIA important protein anamorsin (or ciapin1), an electron transfer protein involved in the assembly of cytosolic Fe-S clusters [42, 56, 58, 63]. Although mNT is able to donate its [2Fe-2S] clusters to apo-acceptor proteins, it remains unclear how mNT is able to exchange Fe-S clusters with mitochondrial proteins.

VDAC actively governs mitochondrial metabolism and function through interaction-based gating [68, 89]. VDAC plays a central role in neurodegenerative diseases (e.g. Alzheimer's disease) [90-94], and destructive processes (e.g. ROS accumulation) [95-98], as well as regulates apoptotic functions in the cell [89]. mNT's placement at the OMM with a redox-sensitive domain suggests that it could be an excellent candidate to modulate the activity of VDAC. Humans have three VDAC paralogs encoded by three separate genes (VDAC1, VDAC2 and VDAC3) [99, 100] and mNT was identified as an interaction partner with all three forms, from multi-species co-fractional studies in which cell lysates were analyzed for proteins that were co-isolated [101, 102]. In this study we focus our investigation on VDAC1 since it interacts with mNT, it is the most abundant channel (including the other two VDAC paralogs) in the mitochondrial membrane, and it controls mitochondrial respiration as well as acts as a transporter of diverse metabolites and ions between the cytosol and the intermembrane space [68, 69, 103]. Passage through VDAC between the cytosol and mitochondrial intermembrane space occurs through modulation of different open and closed states [70]. The expression level of VDAC1 is controlled independently of the expression level of VDAC2 and VDAC3 [104]. In this study we characterize VDAC1 (hereafter referred to as VDAC) interaction with mNT.

Here we report that mNT regulates the channel function of VDAC and that this interaction is dependent on the redox state of mNT's [2Fe-2S] clusters. Additionally, using a combination of hydrogen-deuterium exchange mass

spectrometry (HDX-MS) and computational docking methodologies, we identify the regions of mNT and VDAC involved in association. Importantly, we demonstrate that the VDAC inhibitor 4,4'-diisothiocyanatostilbene-2,2'-disulfonate (DIDS) abrogates the binding of mNT to VDAC *in vitro* and also prevents mNT from transferring its Fe/[2Fe-2S]s *in situ*. Taken together, our results underscore the relevance of the interaction between mNT and VDAC to maintaining cellular homeostasis and the regulation of Fe and [2Fe-2S] clusters in cells.

Results and Discussion

High affinity and redox modulation of VDAC-mNT interaction.

Microscale thermophoresis (MST) was employed to quantify the affinity of the VDAC-mNT interaction. Fluorescently labeled human VDAC in DMPC/CHAPSO bicelles (1% final concentration) was incubated with increasing concentrations of mNT and analyzed by MST and a dissociation constant (K_d) of 76 ± 2 nM was determined (Figure 3-1). Reduction with DTT prevented any detectable binding of mNT to VDAC, indicating that mNT can only bind to VDAC when its [2Fe-2S] clusters are oxidized (e.g., when the protein or lysates are exposed to oxygen; Figure 3-1). The dependency of the interaction of mNT-VDAC on the oxidation state of mNT suggests that it may be part of a response to oxidative stress, as the redox-active mNT is typically in a reduced state under normal cellular conditions [105, 106]. Due to its redox

potential ($E_{m,7}$) of +30 mV, mNT can be oxidized under conditions such as cell stress in disease states, defense, or cell death [57, 107].

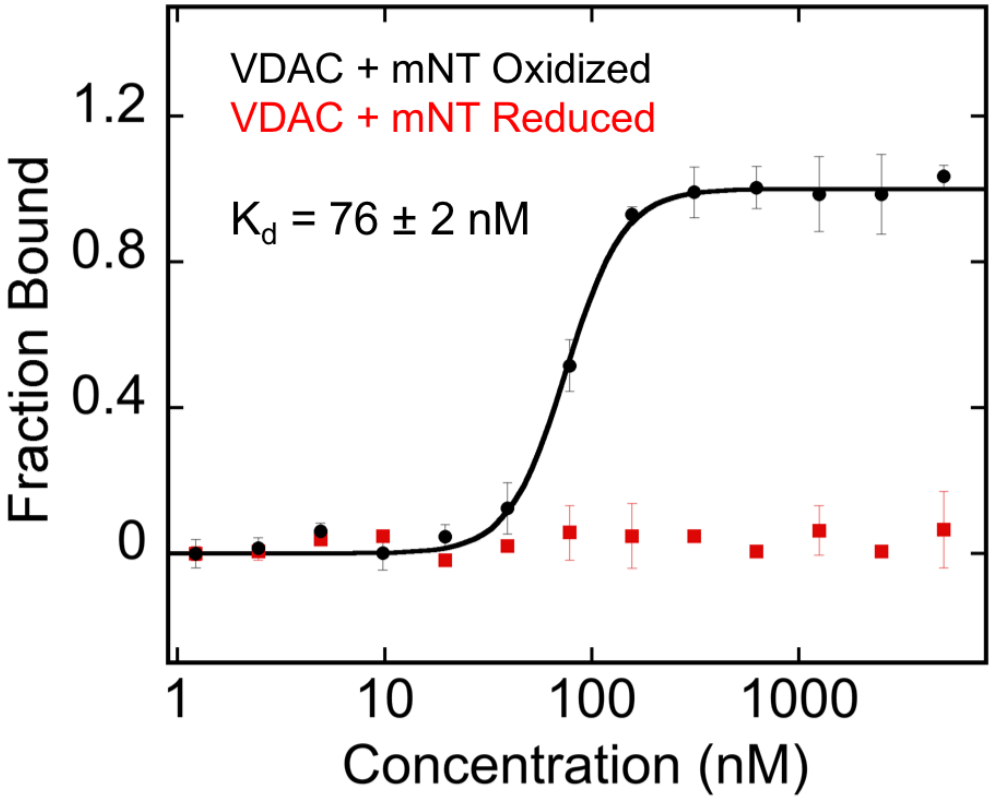

Figure 3-1: mNT binding to VDAC is Redox State-Dependent. MST analysis used to assess the affinity of mNT to fluorescently labeled VDAC reconstituted in 1% DMPC/CHAPSO bicelles under oxidizing conditions results in measured Kd of 76 ± 2 nM (Black). When mNT is reduced with DTT, binding is not observed (Red).

VDAC can adopt a high-conductance “open” state, as well as several low-conductance “closed” states. When VDAC adopts a “closed” conformation [108] it prevents ATP flux across the channels. In addition, VDAC channel permeability can be regulated by binding of Bcl2 family proteins, hexokinase

and tubulin [108-110]. We performed experiments in which VDAC conductance was recorded in the absence or presence of mNT across a range of applied voltages. The characteristic VDAC voltage-dependent conductance pattern was observed in the absence of added mNT protein, with decreasing conductance as voltage is increased above ~35 mV (both positive and negative), as expected [70, 111] (Figure 3-2). In the presence of mNT, the channel conductance was significantly inhibited across the entire voltage range (Figure 3-2). In contrast, the presence of NAF-1, a related NEET protein, had a smaller effect on the conductance changes across the voltage range, and may have a separate function associated with the truncated VDAC-ΔC form as suggested in a previous study [82].

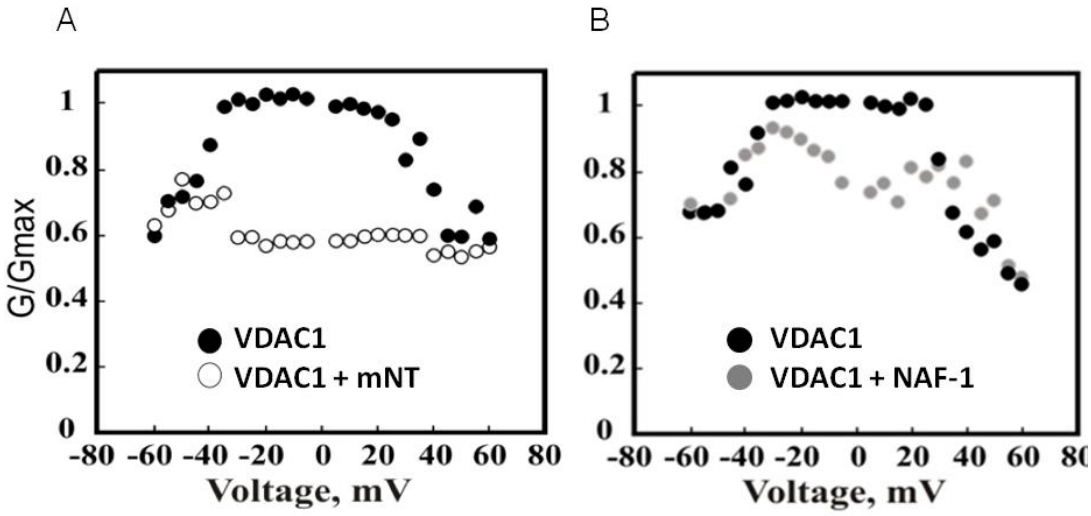

Figure 3-2: VDAC channel conductance is inhibited by mNT. VDAC was reconstituted into a planar lipid bilayer and channel conductance was measured as a function of applied voltage. The recordings were taken before and after the addition of 5 μg/ml mNT (A) or NAF-1 (B). Conductance measurements were normalized to the conductance at 10 mV using the formula: $G/G_{max} = \left(\frac{\text{Conductance}}{\text{Maximal Conductance of Control}}\right)$.

Structural analysis of the VDAC-mNT interaction.

To determine the interaction interface between mNT and VDAC, we utilized hydrogen deuterium exchange mass spectrometry (HDX-MS). Backbone amide protons provide probes for interactions as they can be protected from exchange with the solvent at the binding interface, as well as cause changes in deuterium exchange rates at sites distal to the binding interface [112]. We used the monomeric VDAC-nanodisc complex (VDAC-cND) allowed us to observe affects arising solely from the interaction of VDAC with mNT. Additional support to the mNT-VDAC interaction is MST binding analysis that measures mNT binding to VDAC-cND with a K_d of 210 ± 15 nM (Figure 3-3).

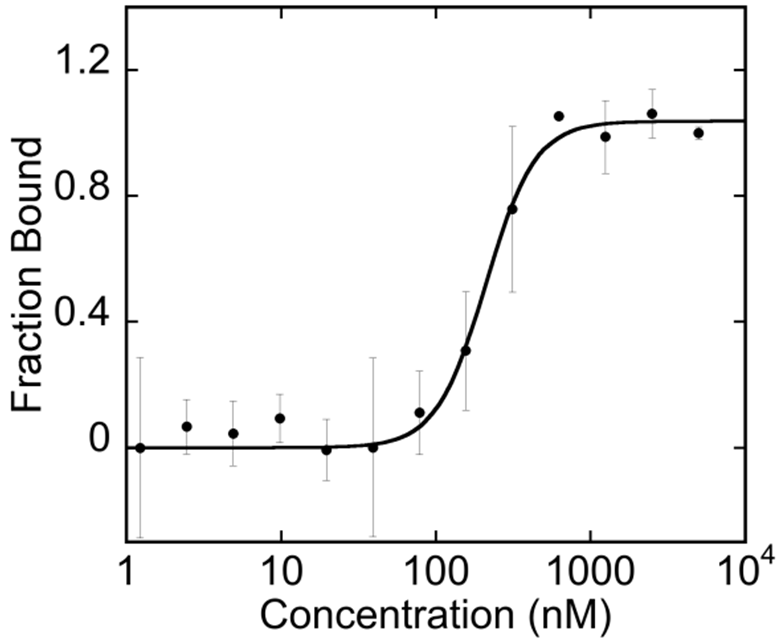

Figure 3-3: MST measurement of mNT binding to VDAC nanodiscs. MST analysis of a serial dilution of mNT binding to fluorescently labeled VDAC assembled in nanodiscs under oxidizing conditions results in a measured K_d of 210 ± 15 nM.

For HDX experiments, protease digestion of mNT resulted in 125 peptide probes and high (89%) sequence coverage. Digestion of the integral membrane protein VDAC demonstrated high sequence coverage as well, with a total of 91 peptide probes. Comparative heat map representations are shown for mNT and VDAC in **Figure 3-4** and **Figure 3-5**.

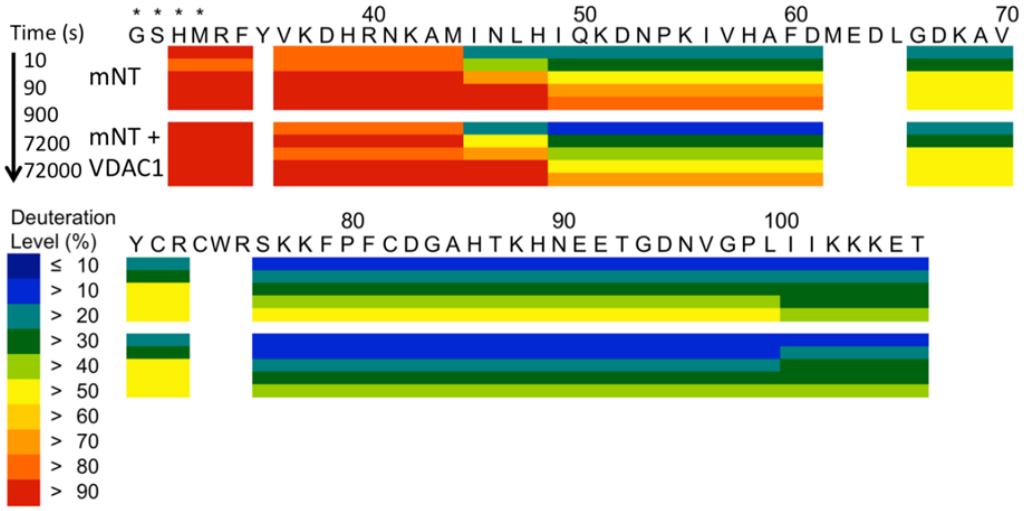

Figure 3-4: Heat map representation of time-dependent deuterium incorporation for mNT in complex VDAC. For time points of 10 s, 90 s, 900 s, 7200 s, and 72000 s, peptide probes are assigned to the primary sequence and color-coded to denote the percentage of deuterium incorporated. The top time course is mNT alone and the bottom is mNT in complex with VDAC.

Deuterium incorporation plots for representative peptide probes for regions with significant changes in protection are shown for both mNT and VDAC, with the regions highlighted on the protein structures (Figures 3-6 and 3-7). The regions of mNT with increased protection upon binding include the [2Fe-2S] cluster-binding region, the strand swapped outer *β*-strand, and the α-

helix within the cluster binding domain. VDAC protection increases at loop regions on the cytosolic side of the pore, with three consecutive loops on the C-terminal end of the barrel and one loop juxtaposed across the surface.

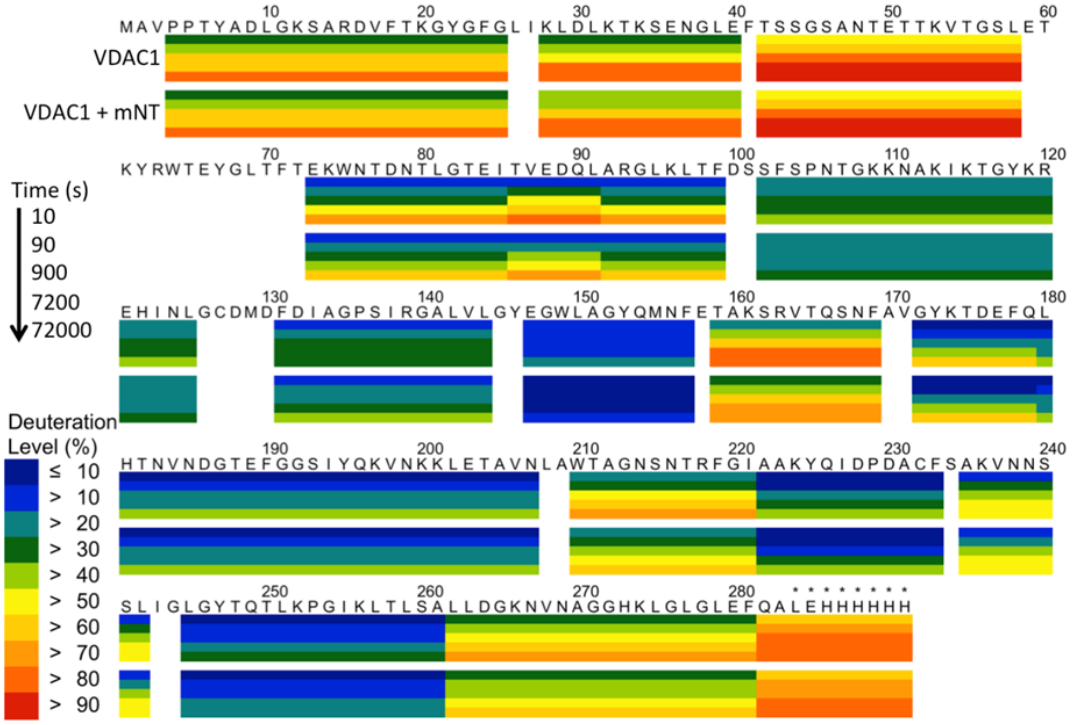

Figure 3-5: Heat map representation of time-dependent deuterium incorporation for VDAC in complex mNT. For time points of 10 s, 90 s, 900 s, 7200 s, and 72000 s, peptide probes are assigned to the primary sequence and color-coded to denote the percentage of deuterium incorporated. The top time course is VDAC alone and the bottom is VDAC in complex with mNT.

The N-terminal helix inside the pore that stabilizes the barrel is unaffected by the binding of mNT, suggesting that mNT does not bind deep enough into the barrel to alter exchange from this region, which can still exchange freely from the mitochondrial facing side of the surface. Peptides with increased hydrogen-deuterium exchange protection extend down the side of the barrel

opposite the internal helical region. This may indicate that mNT forms contacts further down that side, or that changes in local motions from binding are extended down the barrel wall. Taken together, these data indicate that mNT

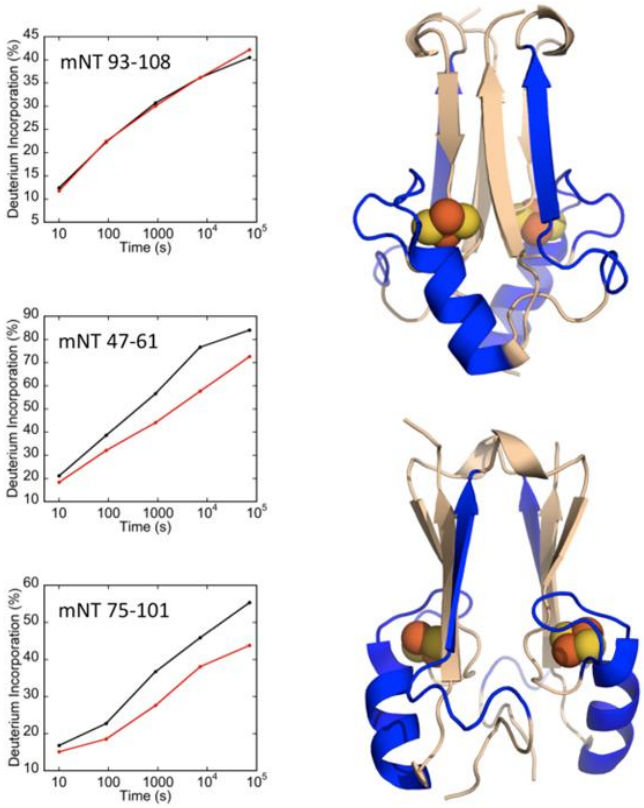

Figure 3-6: Regions of mNT with increased protection upon interaction with VDAC. Selected plots of deuterium incorporation into peptides from regions with significant increases in protection upon complex formation are shown. An additional plot is given (peptide 93-108) that is representative of a region with no significant change in deuterium incorporation upon complex formation. Regions which exhibit significant increases in HD-Exchange protection are highlighted on the mNT crystal structure (PDB ID 2QH7) in blue, while regions with similar protection factors are shown in beige.

binds from the cytosolic to inner-mitochondrial side of the VDAC channel and has specific points of contact, shown by protection changes.

Independent from the HDX-MS experiments, we performed a computational docking analysis of the two proteins (Figure 3-8). **Figure 3-8A** shows the docked model of mNT and VDAC, while **Figure 3-8B** shows the direct-coupling pairs in the two structures that was determined by DCA analysis.

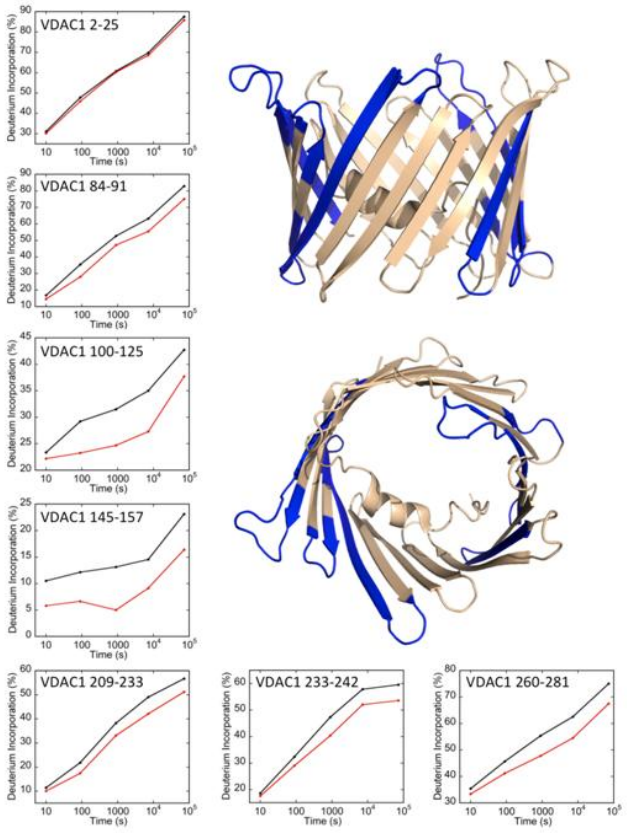

Figure 3-7: Regions of VDAC with increased protection upon interaction with mNT. Selected plots of deuterium incorporation into peptides from regions with significant increases in protection upon complex formation are shown. An additional plot is given (peptide 2-25) that is representative of peptides with no significant change in deuterium incorporation upon complex formation. This unaffected peptide corresponds to the N-terminal alpha-helix inside the VDAC barrel. Regions which exhibiting significant increases in HD-Exchange protection are highlighted on the VDAC crystal structure (PDB ID 5XDO) in blue and those without changes are in beige.

In the docked complex mNT fits into VDAC at an angle with one [2Fe-2S] cluster-binding domain contacting the cytosolic loops above the N-terminal helix and the *β*-cap region fitting in between the N-terminal helix (but not contacting it) and the barrel wall on the opposite side. This docked model matches well with our experimental data, indicating a likely mode of interaction.

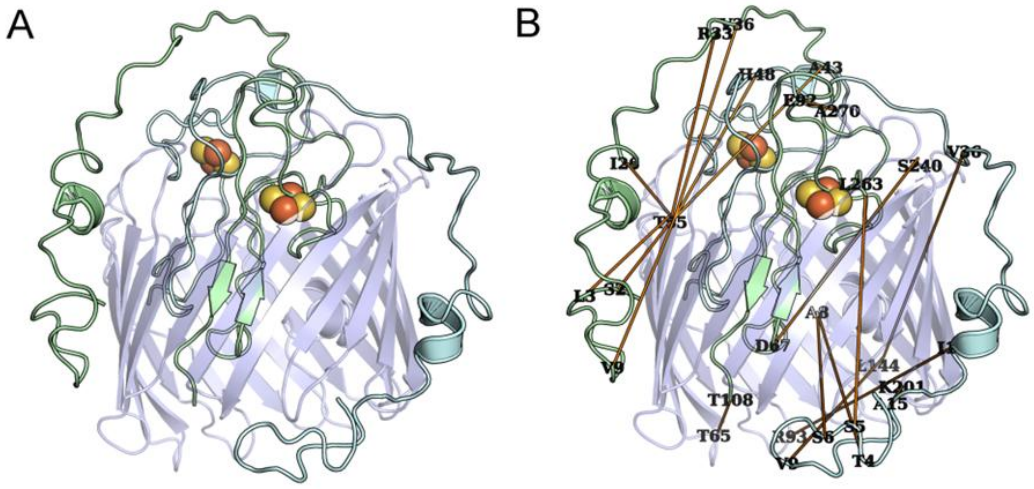

Figure 3-8. The images of modeled binding complex of mNT-VDAC (A) with DCA constraints (B). The pale green and pale cyan cartoons are different chains of mNT, and light purple cartoon is VDAC. Orange lines indicate the top 20 coevolving residue pairs.

The VDAC inhibitor DIDS prevents both mNT-VDAC binding and influences Iron/Fe-S flux between mNT and the mitochondrion.

Using DIDS, a known inhibitor of VDAC channels, we analyzed the binding of mNT and VDAC *in vitro* with MST. Fluorescently labeled VDAC in phospholipid bicelles was pre-incubated with DIDS followed by MST analysis of mNT binding. The presence of DIDS completely prevented detectable

binding of mNT to VDAC (Figure 3-9A). Given this observation, we then determined if inhibiting the interaction would prevent the transfer of iron into the mitochondria *in situ*. We previously discovered that adding oxidized mNT to gently permeabilized cells results in an influx of iron into the mitochondria [46]. Although these studies are not under physiological conditions,

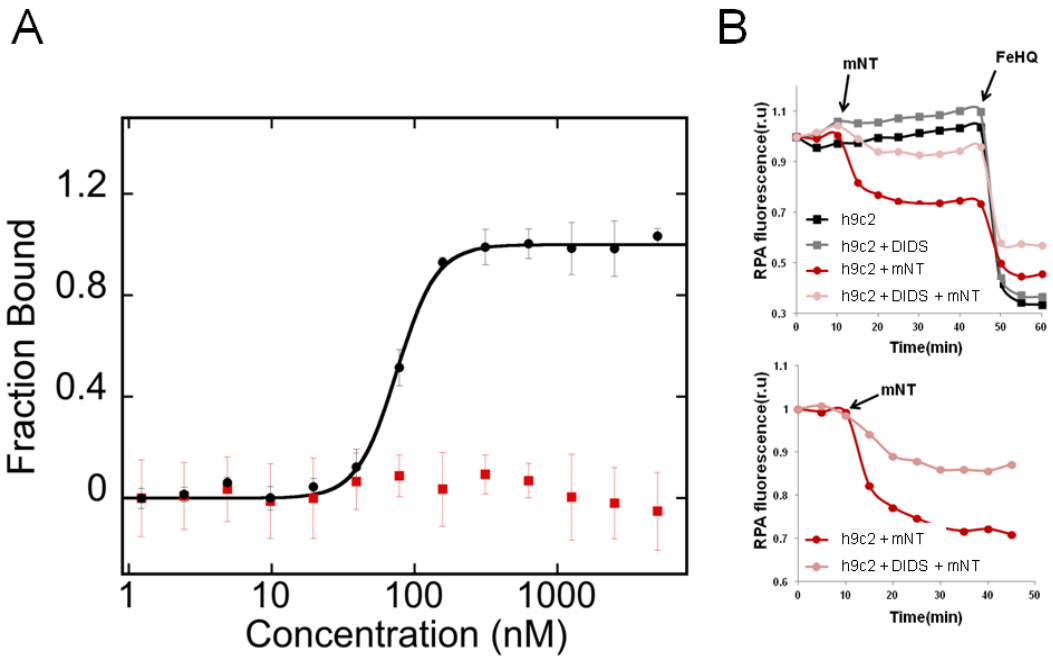

Figure 3-9: DIDS inhibits mNT-VDAC interaction. (A) MST analysis of the effect of DIDS on the binding of mNT to fluorescently labeled VDAC in 1% DMPC/CHAPSO bicelles under oxidizing conditions. *Black* shows mNT and VDAC. *Red* shows DIDS with mNT and VDAC. The final DIDS concentration following mNT addition was 700 µM. (B) The effect of DIDS on mNT-induced changes in mitochondrial iron levels. H9c2 cells were pre-incubated with and without DIDS (100 µM) for 1 hr, labeled with RPA and permeabilized with digitonin to allow the entry of mNT into cells. The change in RPA fluorescence was followed every five minutes. Twenty µM of mNT was added after 10 minutes. Five µM ferrous ammonium sulfate, complexed to equimolar hydroxyquinoline (FeHQ), which is a siderophore that allows iron to pass the membrane, was added after 45 min. RPA fluorescence is expressed in relative units (r.u.) obtained by analyzing individual cell fluorescence with Image J (open software), by averaging five cells per field.

they demonstrate mNT binding to VDAC could also occur within the cellular environment (Figure 3-9B). Soluble mNT was added to gently permeabilized H9c2 cells, which are are useful for studying intracellular metabolic changes. Using rhodamine B-[(1,10-phenanthrolin-5-yl)-aminocarbonyl] benzyl ester (RPA) as an indicator of mitochondrial iron, we monitored the change in fluorescence in response to addition of mNT. RPA is rapidly quenched following addition of mNT, indicating transfer of iron into mitochondria. However, in the presence of DIDS the quenching of RPA was significantly reduced (Figure 3-9B).

Figure 3-10 reconciles all experimental and computational analyses to create a representative model of the complexed mNT and VDAC proteins.

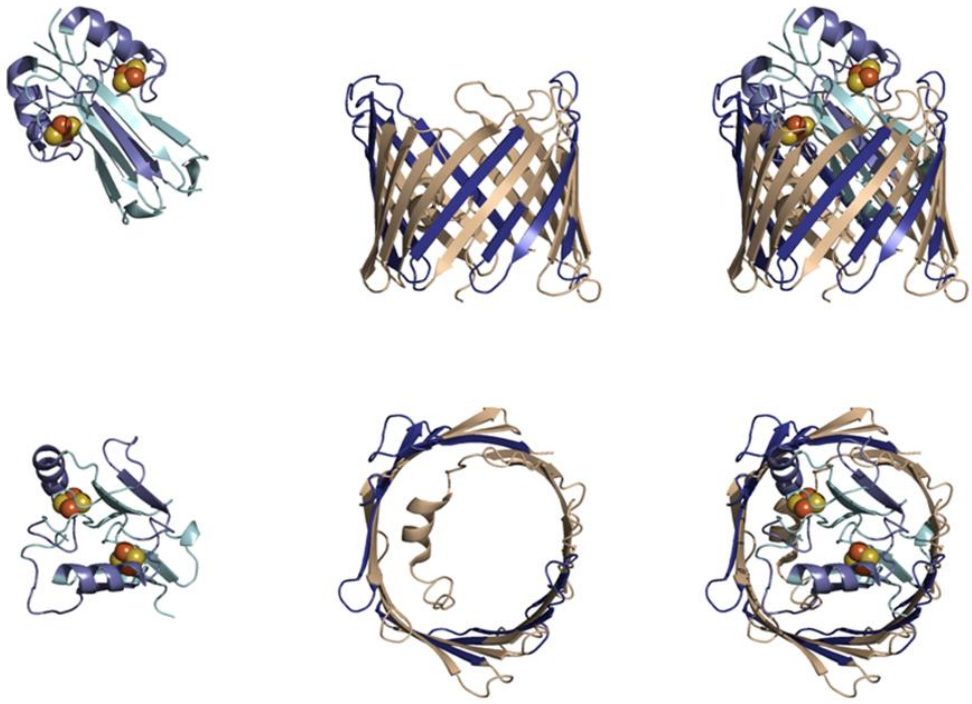

Figure 3-10: Combined Experimental and Computational Model of mNT Docked to VDAC. Data from HDX-MS experiments and Fd-DCA calculations were combined to generate the best model for the docking of the mNT dimer inside the VDAC pore. Increased protection mapping is indicated by darker blues, minimal protection by light blues, and no protection in tan. VDAC PDB ID: 5XDO; MNT PDB ID: 2QH7.

VDAC transports metabolites, such as ATP, ADP, pyruvate and fatty acids, across the OMM between the cytosol and intermembrane space. One effect of VDAC closure is inhibited fatty acid metabolism in the mitochondria, leading to lipid accumulation in the cytosol. Fatty liver disease (liver steatosis) and chronic ethanol exposure are associated with insulin resistance [113, 114]. Insulin resistance and alcohol metabolism are also associated with oxidative stress [115, 116]. A recent study demonstrated that the genetic knockout of mNT prevented liver steatosis in ethanol fed mice [117]. Moreover, exposure to ethanol induces a decrease in mitochondrial function via VDAC closure

[118]. This effect results in a reduction of mitochondrial ATP production, as well as in inhibition of fatty acid oxidation [118]. We have shown with perturbation studies that soluble mNT added to permeabilized cells could transfer its Fe/[2Fe-2S] cluster directly into the mitochondrion [46, 83]. We now show that addition of the VDAC inhibitor DIDS prevents the mitochondrial Fe/[2Fe-2S] accumulation with the addition of soluble mNT, indicating that the interaction with VDAC provides one conduit for this transfer. Our results suggest that, under oxidative stress that could be induced by different sources, VDAC channels are blocked by binding of oxidized mNT with nanomolar affinity and this binding limits channel conductance by favoring the closed state of the channel. Binding of the type-2 diabetes drug pioglitazone stabilizes the oxidized [2Fe-2S] cluster against release [42] and could inhibit the transfer of iron into the mitochondria [58]. However, it must be stated that pioglitazone binding can cause a bottleneck in cytosol/mitochondrial crosstalk and also inhibit the biologically relevant transfer of iron out of the mitochondria and promote ROS accumulation, as we have shown in cancer cells [54].

Because mNT has a redox-active [2Fe-2S] cluster, is linked to the glutathione system, and protects cardiomyocytes from oxidative-stress mediated apoptosis, it may have a role in cellular redox sensing [42, 58, 119, 120]. This idea is further supported by a number of studies showing that mNT's [2Fe-2S] cluster transfer occurs in the more-labile, oxidized state [39, 58, 121, 122]. Therefore it is perhaps unsurprising that only oxidized mNT binds VDAC, as reduction of the cluster has been shown to induce

conformation changes [121]. However cell death, stress, or defense conditions can change the cellular redox state through ROS byproducts of disrupted oxidative phosphorylation, leading to a reduction of the [2Fe-2S] clusters in mNT [123-126]. Such redox-dependent binding supports a proposal that the [2Fe -2S] clusters of mNT act as an on/off switch accompanied by profound alterations of its protein interactions and cellular function. With the mitochondria being the largest source of superoxide and other ROS in the cell, mNT is in ideal proximity for redox sensing and cytosolic communication due to its strategic location on the OMM facing the cytosol [127-130]. Our results establish an important interaction between mNT and VDAC in the OMM that occurs under oxidative conditions. This interaction is potentially part of a stress response that can result in cell death by ferroptosis and may also be a potential source of mitochondrial iron overload during oxidative stress [26, 76, 114].

Materials and Methods

Expression and purification of human mitoNEET and VDAC.

Human mNT was expressed and purified as described [58]. Recombinant human VDAC with a C-terminal 6xHis tag was expressed as described [131]. Nanodiscs containing VDAC were prepared using the covalently circularized cNW9 scaffold protein and DMPC:DMPG at a 3:1 ratio as described [132].

Microscale thermophoresis (MST).

Purified VDAC was fluorescently labeled using the amine reactive RED-NHS NT-647 dye (NanoTemper) according to the manufacturer's protocol, and was studied both in lipid bicelles as well as covalently circularized nanodiscs (cND) [132]. The DMPC/CHAPSO (3:1) bicelle mixture was added to the fluorescently labeled VDAC (in LDAO micelles) to a concentration of 2% and incubated on ice for 30 minutes. The VDAC-bicelle mixture was diluted to 50 nM in 50 mM phosphate buffer, 100 mM NaCl, 2% bicelles, pH 7.0. VDAC was also assembled in the cNDs as recently described by Nasr *et al*., which incorporates a single VDAC protein in each nanodisc [132]. Nanodiscs containing VDAC were fluorescently labeled in lipid bicelles, in the same manner as described above. MST analysis was performed at 22 °C using a Monolith NT.115 system (NanoTemper) using a constant concentration of labeled VDAC in either bicelles or nanodiscs and a 1:1 serial dilution of mNT in 50 mM sodium phosphate, 100 mM NaCl, pH 7.0. MST analysis of VDAC bicelles with reduced mNT was performed in the same buffer at pH 8.0 with the addition of 20 mM DTT. Replicate MST measurements were collected for all VDAC-bicelle and VDAC-nanodiscs mNT binding studies. Data were normalized and fit to the Hill equation with a Hill coefficient >1 using KaleidaGraph software (Synergy Software, Reading, PA).

Gating Experiments.

VDAC from sheep liver mitochondria was solubilized with LDAO and purified using hydroxyapatite resin as described previously [133]. The purified

VDAC was used for channel reconstitution into a planar lipid bilayer. Sheep liver were chosen as the source for VDAC as sheep VDAC exhibits 99.3% sequence identity with the human protein [134] seen in **Figure 3-11**. VDAC was added to a patch clamp *cis* chamber containing 0.5 M NaCl and 10 mM HEPES, pH 7.4. After one or more channels were inserted into the planar lipid bilayers (PLB), current was recorded by voltage-clamping using a Bilayer Clamp BC-525B amplifier (Warner Instruments, Hamden, CT). Current was measured with respect to the *trans* side of the membrane (ground) in the presence and absence of purified mNT and NAF-1.

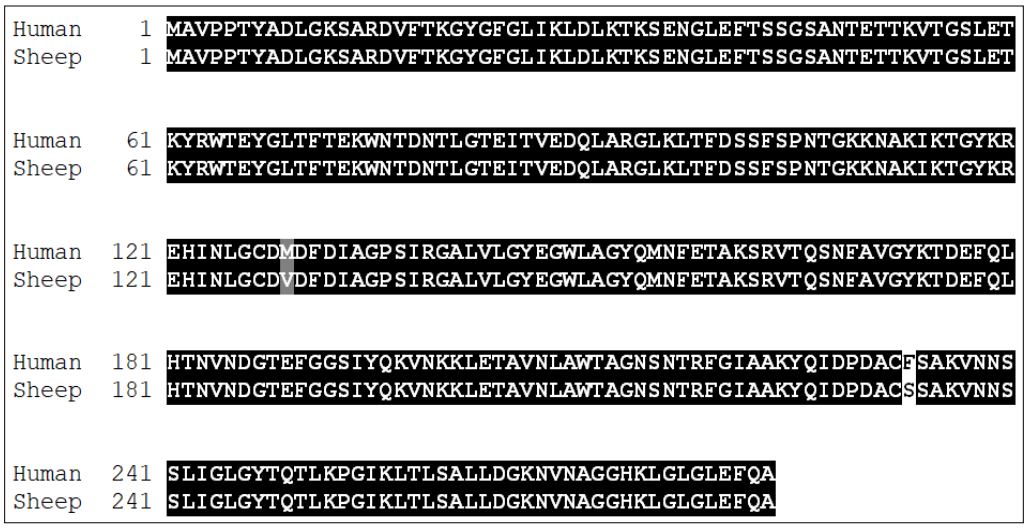

Figure 3-11: **The sequence alignment for human VDAC1 to sheep VDAC1.** There is over 99% sequence identity between human (Accession NP_003365.1) and sheep (Accession NP_001119824.1) with 239 out of 241 residues being the same. Residues varying between the two orthologs are numbers 129 and 174.

The current was digitized on-line using a Digidata 1200 interface board and pCLAMP 6 software (Axon Instruments, Union City, CA).

Cellular studies.

Given the observation that DIDS inhibits the binding of mNT to VDAC *in vitro*, we then determined if inhibiting the interaction would prevent the transfer of iron into the mitochondrion *in situ*. As we previous perturbation studies indicated, the addition of oxidized mNT to gently permeabilized cells results in influx of iron into the mitochondria [58]. Soluble, oxidized mNT was added to gently permeabilized H9C2 cells. Using rhodamine B-[(1,10-phenanthrolin-5-yl)-aminocarbonyl] benzyl ester (RPA) as an indicator of mitochondrial iron, we monitored the change in fluorescence in response to addition of mNT.

Stability analysis.

The potential effect of the lipids and interaction of VDAC on the cluster stability mNT was assessed following the absorption of the [2Fe-2S] clusters over time as described previously [42, 43, 46, 76, 135]. Briefly, 25 μM mNT was incubated in the presence of 25 μM empty nanodiscs (negative control) as well as 25 μM nanodiscs containing VDAC in 50 mM sodium phosphate, 100 mM NaCl, pH 7.0 at 37°C. The absorbance at 458 nm was monitored as a function of time as previously published [39, 60, 76, 122].

Hydrogen deuterium exchange mass spectrometry (HDX-MS).

To elucidate the regions important for the interactions between oxidized mNT and VDAC, we first determined the optimum conditions for final mass spectral analysis of HDX-MS. In an effort to get the maximum coverage of both proteins, we explored a range of denaturant conditions, proteases, and

pHs for final analysis as described [71, 136-141]. Our HDX experiments were carried out in 10 mM sodium phosphate, 100 mM NaCl, pH 7.0 with a final D_2O concentration of 90%. The hydrogen-deuterium exchange reaction was quenched at 4 °C with a final concentration of 500 mM guanidine-HCl, 0.5% formic acid and 10% glycerol in D_2O and flash frozen. Samples were stored at -80 °C until analyzed. Instrument setup and operation were described previously [142]. Both porcine pepsin and fungal protease XIII were used to enhance peptide coverage. Peptides were identified using Sequest software (Thermo Finnigan). Each peptide was evaluated at every time point for quality control. Deuterium content for each time point was calculated using DXMS Explorer (Sierra Analytics).

Computational methodology.

Our protein-protein binding site identification method, Fd-DCA (Fragment docking-Direct Coupling Analysis), was used to predict the highest probability mNT-VDAC binding sites from coevolving residues [143]. These residue-residue couplings were taken as constraints for modeling the initial energetically favorable binding complex of mNT-VDAC [71]. I-TASSER was used to model the N-terminal transmembrane domain (residues 14-31) of mNT as an α-helix, since it was not available in the crystal structure [144]. Then the modeled molecular structure of mNT was visually examined to identify potential candidate surface binding sites for protein-protein interaction. As a result, three sites were obtained, as shown in **Figure 3-12**. The largest binding

site, designated as Site 1, covers the 2Fe-2S cluster region. Site 2 is adjacent to the membrane domain, and Site 3 is relatively small and located in the *β*-cap domain, under Site 1. To discriminate which binding site of mNT interacts with VDAC, direct-coupling analysis (DCA) was performed between mNT and VDAC. The sequences of mNT were collected from UniProt [88, 145]. The sequence alignment of VDAC was obtained from Jackhmmer [146] by using the fast sequence of the PDB entry (5XDO) of VDAC as the template. To join these two sequence alignments, we followed the same rules presented in our previous work [143]. The predicted top 20 coevolving residue pairs between the two proteins are listed in **Table 3-1**.

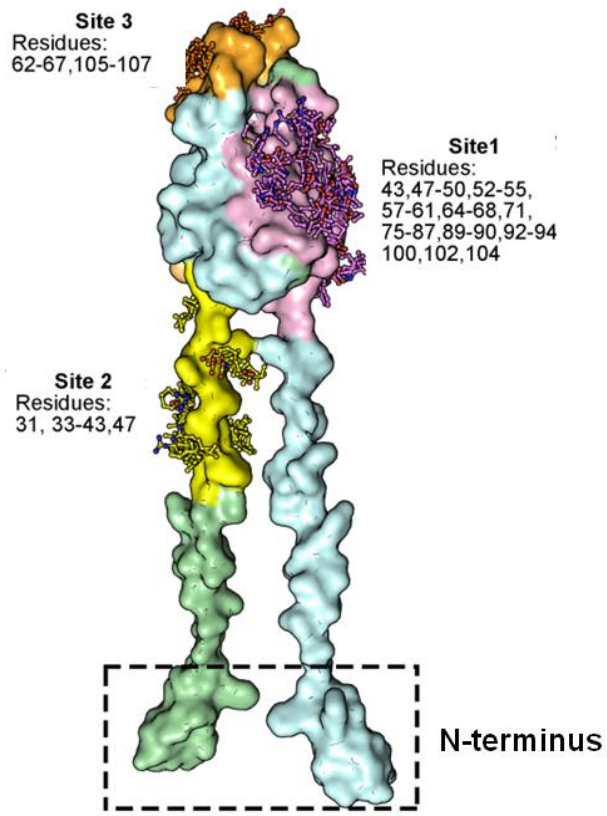

Figure 3-12: Candidate binding sites for VDAC interaction are identified for mNT. The stick-ball models represent the energetically favorable bound fragment-molecular probes, the corresponding surface highlighted with the similar color of probes are identified candidate binding sites.

Interestingly, a part of these coevolving signals are across the soluble domain of mNT and VDAC, and the other part is from the membrane domain of mNT and VDAC. Meanwhile, as shown in Supplemental Table 1 and Supplemental Figure 3, these predicted coevolving residues of mNT are largely overlapped with the residues on identified Site 1 and Site 2. This indicated that VDAC could interact with both binding sites of mNT. Taken these top 20 coevolving residue pairs as the constraints, we docked mNT into VDAC to create a

binding complex and used a Steepest Descent (SD) energy minimization from Gromacs v5.0.5MD to optimize a final, complex structure, shown in **Figure 3-13**.

Table 3-1: Top 20 DI-ranked pairs computed with DCA for interaction between mNT and VDAC.

Residue in mNT	Residue in VDAC	DI	Rank	Residue in mNT	Residue in VDAC	DI	Rank
9	55	1.0067	1	9	144	0.757	11
36	55	0.9503	2	2	55	0.756	12
3	55	0.9102	3	48	55	0.752	13
15	201	0.8463	4	6	8	0.741	14
36	144	0.845	5	43	55	0.715	15
26	55	0.8438	6	5	263	0.713	16
44	144	0.8051	7	4	8	0.707	17
92	270	0.7846	8	67	240	0.696	18
39	55	0.7579	9	108	65	0.688	19
33	55	0.7578	10	19	93	0.684	20

DCA, direct coupling analysis; DI, direct information.

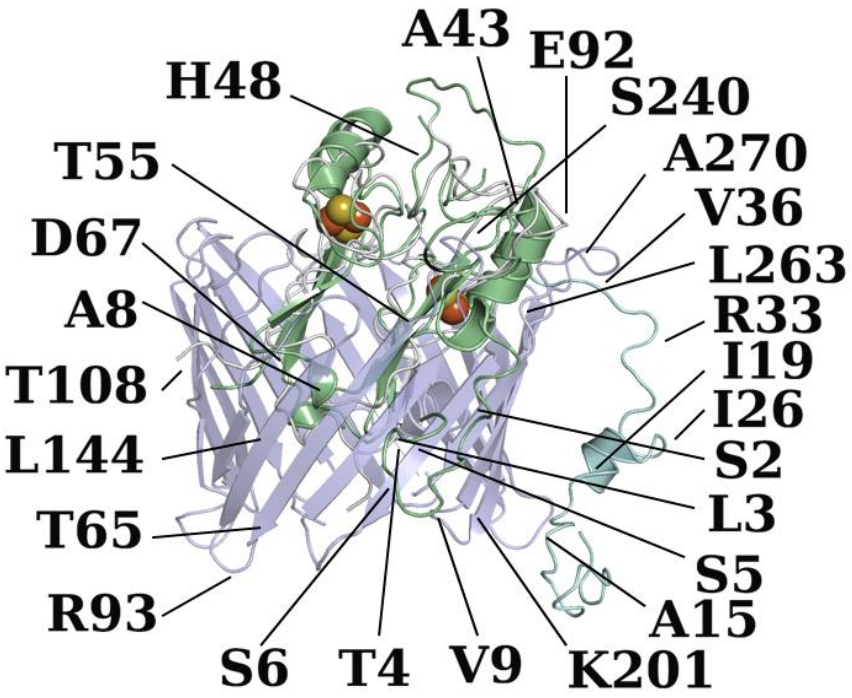

Figure 3-13: Model of mNT Docked to VDAC. The orientation of mNT within the VDAC pore was determined using Fd-DCA. Individual mNT monomers colored blue and green, with calculated direct-interacting residues from *Supplemental Table 1* labeled.

Acknowledgements

Chapter 3 is a reprint as it appears in “Stemming the Flow: MitoNEET Redox-Selectively Controls VDAC Gating” by Jason T Stofleth, Lipper CH, Bai F, Sohn YS, Roy S, Mittler R, Nechushtai R, Onuchic JN, Jennings PA, which has been submitted to the *Proceedings of the National Academy of Sciences* for publication. The dissertation author was a secondary investigator and the primary author of this paper.

Chapter 4

New Connections in Iron-Sulfur Cluster Transport: Glutaredoxin-3 [2Fe-2S] Cluster Transfer is MitoNEET-Specific

Introduction

All organisms from bacteria to mammals utilize iron-sulfur (Fe-S) clusters as cofactors due to their wide range of chemical reactivity and redox characteristics. These iron-sulfur clusters, having varied Fe:S stoichiometry [147] shown in **Figure 4-1**, carry out a diverse array of roles throughout the cell, such as electrical conduits in the photosynthetic and respiration energy transduction pathways, critical catalysts of nitrogen fixation, cellular disulfide redox control, regulate gene expression, catalyze DNA replication and repair, regulate enzymes, control cell cycle, serve as sulfur donors, are part of the oxidative stress response, and act as a cellular iron reserve [147, 148].

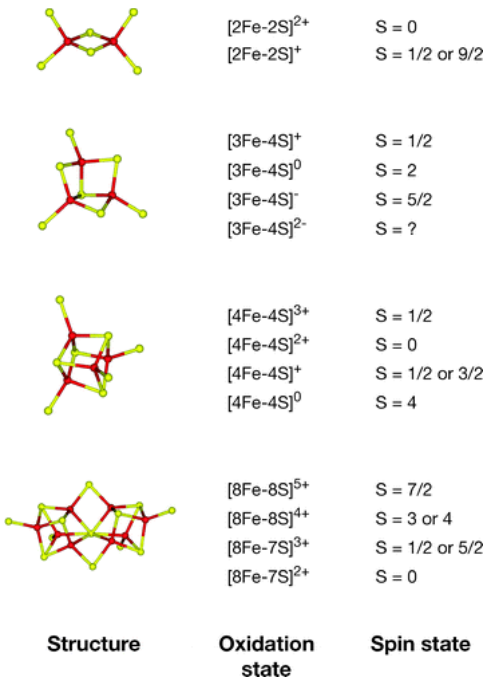

Figure 4-1: Examples of various iron-sulfur cluster stoichiometry found in biological molecules. Biological systems contain [2Fe-2S] clusters, as those discussed in this work, but also utilize higher-order assemblies [147].

Iron is tightly controlled and regulated within the cell to prevent reactive oxygen species (ROS) resulting from peroxides generated by free-iron Fenton chemistry [149-152]. Synthesis of iron-sulfur clusters is therefore a highly regulated, multistep process that requires coordination of a core complex of chaperones, scaffold proteins, electron transfer proteins, cysteine desulferases, ATPases, and nucleotide exchange factors [153].

In mammals the formation of iron-sulfur clusters involves two separate but linked assembly systems. The first is the iron-sulfur cluster assembly pathway (ISC), which occurs in the mitochondrion, and the second is the cytosolic iron-sulfur cluster assembly pathway (CIA) [154-156]. The CIA system is directly responsible for the maturation of both cytosolic and nuclear iron-sulfur proteins, but relies on the ISC as a source of [2Fe-2S] clusters [156-159]. Recent work has demonstrated the existence of multiple, specific iron-sulfur cluster transfer proteins that link the ISC to the CIA through protein to protein transfer of [2Fe-2S] clusters [63, 74, 160].

How the cell takes advantage of free iron or when iron cannot be properly controlled is the essential for many disease states (Table 1-1), and is currently a significant focus of fundamental research as well as new drug development [34]. These small molecule compounds (Table 1-2) can target the intracellular components of pathogens and parasites and add an opportunity for target specificity [161, 162]. In addition, there are numerous drugs that target important proteins within the iron-sulfur assembly pathways, such as pioglitazone, cluvenones, or Mad28 drugs targeting the NEET

proteins. These are able to directly target iron-sulfur clusters of specific proteins in the cell [34]. The NEET proteins have also been studied recently as specific targets for Mad28 in order to combat some types of cancer [76].

At the interface of the ISC and CIA systems is the recently identified class of [2Fe-2S] NEET proteins. MitoNEET (mNT, CISD1), nutrient-deprivation autophagy factor 1 (NAF-1, Miner-1 CISD2), and MiNT (Miner2, CISD3) are localized to the outer mitochondrial membrane, the mitochondrial associating membranes of the ER, and the inner mitochondrion respectively [39]. Each protein contains two [2Fe-2S] clusters with a unique 3Cys-1His coordination site, bestowing these iron-sulfur clusters with specific redox characteristics and pH-sensitive stability; this has been studied in-depth in recent years [40, 42, 56, 106, 122, 163, 164]. The transient properties of the NEET protein 3Cys-1His coordination site make it an ideal candidate for the type of [2Fe-2S] transfer promiscuity that is needed in iron-sulfur regulation, and while it is the first 2Fe-2S protein to have this coordination, it is not surprising that this coordination chemistry has been found in other iron-sulfur cluster transfer proteins [55].

The [2Fe-2S] CDGSH binding motif is conserved across all kingdoms of life, suggesting ancient origins [46, 47, 88]. Both mNT and NAF-1 had been shown to be [2Fe-2S] cluster donor proteins to ferredoxin [58] and anamorsin (Ciapin 1) [63], the critical component of early-CIA machinery [165-167]. Additionally, the anamorsin and NADPH-dependent oxidoreductase 1 (NDOR1) complex can reduce mNT to initiate many critical iron-sulfur repair

functions [64]. This recent advance established a significant link for [2Fe-2S] trafficking and distress communication between the ISC and CIA pathways that involved mNT.

Due to our recent findings that mNT and NAF-1 can donate [2Fe-2S] clusters to anamorsin, which established the NEET proteins role in iron transfer and regulation, we wanted to further investigate links between other CIA and ISC machinery [63]. Since there are a very limited number of unanchored cytosolic [2Fe-2S] proteins, and mNT and NAF-1 are membrane-anchored cytosol-facing proteins, we reasoned that there were unexplored relationships between these few cytosolic [2Fe-2S] proteins and the NEET proteins [158]. In fact the only three cytosolic [2Fe-2S] proteins are aldehyde oxidase 1 (AOX1), xanthine dehydrogenase (XDH), and glutaredoxin-3 (GRX3, *GLRX3*, PICOT). Most significant is that prior to this work there have been no identified, physiologically relevant [2Fe-2S] cluster donor proteins or cellular machinery from which mNT and NAF-1 acquire their [2Fe-2S] clusters. GRX3, being one of very few cytosolic [2Fe-2S] proteins, is linked to the CIA pathway, and is an established intermediate iron-sulfur carrier for cellular iron-sulfur cluster biogenesis; so we reasoned that it was a potential donor or acceptor of iron-sulfur clusters from mNT and NAF-1 [74, 79, 168].

Each Grx3 monomeric subunit contains an inactive N-terminal thioredoxin domain (Trx) that appears to be primarily responsible for mediating protein-protein interactions and is necessary for [2Fe-2S] cluster transfer. The Trx domain is followed by two separate C-terminal glutaredoxin (Grx) [2Fe-2S]

cluster-coordinating domains termed GrxA and GrxB [74], seen in **Figure 4-2**. Holo-GRX3 contains six subunits, composed of two 335 amino acid monomers and four glutathione ligands. GRX3 is a monothiol glutaredoxin, in which each monomer contributes a single bridging cysteine residue to coordinate the [2Fe-2S] cluster, and the central cysteine of a GSH serves to provide an additional thiol-ligand each, giving it a stoichiometry of 2Grx3 : 4GSH : 2[2Fe-2S]; visualized in **Figure 4-3** [73].

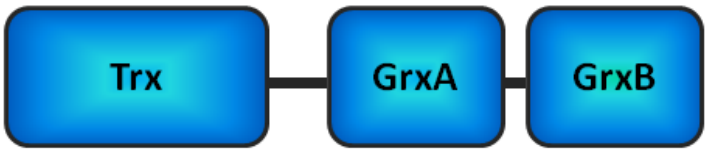

Figure 4-2: The domain organization of the Grx3 monomer. In order from N-terminus to C-terminus, GRX3 contains one thioredoxin-like domain (Trx), followed by two Grx domains (GrxA and GrxB). Each Grx domain is responsible for contributing a single cysteine ligand (monothiol) to each [2Fe-2S] cluster.

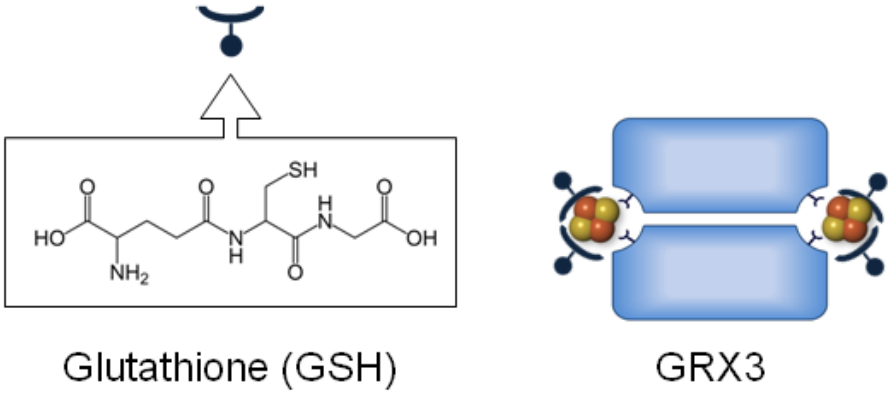

Figure 4-3: GRX3 Subunit Stoichiometry. (Left) The glutathione (GSH) structure consist of glutamate-cysteine-glycine amino acids and its cartoon representation. **(Right)** Holo-GRX3 is composed of two 37 kDa Grx3 monomers that each contributes a single cysteine ligand to each [2Fe-2S] cluster, distinguishing it as a monothiol glutaredoxin. Two additional GSH subunits each also contribute a single cysteine, giving each [2Fe-2S] cluster a 4Cys-coordination chemistry, and an overall holo-GRX3 subunit stoichiometry of 2Grx3 : 4GSH : 2[2Fe-2S].

In addition, GRX3 can exist as a heterodimeric bridged complexes in which a monothiol iron-sulfur ligating BOLA2 monomer replaces one Grx3 subunit to carry out modified iron-sulfur transport activities within the cell [160, 169, 170].

One component of the inner mitochondrion to cytoplasm iron-sulfur relay is through the ATP-binding cassette sub-family B member 7 ($ABCB_7$) active transporter which spans and actively transports from the matrix through the inner mitochondrial membrane. GSH-coordinated [2Fe-2S] clusters as well as GSH-trisulfides are demonstrated substrates, with GSH having a inner-mitochondrial binding site within the inner cavity of $ABCB_7$ (paralogs are Atm1 in yeast, ATM3 in arabadopsis) [171-174]. While the phenomenon of [2Fe-2S] transport from the intermembrane space to the cytosol is not yet fully

elucidated, the role of GRX3 at this interface is a hot topic of current investigation [175].

GSH also plays an essential role in many other steps of cellular iron metabolism as well as cytosolic thiol-redox control, further suggesting a significant role in iron metabolism and iron-sulfur cluster transport for GRX3 [176-178]. GSH recycling is critical as cells must maintain their levels of free GSH pools. Free GSH acts as an important redox regulator by cysteine/disulfide exchange with an $E_{m,7}$ of -240 mV (-220 to -240 mV range based on data) and serves to neutralize ROS [179-182]. Besides having a redox role, GSH can act as a sulfur source in the cell in its free form in both the mitochondrion and the cytosol [183], and low levels are associated with mitochondrial DNA damage and cell-death [179, 184, 185]. The GSH role of greatest interest for this study is that GSH can act as a ligand for a variety of metals [186], but most importantly it can carry [2Fe-2S] clusters with a [2Fe-2S](GS)$_4$ coordination stoichiometry [187-189] and has an established role in iron-sulfur cluster transport and assembly into proteins in both the mitochondrion and cytosol [188, 190, 191]. It is with these [2Fe-2S](GS)$_4$ clusters that an inner mitochondrial membrane active transporter, ABCB$_7$, is able to export [2Fe-2S] from the mitochondrial matrix to the intermembrane space [171, 192]. When ABCB$_7$ expression is disrupted in various species, ROS-mediated cell death and mitochondrial iron-accumulation occur [193-195]

While the phenomenon of [2Fe-2S] transport from the intermembrane space to the cytosol is not yet fully elucidated, the role of GRX3 at this

interface is currently expanding [175]. It has been recently demonstrated that GRX3 can transfer [2Fe-2S] clusters to anamorsin, establishing a cytosolic link between the ISC and CIA. Taken together with the ability of mNT and NAF-1 to also transfer their clusters and for GRX3-BolA heterodimers to do so [170], anamorsin appears to have at least four potential [2Fe-2S] cluster donors.

In order to investigate whether [2Fe-2S] cluster transfer could occur between NEET proteins and GRX3, we expressed and purified full-length human GRX3 and the soluble domains of human mNT and NAF-1. Using a well-established protocol to measure iron-sulfur cluster transfer between donor holo-proteins and [2Fe-2S] cluster apo-acceptor proteins, we examined the unique visible absorption spectrum due to the iron-sulfur and associated ligands at 410 nm for GRX3 and 458 nm for mNT and NAF-1 [58, 60, 74, 160]. We also wanted to explore any variations in between mNT and NAF-1, since the two are structurally similar paralogs with 68.7% sequence identity and are qualitatively similar in overall structure. NAF-1 and mNT having distinctly different roles in the cell are supported by the following: The varied stability half-life of [2Fe-2S] clusters at low pH, variations in ferredoxin and anamorsin transfer rates, unequal drug binding affinities, different levels of upregulation in cancers, different cellular localization, and that mNT can transfer [2Fe-2S] to NAF-1 unidirectionally [26, 46, 66, 67, 196].

We identified that holo-GRX3 transfers [2Fe-2S] clusters to apo-mNT, yet there is no detectable transfer [2Fe-2S] clusters from holo-GRX-3 to apo-NAF-1. This work identifies the first identified [2Fe-2S] cluster donor to mNT,

and suggests that despite many similarities between mNT and NAF-1, there is a divergence in their roles at the crossroads of the ISC and CIA pathways.

Results

GRX3 transfers [2Fe-2S] clusters to apo-mitoNEET

GRX3, mNT, and NAF-1 contain two [2Fe-2S] cluster binding sites in which coordinating residues are contributed equally from each dimer. The monothiol GRX3 ligates each [2Fe-2S] cluster using a 4-Cys coordination site, with a single cysteine contribution from each glutaredoxin monomer and a single cysteine from two additional glutathione subunits per cluster. As a result the holo-protein has a characteristic visible absorption spectrum with a 410 nm absorption peak, seen in **Figure 4-4**. Conversely, NAF-1 and mNT have a 3-Cys:1-His cluster coordination site, yielding a visible absorption peak at 458 nm (Figure 4-3B). The non-overlapping peaks make it possible to measure the presence of [2Fe-2S] clusters with each protein's specific ligand in solution, and to monitor the transfer of [2Fe-2S] clusters between the two different ligand environments as described previously [56, 58, 63, 76, 82].

Therefore, we expected a peak shift from 410 nm (Figure 4-5A) to 458 nm (Figure 4-5B) if GRX3 transfers clusters to either NEET protein, or from 458 nm (Figure 4-5B) to 410 nm (Figure 4-5A) if NEET proteins transfer to GRX3.

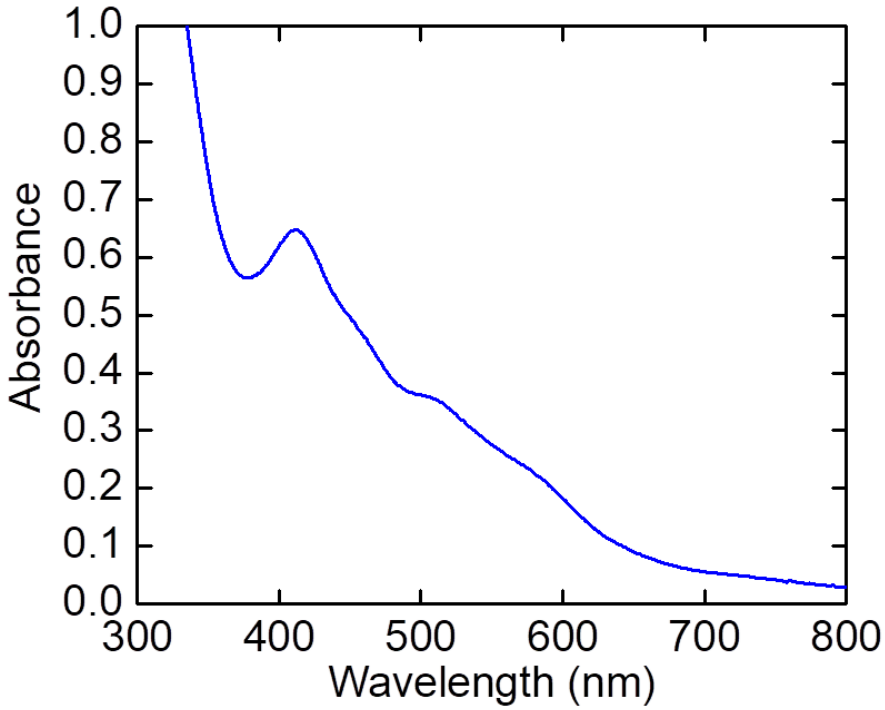

Figure 4-4: Characteristic GRX3 UV-Visible Absorption Spectrum. Holo-GRX3 has a 410 nm absorption peak that is characteristic to the unique 4-Cys ligand environment of the [2Fe-2S] clusters.

The distinct non-overlap is clearly viewed in **Figure 4-5C**. This approach is an established technique and has been demonstrated for mNT and NAF-1 [2Fe-2S] cluster transfer to apo-ferredoxin [58], as well as mNT and NAF-1 [2Fe-2S] cluster transfer to apo-anamorsin (Dre2 in yeast), the early component of CIA machinery [63, 167, 197].

In order to examine whether mNT or NAF-1 could accept clusters from GRX3, we purified and created the apo-form of both proteins using low pH to facilitate cluster loss, as previously described [43, 76, 77]. GRX3 readily forms the monomeric apo-protein in the presence of oxygen and is purified away

from any remaining dimer using size-exclusion chromatography. Anaerobically reconstituted GRX3 was combined with either apo-NAF-1 or apo-mNT, and UV-visible spectra were recorded before, shown in **Figure 4-6** and **Figure 4-7**, respectively. Alternatively, apo-GRX3 was combined with holo-NAF-1 or holo-mNT to assess the alternative transfer direction (data not shown).

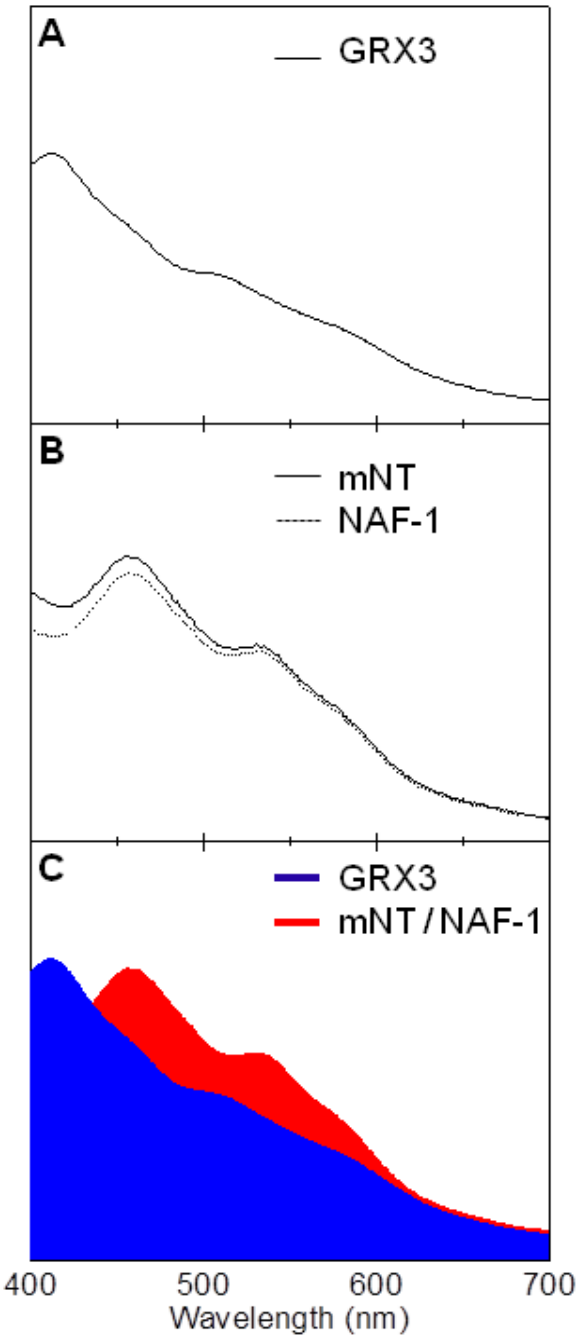

Figure 4-5: Observable visible range absorption peak differences between NEET proteins and GRX3. GRX3 peak at 410 nm **(A)**, NEET protein peak at 458 nm **(B)**. A directional [2Fe-2S] cluster transfer will yield a distinct, non-overlapping absorbance peak shift as the [2Fe-2S] clusters are lost from one holo-protein and gained by the other apo-protein **(C)**.

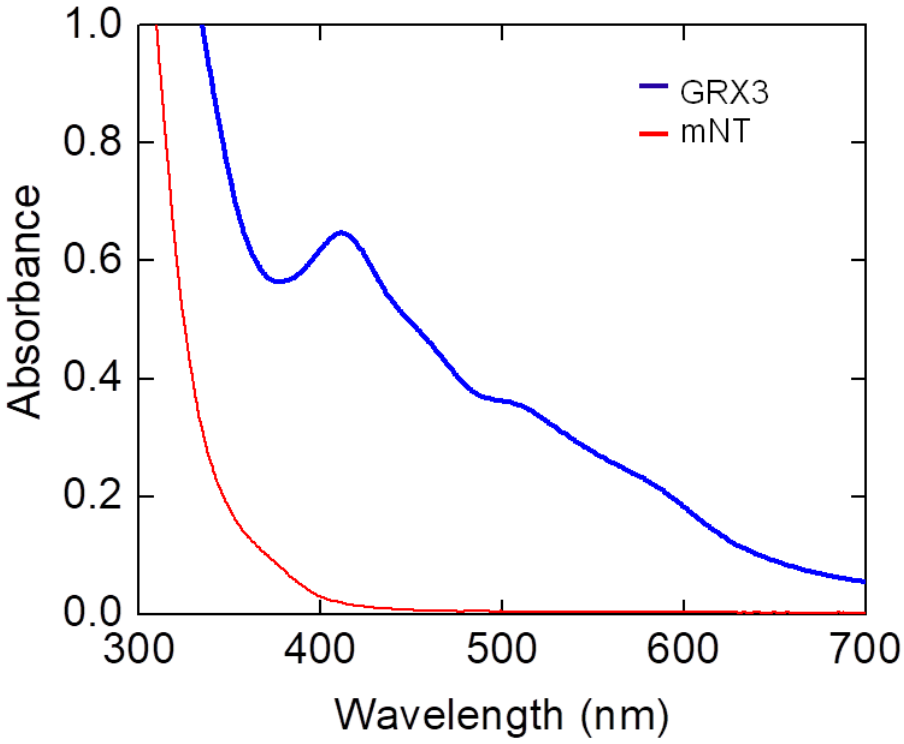

Figure 4-6: Pre-transfer assay holo-GRX3 and apo-mNT spectra. Prior to mixing the holo-GRX3 with apo-mNT, the individual UV-visible spectra were taken as a reference for the starting absorption and to ensure that apo-NAF-1 had no significant absorbance at 458 nm due to complete [2Fe-2S] cluster loss.

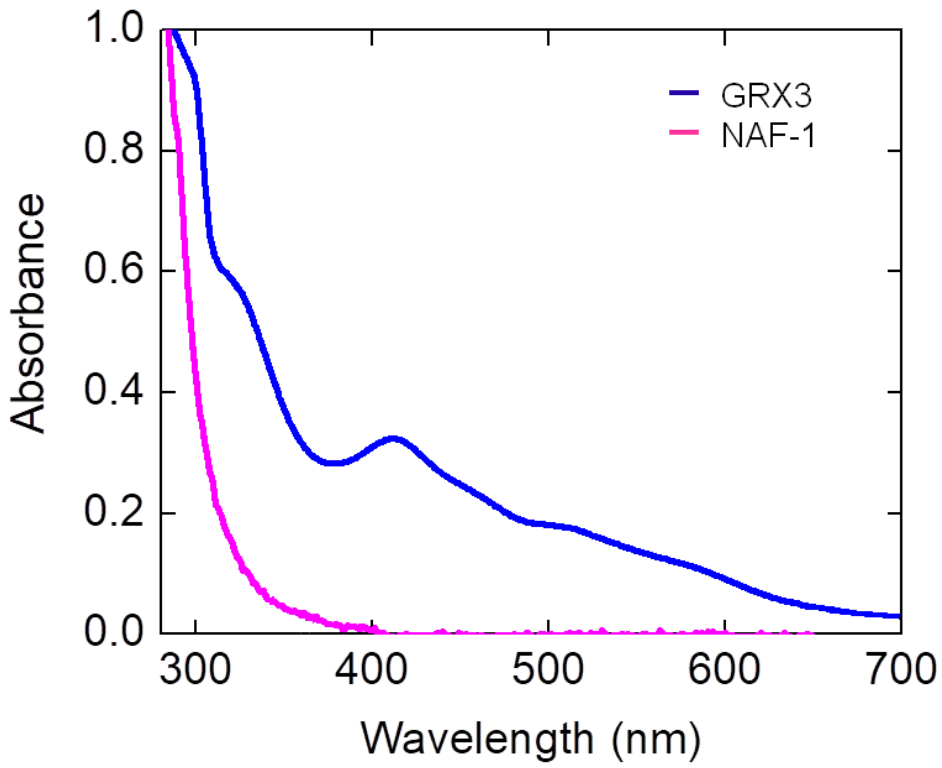

Figure 4-7: Pre-transfer assay holo-GRX3 and apo-NAF-1 spectra. Prior to mixing the holo-GRX3 with apo-NAF-1, the individual UV-visible spectra were taken as a reference for the starting absorption and to ensure that apo-NAF-1 had no significant absorbance at 458 nm due to complete [2Fe-2S] cluster loss.

We observed that GRX3 is able to transfer [2Fe-2S] clusters to mNT, as a recovery of the characteristic mNT spectrum 458 nm peak from the non-absorptive apo-mNT was observed in conjunction with the depletion of any peak at 410 nm. The spectral overlay for chemically reconstituted GRX3 (pre-transfer) and the recovered mNT plus apo-GRX3 (post-transfer) is shown in **Figure 4-8**, validating our expectations for a 410 nm to 458 nm peak shift, previously described in **Figure 4-3**. **Figure 4-8** summarizes the spectral shift through the course of the reaction, and **Figure 4-9** demonstrates the recovery

and reforming of dimeric holo-mNT with two [2Fe-2S] clusters from monomeric apo-mNT through the course of the reaction.

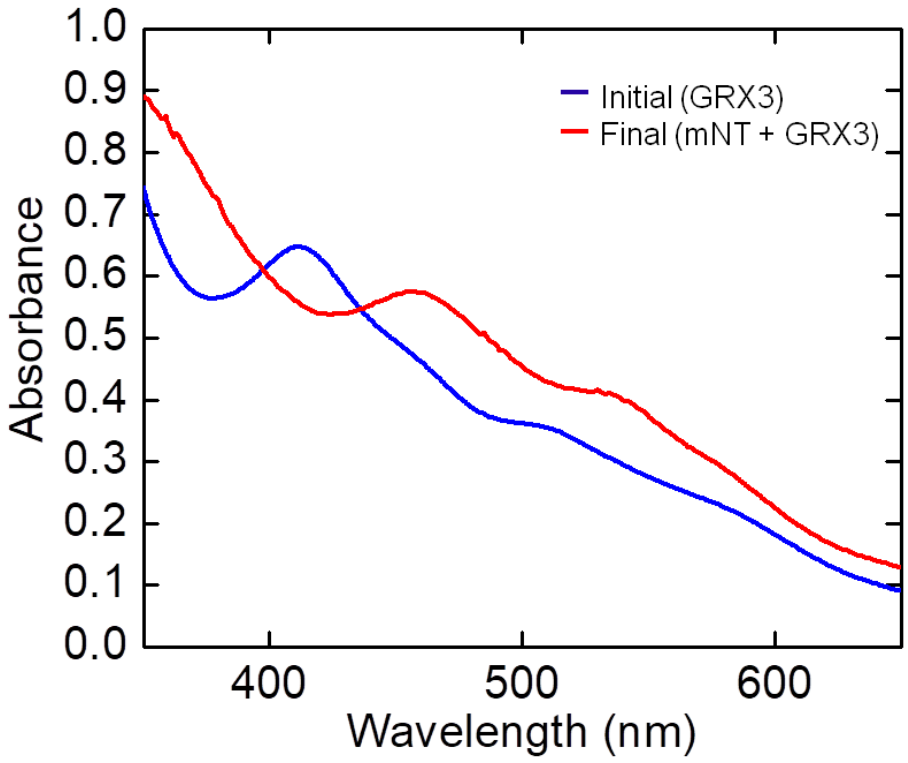

Figure 4-8: Initial and final spectra of GRX3 to mNT [2Fe-2S] cluster transfer. The pre-assay visible-range spectrum with of GRX3 (blue) with a peak at 410 nm, and the post-assay combined spectrum of mNT + apo-GRX3 (red) with a peak at 458 nm (red).

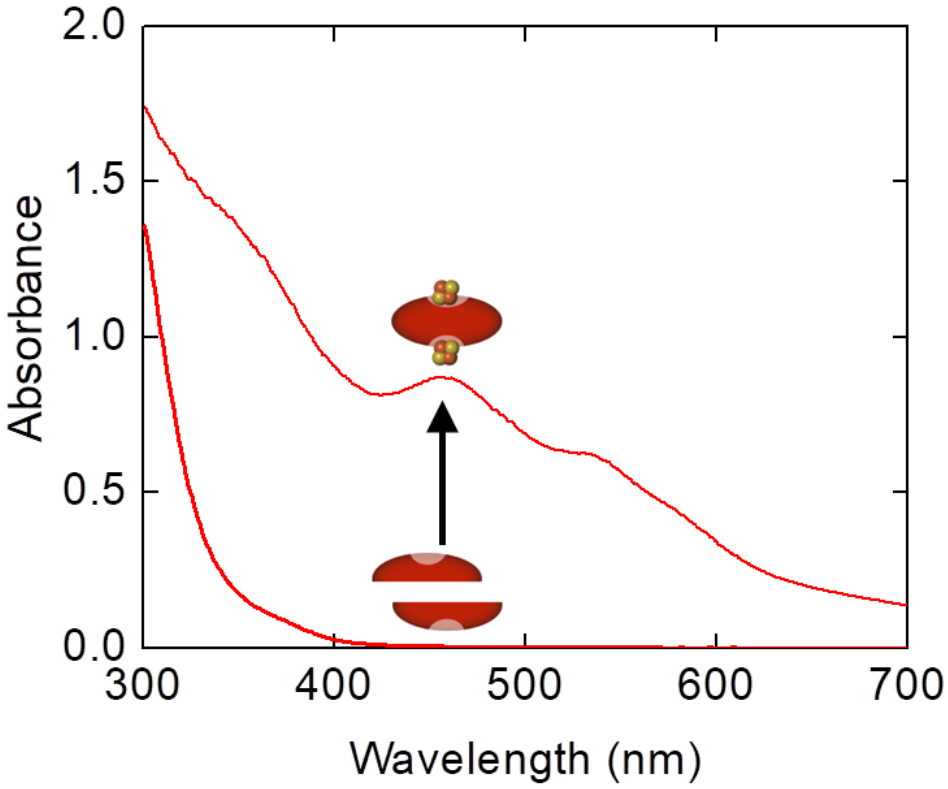

Figure 4-9: [2Fe-2S] cluster transfer from GRX3 allows mNT to recover the 458 nm absorbance peak. Monomeric apo-mNT has no peak at 458 nm, but the transfer of two [2Fe-2S] clusters from holo-GRX3 allows it to both reconstitute and reform a dimer. Only dimeric holo-mNT exhibits the characteristic 458 nm absorption peak.

GRX3 does not transfer [2Fe-2S] clusters to apo-NAF-1

In an identical set of experiments with apo-NAF-1 and reconstituted holo-GRX3 (data not shown), we did not observe a similar transfer of [2Fe-2S] clusters, as no 458 nm peak developed despite the ability of the apo-NAF-1 to be chemically reconstituted in parallel to the GRX3 transfer (Figure 4-10).

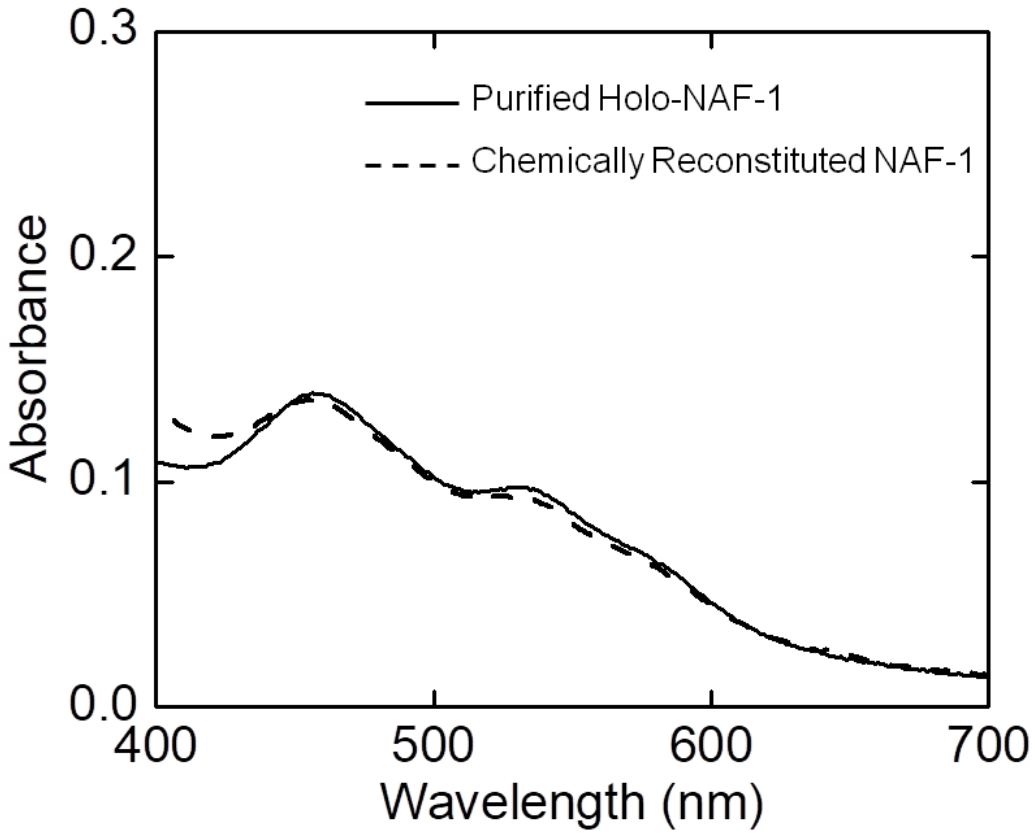

Figure 4-10: Holo-NAF-1 Purified and Chemical Reconstitution Spectral Overlay. To ensure that holo-NAF-1 was able to be recovered from the apo-form of the protein, a chemical reconstitution was run in parallel to all transfer assays. Here, the visible-range spectrum for purified holo-NAF-1 is shown overlaid with the spectrum for the chemically reconstituted holo-NAF-1. Using previously created apo-NAF-1, chemical reconstitution was performed anaerobically under argon gas at room temperature, using a buffer containing 50 mM Tris (pH 8.0), 100 mM NaCl, 3 mM DTT, with $FeCl_3$ and Na_2S added stepwise to a final concentration of 500 µM. Since the reaction is diffusion-based, the mixture was incubated for 12-18 hrs anaerobically, followed by buffer exchange to remove excess iron and sulfide ions.

To confirm that the visible spectrum of mNT that was recovered as a result of the transfer matched that of purified mNT, we overlaid holo-mNT spectra from purification, chemical reconstitution, and transfer (Figure 4-11).

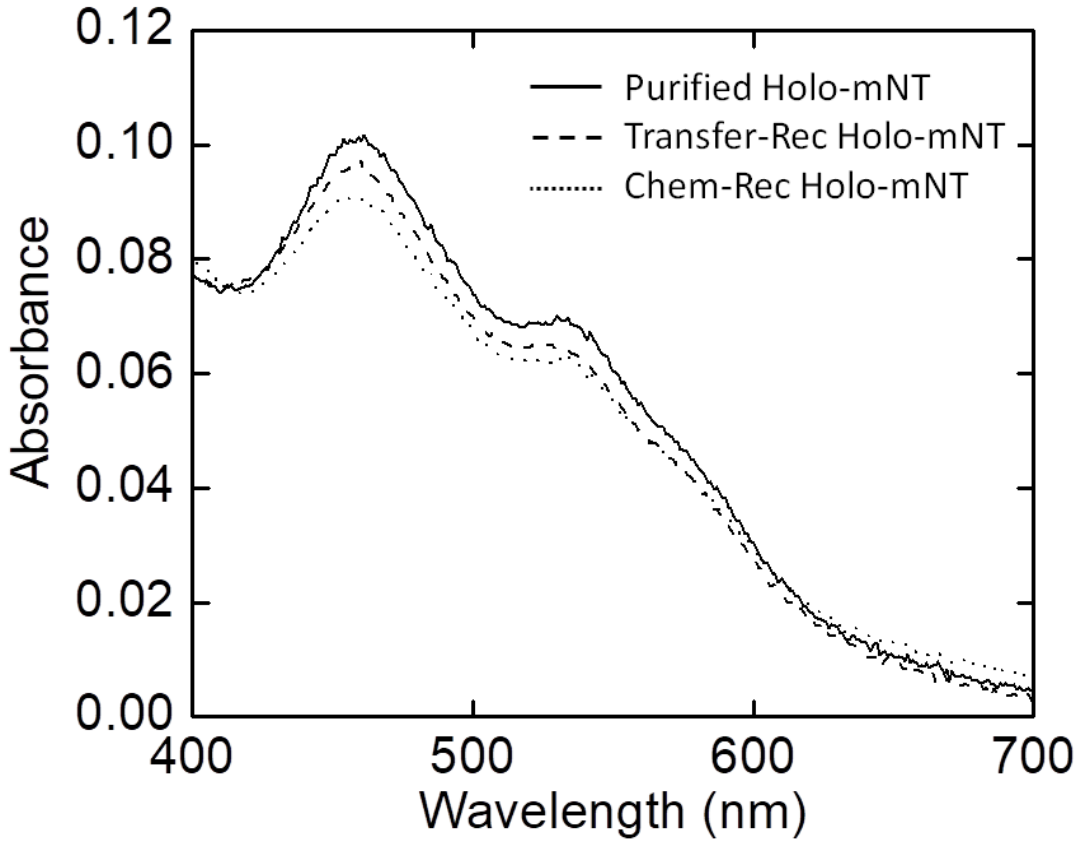

Figure 4-11: Holo-mNT Visible-Range Spectrum Overlays. To show that all forms of holo-mNT used in these experiments had the same characteristic absorption spectrum, GRX3-transfer-recovered (Transfer-Rec) and chemically reconstituted (Chem-Rec) spectra were compared to the purified holo-mNT spectrum as a reference. The sample dilutions were varied slightly in order to visibly distinguish between each spectrum.

Discussion

With these finding we demonstrate that holo-GRX3 is able to donate two [2Fe-2S] clusters to reform dimeric holo-mNT from monomeric apo-mNT. The ratio of absorbance at 280 nm to 458 nm (~2.3 : 1) shows that there is one [2Fe-2S] cluster per monomer, based on the molar extinction coefficient of the peptide monomer at 280 nm and the extinction coefficient of the individual 3Cys-1His coordinated [2Fe-2S] [121]. This effect is represented in **Figure 4-9**, showing the non-absorptive monomer versus the absorptive dimer of mNT.

This process is not simply diffusion-driven due to a few key reasons: the relatively fast time to transfer completion, the uni-directionality of cluster transfer, and the high yield of recovered mNT dimer. The transfer time took only minutes, such that sample extraction from the anaerobic glove box to take spectral measurements was slower than the rate of completion (no additional recover at 458 nm over time). Secondly, the loss of the 410 nm absorption peak from GRX3 was complete after transfer at near stoichiometric amounts of the two proteins, demonstrated in **Figure 4-12**. GRX3 is fairly stable in anaerobic conditions, so long as there is an excess of GSH in the buffer. Chemically reconstituted GRX3 would retain the same relative intensity of its characteristic brown color for over a week at room temperature in the anaerobic glove box, so it is not likely that the rapid reconstitution of holo-mNT is due to instability of holo-GRX3 releasing free iron and sulfides in to solution.

Conversely, holo-mNT does not transfer [2Fe-2S] clusters to apo-GRX3, meaning there was definitive transfer directionality at neutral pH. Lastly, chemical reconstitution of both mNT and NAF-1, in comparison to GRX3-mNT transfer assays, yield holo-proteins indicating that the NAF-1 construct was functional and could recover a [2Fe-2S] cluster; however GRX3 is not a partner protein.

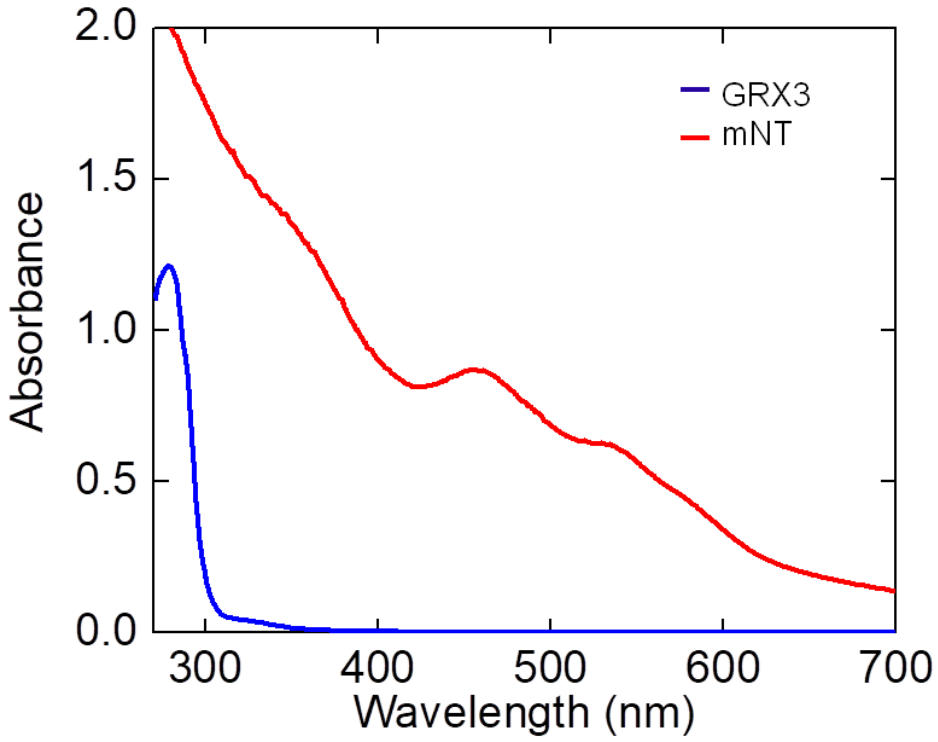

Figure 4-12: GRX3 loses the 410 nm peak and mNT regains the 458 nm peak from the transfer assay. GRX3 cluster loss during the transfer assay is complete, while mNT regains its 458 nm peak from the holo-form of the protein. The proteins are shown in nearly equimolar amounts. The ε_{280} of GRX is 3.4 $mM^{-1}cm^{-1}$, and the ε_{280} of mNT is 8.6 $mM^{-1}cm^{-1}$.

Prior to these findings, the steps that linked [2Fe-2S] cluster transfer between the ISC and CIA were best described by **Figure 4-13**, a modified

version from [63] which shows the identified steps of [2Fe-2S] cluster transfer as black arrows, and red arrows represent necessary, but yet uncharacterized steps. Iron-sulfur clusters are assembled by the mitochondrial ISC system, but the means by which they are exported in a controlled fashion to cytosolic iron-sulfur proteins, such as mNT and GRX3 is unclear. While it was newly discovered that mNT is a transfer source of [2Fe-2S] clusters for NAF-1 [67], the donor source of mNT [2Fe-2S] clusters was undiscovered. Our lab had identified that both mNT and NAF-1 can donate iron-sulfur to anamorsin [63], while other work concurrently demonstrated that GRX3 can also supply iron-sulfur clusters to anamorsin [74].

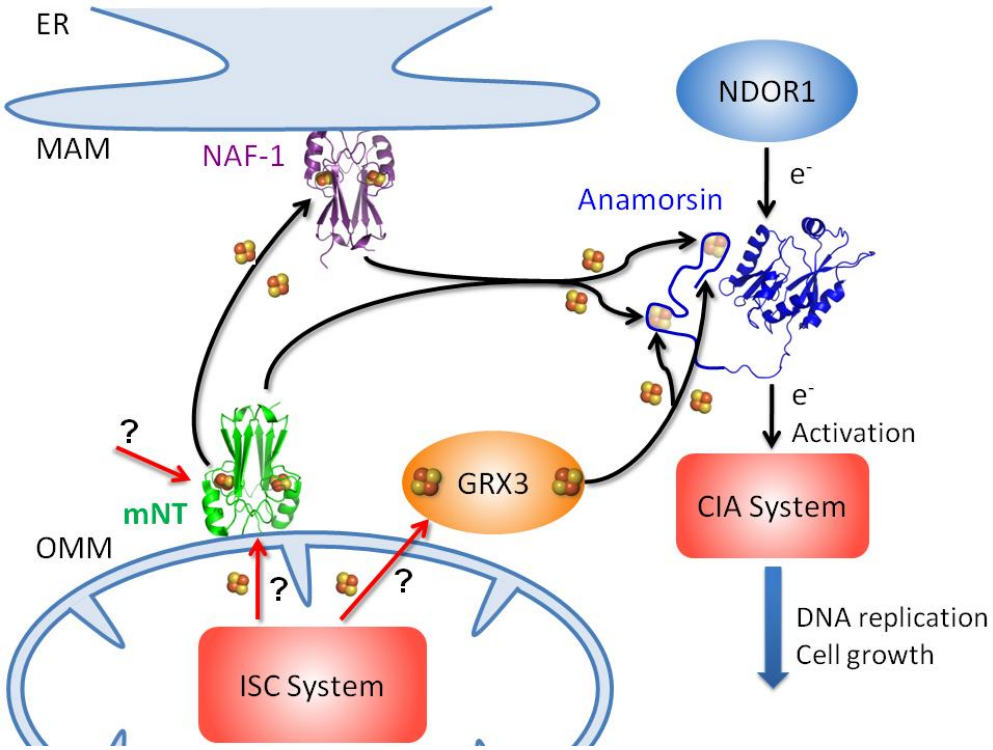

Figure 4-13: Schematic that summarizes the course of iron-sulfur transport prior to this work. Iron-sulfur cluster are made inside the mitochondrion and exported through a mechanism that is currently unresolved (red arrows). GRX3 and mNT are early cytosolic mediators of [2Fe-2S] cluster transport, and critical to bridge the ISC to the CIA, yet precisely how they are able to acquire clusters was unresolved [63].

The implications of this work are that we have established GRX3 as a donor of [2Fe-2S] clusters to mNT, the only identified cluster donor to date. Additionally, we have distinguished yet another key difference between the roles mNT and NAF-1 play in cells, despite these two proteins having moderate sequence conservation (Figure 4-14) and a high degree of structural similarity (Figure 4-15)[56]. However, as evidenced in **Figure 4-15**, [66], the

surface electrostatics vary moderately between the two proteins, and while the structural organization is similar, each is quite distinct.

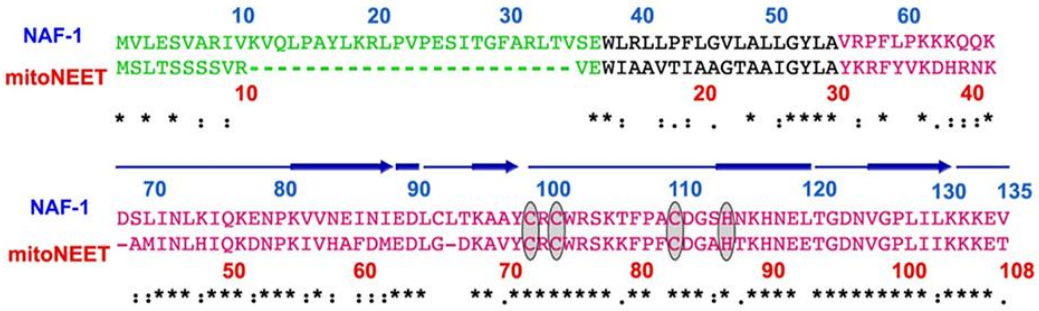

Figure 4-14: The amino acid sequence alignment comparing NAF-1 to mNT. NAF-1 and mitoNEET amino acid sequences: letters in green denote the water soluble C-terminus, those in black denote the trans-membrane segment, and the soluble part facing the cytoplasm is shown in pink. The symbols denote the level of similarity between the amino acids: asterisk, identity; colon, high similarity; period, poor similarity; no sign, no similarity. The blue line above the sequence corresponding to the soluble portion of the sequence indicates secondary structure elements: arrow for beta sheet and a thick line for alpha helix. The thin lines indicate no secondary structure [56].

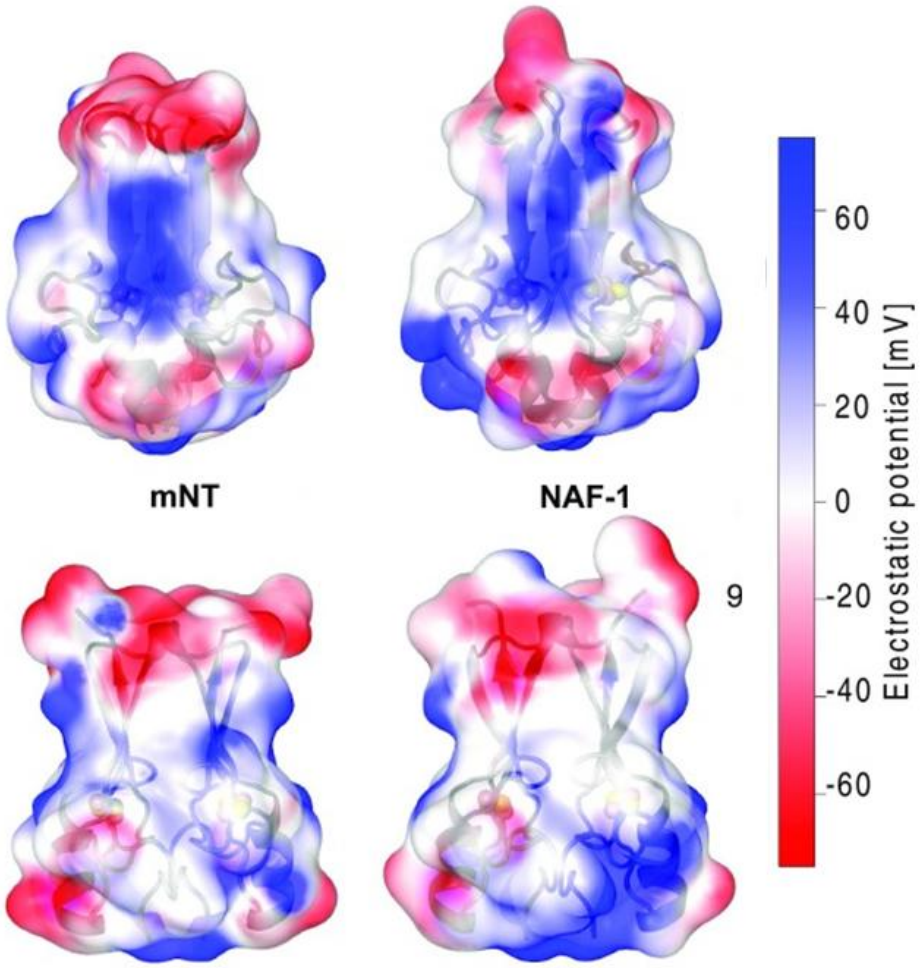

Figure 4-15: Electrostatic potential on the surface of mNT and NAF-1. The electrostatic potential values (estimated using NEET proteins' force files and APBS electrostatic) of mNT and NAF-1 are here reported over each protein surface. The side facing the plane of the β-sheet (top) and the side view (bottom) are here reported. The color code refers to the electrostatic potential values reported on the right [66].

Considering that the N-terminal Trx domain of GRX3 is responsible for protein recognition and necessary for [2Fe-2S] cluster transfer to anamorsin [74], it is probable that the N-terminal domain is also able to distinguish between the surface of mNT and NAF-1 in order to impart the transfer

selectivity. This selectivity may be a useful tool for further investigations of these proteins, including asking whether GRX3-BolA2 heterodimers have the same transfer potential to NEET proteins as GRX3 homodimers, or if they have an alternative selectivity. These homodimers also have the parallel ability to transfer [2Fe-2S] to anamorsin, just as GRX3 homodimers do [170], but there is likely a functional divergence that will help us to understand their role in the cell, as total functional overlap, without any alternative gain-of-function would seem unlikely. Moreover, this selectivity variation may be useful for designing better therapeutics at targeting iron-sulfur proteins, to treat metabolic disorders, allow signaling in cancer cells or other pathogen or parasite cells to release iron and self-destruct through ROS formation or ferroptosis.

Figure 4-16 graphically summarizes the updates to the previous schematic of [Fe-2S] transfer steps that link the ISC to the CIA (Figure 4-13). In connecting the individual steps, it has become evident that iron-sulfur transport utilizes some parallel transfer steps for redundancy in critical functions, and even has the ability for a feedback mechanism. This would likely allow the cell to regulate the flow of iron in times of abundance or scarcity, when control of free iron is essential. This would mean that mNT has a potential role as an iron-sulfur *bank*, when iron can be safely stashed away in a controlled fashion. This idea matches previous studies aimed at resolving the effects of depleted mNT and corresponding mitochondrial iron and ROS

accumulation [46, 50, 83, 123], and likely explains why mNT is upregulated in some cancers [26, 198].

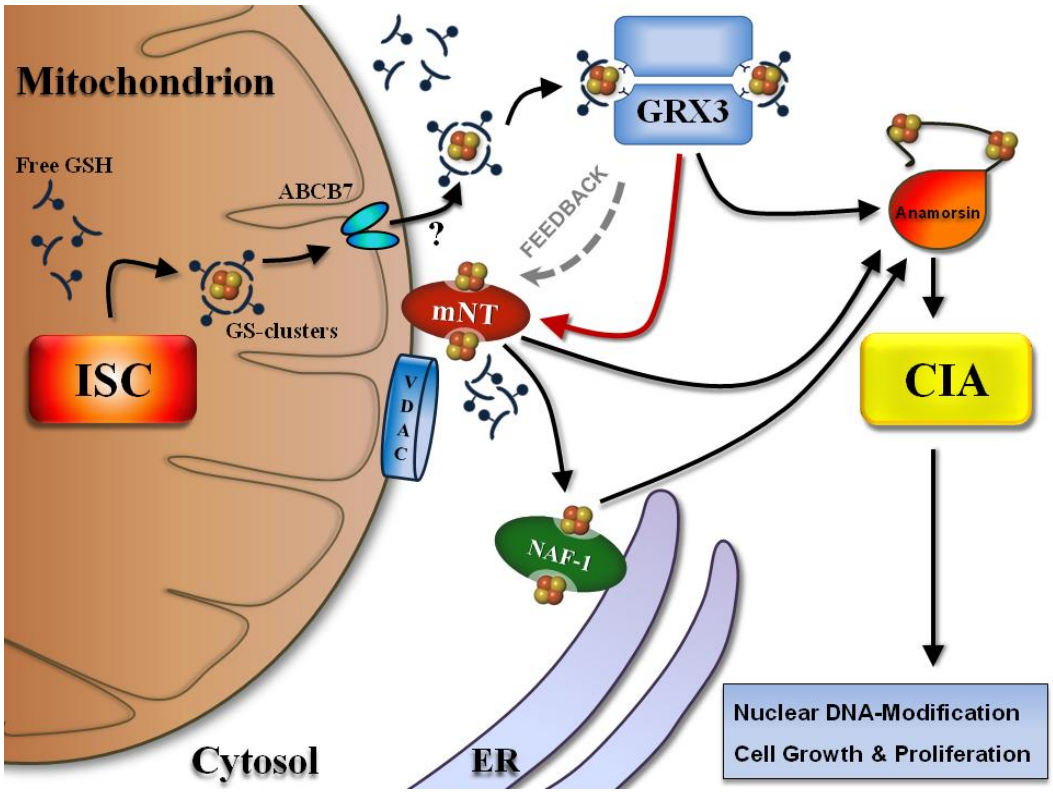

Figure 4-16: Updated model for the roles of GRX3, mNT, and NAF-1 in linking the ISC to the CIA. [2Fe-2S] clusters are assembled in the ISC and carried by four coordinated glutathiones (GS). $[2Fe\text{-}2S](GS)_4$ is then actively transported out of the matrix by the ABCB_7 transporter and the clusters are exported across the outer mitochondrial membrane by a currently-unresolved method (arrow with ?). $[2Fe\text{-}2S](GS)_4$ is then assembles into holo-GRX3. GRX3 can either deliver [2Fe-2S] clusters to the CIA for assembling nuclear iron-sulfur proteins and for cell growth proteins or to mNT as an iron-reserve and to recycle GSH (Red arrow represents our findings). mNT also has the ability to deliver [2Fe-2S] clusters to the cytosolic anamorsin and the CIA, so that when cellular demand for iron increases, mNT can supply it.

Chapter 4, in part, is a preprint as it will appear when submitted for publication, titled “New Connections in Iron-Sulfur Cluster Transport: GRX3 [2Fe-2S] Cluster Transfer is mitoNEET-Specific” by Stofleth JT, Jennings PA; which is being prepared for submission. The dissertation author was the primary investigator and author of this paper.

Chapter 5

Conclusions and Future Directions

Prior to this work, the NEET proteins had been demonstrated to function as iron-sulfur cluster trafficking proteins. Their ability to transfer iron-sulfur to anamorsin and ferredoxin in a directional manner was a key finding to support this role. With the identification of GRX3 as an iron-sulfur cluster donor for mNT, the connection of mNT and NAF-1 the ISC and CIA is now linked. Further *in vivo* studies will help resolve the cellular conditions that drive these iron-sulfur transfers. Whether they are due to perturbations of redox or other insult, or rather a part of homeostasis will help develop the understanding of iron-regulation in the cell.

We hypothesize that if mNT delivers iron/[2Fe-2S] to the mitochondrion, then the process is very likely reversible based on cellular conditions, such as cytosolic:mitochondrial iron availability, cell death signaling such as ferroptosis, or overcoming dysfunctional parallel pathways linking the ISC-CIA (GRX3, mNT, and NAF-1 all transfer to anamorsin). Since iron regulation is tightly controlled, as discussed earlier, it is more likely that mNT transfers the [2Fe-2S] cluster rather than reassemble iron-sulfur by diffusion when iron is exported. This would require mNT to access either a membrane-spanning iron-sulfur transporter, perhaps a subtype of the $ABCB_7$ active transporter class that is yet uncharacterized in the outer mitochondrial membrane. Or, perhaps it uses VDAC, as it can access the interior and is using this feature to deliver iron to an inner-mitochondrial source, such as the inner-mitochondrial GSH pools [199].

A good experiment to investigate VDAC as an outer mitochondrial membrane iron/Fe-S conduit would be to see if VDAC open–gated conformation can allow the passage of [2Fe-2S](GS)$_4$ clusters, and then if [2Fe-2S](GS)$_4$ clusters can transfer their iron-sulfur clusters directly to mNT. It would be best to conduct these studies in artificial bilayers, such as liposomes or even nanodiscs, and alternatively one of many other available current options for bilayer studies [200]. The advantage to using natural lipids for proteolipisomes or nanodiscs is that artificial detergents for solubility is no longer necessary, as the chemistry and micelle characteristics may adversely influence protein structure. Since the full-length mNT construct contains one N-terminal membrane spanning domain per monomer, studying the viability of this transfer in an environment that more accurately mimics the conditions and spatial relationships on the mitochondrial membrane. There may be some added effect of having the two mNT helical regions in proximity to VDAC that drive conformation changes, cluster release, or mNT insertion into the VDAC pore that can be investigated further. To date there is no published record of these investigations.

Another experiment to assess the viability of VDAC as an iron-sulfur conduit would be to examine a VDAC and GRX3 monomer interaction using a quantitative binding assay, in order to determine the potential of GRX3 using VDAC to access iron/[2Fe-2S], similar to that proposed for mNT above. A good control to these experiments would be to use shRNA to knockdown the mitochondrial ABCB$_7$ transporter levels and see if VDAC production is

upregulated or if GRX3 levels are upregulated or downregulated as a result. Alternatively shRNA knockdowns of mNT and GRX3 that look for alterations to VDAC and $ABCB_7$ mRNA and protein expression could provide more clues.

Continuing exploration of iron-sulfur transport between the ISC & CIA

An additional set of experiments I would suggest to follow up to the findings presented in Chapter 4 would be to produce and isolate Grx3-BolA heterodimers, which have already been shown to supply [2Fe-2S] clusters to apo-anamorsin in parallel with mNT and GRX3 homodimers [170]. I would also attempt to evaluate their potential as NAF-1 iron-sulfur cluster donors, as a means to alternatively regulate NEET protein targets and varied downstream signaling within the cell.

Since the Trx domain of GRX3 was necessary for [2Fe-2S] cluster transfer to anamorsin [74], it would be interesting to see if the same loss of function occurs with the GRX3 to mNT iron-sulfur transfer. Following the same procedure that I developed for full-length GRX3, the holo-protein with only the GrxA and GrxB domains could be anaerobically reconstituted and set up to transfer to apo-mNT.

Research focused on characterizing new iron-sulfur partners for the NEET proteins is a promising direction, as the network of iron-sulfur cluster transfer is far from complete. I would suggest developing an anaerobic reconstitution protocol for AOX1 and XHD. It is likely that one of the proteins described in this study acts as an iron-sulfur donor to these, but whether it is

mNT, NAF-1, GRX3, [2Fe-2S]$(GS)_4$ clusters, or another factor is completely uncharacterized. With the information currently available, it is difficult to state which of these (or even if there are multiple) would be the most likely to be the donor.

Creating Gallium-sulfur cluster proteins for NMR studies

Lastly, I would like to end by discussing a project that has been a very dear to me, but would be a bit of a long shot, and I never had the time to attempt it. A major problem for our lab is that at any given time, it is half-filled with NMR experts; yet the paramagnetic iron-sulfur clusters prevent such experiments from resolving changes in structure at amino acids near the cluster. Since most of the critical alterations and even drug binding occur near to the cluster, assessing the amino acids nearby is critical. Using the modified mNT and NAF-1 reconstitution protocol from Chapter 2, I would attempt to incorporate a diamagnetic [2Ga-2S] cluster. This has been documented in cyanobacterial ferredoxins, and would be a major advantage for NMR experiments to examine solution-based drug-binding studies [201-204]. The protein preparation would relatively easy to achieve if one substituted $GaCl_3$ for $FeCl_3$ in the reconstitution protocol. Then for isolation of dimeric [2Ga-2S] mNT, the sample would be concentrated and loaded onto the S-200 size-exclusion column described in the GRX3 purification protocol, and separated based on dimer versus monomeric mNT or NAF-1 elution profile detailed in **Figure 5-1** [205].

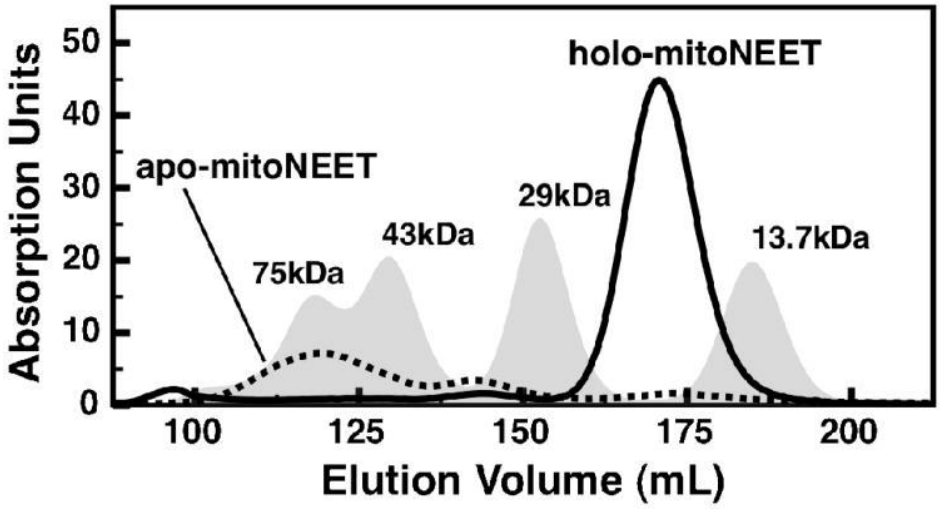

Figure 5-1: Size-exclusion chromatography elution profile for mNT. Size-exclusion chromatograms for wild-type mitoNEET: holo-mitoNEET (solid trace) and apo-mitoNEET (dotted trace). A set of four protein standards is reported for comparison (gray peaks): Ribonuclease A (13.7 kDa), Carbonic Anhydrase (29 kDa), Ovalbumin (43 kDa), and Conalbumin (75 kDa). All chromatograms are calculated from absorbance at 280 nm [205].

If this produced stable, dimeric mNT/NAF-1 holo-protein, it would be expected to have a similar elution profile, but would remain colorless, as demonstrated for a [2Ga-2S] ferredoxin that was reconstituted successfully in **Figure 5-2** [201].

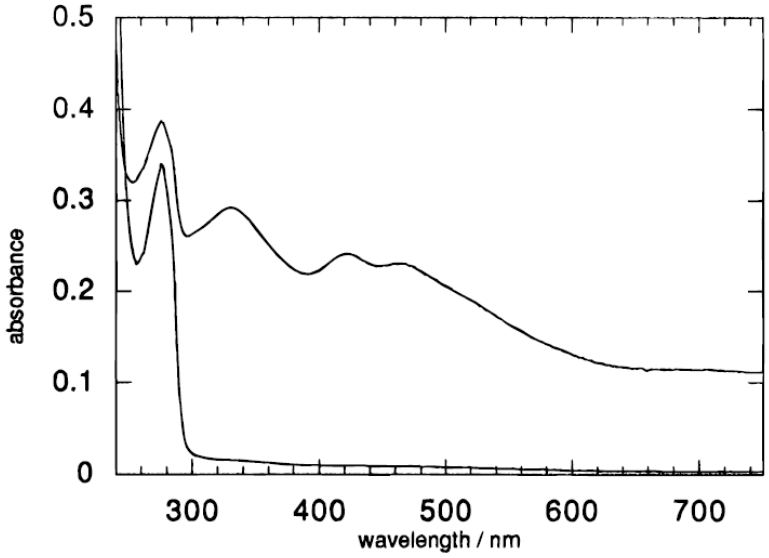

Figure 5-2: Spectral overlay for a [2Fe-2S] cluster substituted for a [2Ga-2S] cluster in ferredoxin. The gallium-sulfur cluster has no absorption in the visible region, so UV-Visible spectroscopy is not useful for monitoring cofactor content, as is typical for iron-sulfur cluster proteins [201].

Additional controls would be necessary to determine the protein viability as a replacement for the properties conferred by true [2Fe-2S] cluster, but would be fairly simple workflow since most of the reconstitution conditions have been determined and optimized. CD is typically used for analysis and confirmation of protein structure [201], and mass spectrometry could confirm the changes from iron to gallium in the molecular weight of the holo-protein. In addition an assay that can detect trace iron, showing none was present in the dimeric mNT or NAF-1 structure would support that the gallium replacement was successful.

A new crystal structure would need to be determined, showing the 3Cys:1His coordination site had not changed by altering secondary or tertiary protein structural conformation would be a key piece of data. Two sets of quantitative binding studies when evaluating drug binding would also be needed to ensure that the iron to gallium switch had not altered some aspect of the small molecule binding affinity. If creating [2Ga-2S] cluster NEET proteins is feasible, it would provide a means to better understand small molecule binding for the first time using structural NMR methods. Especially since the crystal structure of NEET proteins bound to pioglitazone, cluvenone, and MAD28 has remained elusive, in part due to the highly hydrophobic, insoluble nature of these drugs. So far, attempts at drug-protein co-crystallization and crystal-soaking with the drugs has been unsuccessful. Using solution NMR for these studies offers a major advantage in that the demands for drug concentration would be within the aqueous solubility range, is sensitive to low-affinity binding (K_d of mM to nM), and can even measure K_d [206-208]. A well characterized protocol for the [2Ga-2S] cluster NEET proteins could foster further collaborative projects and grants with Professor Emmanuel Theodorakis' group (here at UCSD), aimed at resolving the amino acid residue changes near the cluster that are directly involved in drug binding, and the local amino acids that exhibit chemical shifts as a result.

References

1. Holliday, G.L., J.M. Thornton, A. Marquet, A.G. Smith, F. Rebeille, R. Mendel, H.L. Schubert, A.D. Lawrence, and M.J. Warren, *Evolution of enzymes and pathways for the biosynthesis of cofactors.* Nat Prod Rep, 2007. **24**(5): p. 972-87.

2. Aggett, P.J., *Physiology and metabolism of essential trace elements: an outline.* Clin Endocrinol Metab, 1985. **14**(3): p. 513-43.

3. Einsle, O., F.A. Tezcan, S.L. Andrade, B. Schmid, M. Yoshida, J.B. Howard, and D.C. Rees, *Nitrogenase MoFe-protein at 1.16 A resolution: a central ligand in the FeMo-cofactor.* Science, 2002. **297**(5587): p. 1696-700.

4. Djurdjevic, I., O. Einsle, and L. Decamps, *Nitrogenase Cofactor: Inspiration for Model Chemistry.* Chem Asian J, 2017. **12**(13): p. 1447-1455.

5. Nouet, C., P. Motte, and M. Hanikenne, *Chloroplastic and mitochondrial metal homeostasis.* Trends Plant Sci, 2011. **16**(7): p. 395-404.

6. Burkhead, J.L., K.A. Reynolds, S.E. Abdel-Ghany, C.M. Cohu, and M. Pilon, *Copper homeostasis.* New Phytol, 2009. **182**(4): p. 799-816.

7. Kaplan, J. and D.M. Ward, *The essential nature of iron usage and regulation.* Curr Biol, 2013. **23**(15): p. R642-6.

8. MacKenzie, E.L., K. Iwasaki, and Y. Tsuji, *Intracellular iron transport and storage: from molecular mechanisms to health implications.* Antioxid Redox Signal, 2008. **10**(6): p. 997-1030.

9. Muckenthaler, M.U., S. Rivella, M.W. Hentze, and B. Galy, *A Red Carpet for Iron Metabolism.* Cell, 2017. **168**(3): p. 344-361.

10. Cabantchik, Z.I., *Labile iron in cells and body fluids: physiology, pathology, and pharmacology.* Front Pharmacol, 2014. **5**: p. 45.

11. Rouault, T.A. and W.H. Tong, *Iron-sulphur cluster biogenesis and mitochondrial iron homeostasis.* Nat Rev Mol Cell Biol, 2005. **6**(4): p. 345-51.

12. Lu, Y., N. Yeung, N. Sieracki, and N.M. Marshall, *Design of functional metalloproteins.* Nature, 2009. **460**(7257): p. 855-62.

13. Zhang, D.L., J. Wu, B.N. Shah, K.C. Greutelaers, M.C. Ghosh, H. Ollivierre, X.Z. Su, P.E. Thuma, G. Bedu-Addo, F.P. Mockenhaupt, V.R. Gordeuk, and T.A. Rouault, *Erythrocytic ferroportin reduces intracellular*

iron accumulation, hemolysis, and malaria risk. Science, 2018. **359**(6383): p. 1520-1523.

14. Weinberg, E.D. and J. Moon, *Malaria and iron: history and review.* Drug Metab Rev, 2009. **41**(4): p. 644-62.

15. Carver, P.L., *The Battle for Iron between Humans and Microbes.* Curr Med Chem, 2018. **25**(1): p. 85-96.

16. Stijlemans, B., A. Beschin, S. Magez, J.A. Van Ginderachter, and P. De Baetselier, *Iron Homeostasis and Trypanosoma brucei Associated Immunopathogenicity Development: A Battle/Quest for Iron.* Biomed Res Int, 2015. **2015**: p. 819389.

17. Skaar, E.P., *The battle for iron between bacterial pathogens and their vertebrate hosts.* PLoS Pathog, 2010. **6**(8): p. e1000949.

18. Cassat, J.E. and E.P. Skaar, *Iron in infection and immunity.* Cell Host Microbe, 2013. **13**(5): p. 509-519.

19. Zauberman, A., Y. Vagima, A. Tidhar, M. Aftalion, D. Gur, S. Rotem, T. Chitlaru, Y. Levy, and E. Mamroud, *Host Iron Nutritional Immunity Induced by a Live Yersinia pestis Vaccine Strain Is Associated with Immediate Protection against Plague.* Front Cell Infect Microbiol, 2017. **7**: p. 277.

20. Manz, D.H., N.L. Blanchette, B.T. Paul, F.M. Torti, and S.V. Torti, *Iron and cancer: recent insights.* Ann N Y Acad Sci, 2016. **1368**(1): p. 149-61.

21. Basuli, D., L. Tesfay, Z. Deng, B. Paul, Y. Yamamoto, G. Ning, W. Xian, F. McKeon, M. Lynch, C.P. Crum, P. Hegde, M. Brewer, X. Wang, L.D. Miller, N. Dyment, F.M. Torti, and S.V. Torti, *Iron addiction: a novel therapeutic target in ovarian cancer.* Oncogene, 2017. **36**(29): p. 4089-4099.

22. Torti, S.V. and F.M. Torti, *Iron and cancer: more ore to be mined.* Nat Rev Cancer, 2013. **13**(5): p. 342-55.

23. Rohlena, J., L.F. Dong, and J. Neuzil, *Targeting the mitochondrial electron transport chain complexes for the induction of apoptosis and cancer treatment.* Curr Pharm Biotechnol, 2013. **14**(3): p. 377-89.

24. Nayak, A.P., A. Kapur, L. Barroilhet, and M.S. Patankar, *Oxidative Phosphorylation: A Target for Novel Therapeutic Strategies Against Ovarian Cancer.* Cancers (Basel), 2018. **10**(9).

25. Liberti, M.V. and J.W. Locasale, *The Warburg Effect: How Does it Benefit Cancer Cells?* Trends Biochem Sci, 2016. **41**(3): p. 211-218.

26. Sohn, Y.S., S. Tamir, L. Song, D. Michaeli, I. Matouk, A.R. Conlan, Y. Harir, S.H. Holt, V. Shulaev, M.L. Paddock, A. Hochberg, I.Z. Cabanchick, J.N. Onuchic, P.A. Jennings, R. Nechushtai, and R. Mittler, *NAF-1 and mitoNEET are central to human breast cancer proliferation by maintaining mitochondrial homeostasis and promoting tumor growth.* Proc Natl Acad Sci U S A, 2013. **110**(36): p. 14676-81.

27. Urra, F.A., F. Munoz, A. Lovy, and C. Cardenas, *The Mitochondrial Complex(I)ty of Cancer.* Front Oncol, 2017. **7**: p. 118.

28. Sullivan, L.B. and N.S. Chandel, *Mitochondrial reactive oxygen species and cancer.* Cancer Metab, 2014. **2**: p. 17.

29. Wachnowsky, C., I. Fidai, and J.A. Cowan, *Iron-sulfur cluster biosynthesis and trafficking - impact on human disease conditions.* Metallomics, 2018. **10**(1): p. 9-29.

30. Ventola, C.L., *The antibiotic resistance crisis: part 1: causes and threats.* P T, 2015. **40**(4): p. 277-83.

31. Ventola, C.L., *The antibiotic resistance crisis: part 2: management strategies and new agents.* P T, 2015. **40**(5): p. 344-52.

32. Sanganyado, E. and W. Gwenzi, *Antibiotic resistance in drinking water systems: Occurrence, removal, and human health risks.* Sci Total Environ, 2019. **669**: p. 785-797.

33. Danner, M.C., A. Robertson, V. Behrends, and J. Reiss, *Antibiotic pollution in surface fresh waters: Occurrence and effects.* Sci Total Environ, 2019. **664**: p. 793-804.

34. Vernis, L., N. El Banna, D. Baille, E. Hatem, A. Heneman, and M.E. Huang, *Fe-S Clusters Emerging as Targets of Therapeutic Drugs.* Oxid Med Cell Longev, 2017. **2017**: p. 3647657.

35. Colca, J.R., W.G. McDonald, D.J. Waldon, J.W. Leone, J.M. Lull, C.A. Bannow, E.T. Lund, and W.R. Mathews, *Identification of a novel mitochondrial protein ("mitoNEET") cross-linked specifically by a thiazolidinedione photoprobe.* Am J Physiol Endocrinol Metab, 2004. **286**(2): p. E252-60.

36. Tyagi, S., P. Gupta, A.S. Saini, C. Kaushal, and S. Sharma, *The peroxisome proliferator-activated receptor: A family of nuclear receptors*

role in various diseases. J Adv Pharm Technol Res, 2011. **2**(4): p. 236-40.

37. Kubota, N., Y. Terauchi, T. Kubota, H. Kumagai, S. Itoh, H. Satoh, W. Yano, H. Ogata, K. Tokuyama, I. Takamoto, T. Mineyama, M. Ishikawa, M. Moroi, K. Sugi, T. Yamauchi, K. Ueki, K. Tobe, T. Noda, R. Nagai, and T. Kadowaki, *Pioglitazone ameliorates insulin resistance and diabetes by both adiponectin-dependent and -independent pathways.* J Biol Chem, 2006. **281**(13): p. 8748-55.

38. Norris, A.W., L. Chen, S.J. Fisher, I. Szanto, M. Ristow, A.C. Jozsi, M.F. Hirshman, E.D. Rosen, L.J. Goodyear, F.J. Gonzalez, B.M. Spiegelman, and C.R. Kahn, *Muscle-specific PPARgamma-deficient mice develop increased adiposity and insulin resistance but respond to thiazolidinediones.* J Clin Invest, 2003. **112**(4): p. 608-18.

39. Wiley, S.E., A.N. Murphy, S.A. Ross, P. van der Geer, and J.E. Dixon, *MitoNEET is an iron-containing outer mitochondrial membrane protein that regulates oxidative capacity.* Proceedings of the National Academy of Sciences of the United States of America, 2007. **104**(13): p. 5318-5323.

40. Conlan, A.R., H.L. Axelrod, A.E. Cohen, E.C. Abresch, J. Zuris, D. Yee, R. Nechushtai, P.A. Jennings, and M.L. Paddock, *Crystal structure of Miner1: The redox-active 2Fe-2S protein causative in Wolfram Syndrome 2.* J Mol Biol, 2009. **392**(1): p. 143-53.

41. Lin, J., T. Zhou, K. Ye, and J. Wang, *Crystal structure of human mitoNEET reveals distinct groups of iron sulfur proteins.* Proc Natl Acad Sci U S A, 2007. **104**(37): p. 14640-5.

42. Paddock, M.L., S.E. Wiley, H.L. Axelrod, A.E. Cohen, M. Roy, E.C. Abresch, D. Capraro, A.N. Murphy, R. Nechushtai, J.E. Dixon, and P.A. Jennings, *MitoNEET is a uniquely folded 2Fe 2S outer mitochondrial membrane protein stabilized by pioglitazone.* Proc Natl Acad Sci U S A, 2007. **104**(36): p. 14342-7.

43. Wiley, S.E., M.L. Paddock, E.C. Abresch, L. Gross, P. van der Geer, R. Nechushtai, A.N. Murphy, P.A. Jennings, and J.E. Dixon, *The outer mitochondrial membrane protein mitoNEET contains a novel redox-active 2Fe-2S cluster.* J Biol Chem, 2007. **282**(33): p. 23745-9.

44. Hou, X., R. Liu, S. Ross, E.J. Smart, H. Zhu, and W. Gong, *Crystallographic studies of human MitoNEET.* J Biol Chem, 2007. **282**(46): p. 33242-6.

45. Inupakutika, M.A., S. Sengupta, R. Nechushtai, P.A. Jennings, J.N. Onuchic, R.K. Azad, P. Padilla, and R. Mittler, *Phylogenetic analysis of eukaryotic NEET proteins uncovers a link between a key gene duplication event and the evolution of vertebrates.* Sci Rep, 2017. **7**: p. 42571.

46. Tamir, S., M.L. Paddock, M. Darash-Yahana-Baram, S.H. Holt, Y.S. Sohn, L. Agranat, D. Michaeli, J.T. Stofleth, C.H. Lipper, F. Morcos, I.Z. Cabantchik, J.N. Onuchic, P.A. Jennings, R. Mittler, and R. Nechushtai, *Structure-function analysis of NEET proteins uncovers their role as key regulators of iron and ROS homeostasis in health and disease.* Biochim Biophys Acta, 2015. **1853**(6): p. 1294-315.

47. Lin, J., L. Zhang, S. Lai, and K. Ye, *Structure and molecular evolution of CDGSH iron-sulfur domains.* PLoS One, 2011. **6**(9): p. e24790.

48. Amr, S., C. Heisey, M. Zhang, X.J. Xia, K.H. Shows, K. Ajlouni, A. Pandya, L.S. Satin, H. El-Shanti, and R. Shiang, *A homozygous mutation in a novel zinc-finger protein, ERIS, is responsible for Wolfram syndrome 2.* Am J Hum Genet, 2007. **81**(4): p. 673-83.

49. Chen, Y.F., C.H. Kao, Y.T. Chen, C.H. Wang, C.Y. Wu, C.Y. Tsai, F.C. Liu, C.W. Yang, Y.H. Wei, M.T. Hsu, S.F. Tsai, and T.F. Tsai, *Cisd2 deficiency drives premature aging and causes mitochondria-mediated defects in mice.* Genes Dev, 2009. **23**(10): p. 1183-94.

50. Geldenhuys, W.J., S.A. Benkovic, L. Lin, H.M. Yonutas, S.D. Crish, P.G. Sullivan, A.S. Darvesh, C.M. Brown, and J.R. Richardson, *MitoNEET (CISD1) Knockout Mice Show Signs of Striatal Mitochondrial Dysfunction and a Parkinson's Disease Phenotype.* ACS Chem Neurosci, 2017. **8**(12): p. 2759-2765.

51. Vernay, A., A. Marchetti, A. Sabra, T.N. Jauslin, M. Rosselin, P.E. Scherer, N. Demaurex, L. Orci, and P. Cosson, *MitoNEET-dependent formation of intermitochondrial junctions.* Proc Natl Acad Sci U S A, 2017. **114**(31): p. 8277-8282.

52. Logan, S.J., L. Yin, W.J. Geldenhuys, M.K. Enrick, K.M. Stevanov, R.T. Carroll, V.A. Ohanyan, C.L. Kolz, and W.M. Chilian, *Novel thiazolidinedione mitoNEET ligand-1 acutely improves cardiac stem cell survival under oxidative stress.* Basic Res Cardiol, 2015. **110**(2): p. 19.

53. Stauch, K.L., L.M. Villeneuve, S. Totusek, B. Lamberty, P. Ciborowski, and H.S. Fox, *Quantitative Proteomics of Presynaptic Mitochondria Reveal an Overexpression and Biological Relevance of Neuronal MitoNEET in Postnatal Brain Development.* Dev Neurobiol, 2019.

54. Darash-Yahana, M., Y. Pozniak, M. Lu, Y.S. Sohn, O. Karmi, S. Tamir, F. Bai, L. Song, P.A. Jennings, E. Pikarsky, T. Geiger, J.N. Onuchic, R. Mittler, and R. Nechushtai, *Breast cancer tumorigenicity is dependent on high expression levels of NAF-1 and the lability of its Fe-S clusters.* Proc Natl Acad Sci U S A, 2016. **113**(39): p. 10890-5.

55. Qi, W. and J.A. Cowan, *Structural, Mechanistic and Coordination Chemistry of Relevance to the Biosynthesis of Iron-Sulfur and Related Iron Cofactors.* Coord Chem Rev, 2011. **255**(7-8): p. 688-699.

56. Tamir, S., J.A. Zuris, L. Agranat, C.H. Lipper, A.R. Conlan, D. Michaeli, Y. Harir, M.L. Paddock, R. Mittler, Z.I. Cabantchik, P.A. Jennings, and R. Nechushtai, *Nutrient-deprivation autophagy factor-1 (NAF-1): biochemical properties of a novel cellular target for anti-diabetic drugs.* PLoS One, 2013. **8**(5): p. e61202.

57. Zuris, J.A., D.A. Halim, A.R. Conlan, E.C. Abresch, R. Nechushtai, M.L. Paddock, and P.A. Jennings, *Engineering the redox potential over a wide range within a new class of FeS proteins.* J Am Chem Soc, 2010. **132**(38): p. 13120-2.

58. Zuris, J.A., Y. Harir, A.R. Conlan, M. Shvartsman, D. Michaeli, S. Tamir, M.L. Paddock, J.N. Onuchic, R. Mittler, Z.I. Cabantchik, P.A. Jennings, and R. Nechushtai, *Facile transfer of [2Fe-2S] clusters from the diabetes drug target mitoNEET to an apo-acceptor protein.* Proc Natl Acad Sci U S A, 2011. **108**(32): p. 13047-52.

59. Geldenhuys, W.J., R. Skolik, M.E. Konkle, M.A. Menze, T.E. Long, and A.R. Robart, *Binding of thiazolidinediones to the endoplasmic reticulum protein nutrient-deprivation autophagy factor-1.* Bioorg Med Chem Lett, 2019. **29**(7): p. 901-904.

60. Zuris, J.A., S.S. Ali, H. Yeh, T.A. Nguyen, R. Nechushtai, M.L. Paddock, and P.A. Jennings, *NADPH inhibits [2Fe-2S] cluster protein transfer from diabetes drug target MitoNEET to an apo-acceptor protein.* J Biol Chem, 2012. **287**(15): p. 11649-55.

61. Tamir, S., Y. Eisenberg-Domovich, A.R. Conlan, J.T. Stofleth, C.H. Lipper, M.L. Paddock, R. Mittler, P.A. Jennings, O. Livnah, and R. Nechushtai, *A point mutation in the [2Fe-2S] cluster binding region of the NAF-1 protein (H114C) dramatically hinders the cluster donor properties.* Acta Crystallogr D Biol Crystallogr, 2014. **70**(Pt 6): p. 1572-8.

62. Pesce, L., V. Calandrini, H.B. Marjault, C.H. Lipper, G. Rossetti, R. Mittler, P.A. Jennings, A. Bauer, R. Nechushtai, and P. Carloni, *Molecular Dynamics Simulations of the [2Fe-2S] Cluster-Binding*

Domain of NEET Proteins Reveal Key Molecular Determinants That Induce Their Cluster Transfer/Release. J Phys Chem B, 2017.

63. Lipper, C.H., M.L. Paddock, J.N. Onuchic, R. Mittler, R. Nechushtai, and P.A. Jennings, *Cancer-Related NEET Proteins Transfer 2Fe-2S Clusters to Anamorsin, a Protein Required for Cytosolic Iron-Sulfur Cluster Biogenesis.* PLoS One, 2015. **10**(10): p. e0139699.

64. Camponeschi, F., S. Ciofi-Baffoni, and L. Banci, *Anamorsin/Ndor1 Complex Reduces [2Fe-2S]-MitoNEET via a Transient Protein-Protein Interaction.* J Am Chem Soc, 2017. **139**(28): p. 9479-9482.

65. Saito, Y., H. Shibayama, H. Tanaka, A. Tanimura, and Y. Kanakura, *A cell-death-defying factor, anamorsin mediates cell growth through inactivation of PKC and p38MAPK.* Biochem Biophys Res Commun, 2011. **405**(2): p. 303-7.

66. Karmi, O., H.B. Marjault, L. Pesce, P. Carloni, J.N. Onuchic, P.A. Jennings, R. Mittler, and R. Nechushtai, *The unique fold and lability of the [2Fe-2S] clusters of NEET proteins mediate their key functions in health and disease.* J Biol Inorg Chem, 2018. **23**(4): p. 599-612.

67. Karmi, O., S.H. Holt, L. Song, S. Tamir, Y. Luo, F. Bai, A. Adenwalla, M. Darash-Yahana, Y.S. Sohn, P.A. Jennings, R.K. Azad, J.N. Onuchic, F. Morcos, R. Nechushtai, and R. Mittler, *Interactions between mitoNEET and NAF-1 in cells.* PLoS One, 2017. **12**(4): p. e0175796.

68. Lemasters, J.J. and E. Holmuhamedov, *Voltage-dependent anion channel (VDAC) as mitochondrial governator--thinking outside the box.* Biochim Biophys Acta, 2006. **1762**(2): p. 181-90.

69. Benz, R., *Permeation of hydrophilic solutes through mitochondrial outer membranes: review on mitochondrial porins.* Biochim Biophys Acta, 1994. **1197**(2): p. 167-96.

70. Pavlov, E., S.M. Grigoriev, L.M. Dejean, C.L. Zweihorn, C.A. Mannella, and K.W. Kinnally, *The mitochondrial channel VDAC has a cation-selective open state.* Biochim Biophys Acta, 2005. **1710**(2-3): p. 96-102.

71. Tamir, S., S. Rotem-Bamberger, C. Katz, F. Morcos, K.L. Hailey, J.A. Zuris, C. Wang, A.R. Conlan, C.H. Lipper, M.L. Paddock, R. Mittler, J.N. Onuchic, P.A. Jennings, A. Friedler, and R. Nechushtai, *Integrated strategy reveals the protein interface between cancer targets Bcl-2 and NAF-1.* Proc Natl Acad Sci U S A, 2014. **111**(14): p. 5177-82.

72. Chang, N.C., M. Nguyen, M. Germain, and G.C. Shore, *Antagonism of Beclin 1-dependent autophagy by BCL-2 at the endoplasmic reticulum requires NAF-1.* EMBO J, 2010. **29**(3): p. 606-18.

73. Haunhorst, P., C. Berndt, S. Eitner, J.R. Godoy, and C.H. Lillig, *Characterization of the human monothiol glutaredoxin 3 (PICOT) as iron-sulfur protein.* Biochem Biophys Res Commun, 2010. **394**(2): p. 372-6.

74. Banci, L., S. Ciofi-Baffoni, K. Gajda, R. Muzzioli, R. Peruzzini, and J. Winkelmann, *N-terminal domains mediate [2Fe-2S] cluster transfer from glutaredoxin-3 to anamorsin.* Nat Chem Biol, 2015. **11**(10): p. 772-8.

75. Conlan, A.R., M.L. Paddock, H.L. Axelrod, A.E. Cohen, E.C. Abresch, S. Wiley, M. Roy, R. Nechushtai, and P.A. Jennings, *The novel 2Fe-2S outer mitochondrial protein mitoNEET displays conformational flexibility in its N-terminal cytoplasmic tethering domain.* Acta Crystallogr Sect F Struct Biol Cryst Commun, 2009. **65**(Pt 7): p. 654-9.

76. Bai, F., F. Morcos, Y.S. Sohn, M. Darash-Yahana, C.O. Rezende, C.H. Lipper, M.L. Paddock, L. Song, Y. Luo, S.H. Holt, S. Tamir, E.A. Theodorakis, P.A. Jennings, J.N. Onuchic, R. Mittler, and R. Nechushtai, *The Fe-S cluster-containing NEET proteins mitoNEET and NAF-1 as chemotherapeutic targets in breast cancer.* Proc Natl Acad Sci U S A, 2015. **112**(12): p. 3698-703.

77. Bak, D.W. and S.J. Elliott, *Conserved Hydrogen Bonding Networks of MitoNEET Tune Fe-S Cluster Binding and Structural Stability.* Biochemistry, 2013. **52**(27): p. 4687-4696.

78. Vranish, J.N., W.K. Russell, L.E. Yu, R.M. Cox, D.H. Russell, and D.P. Barondeau, *Fluorescent probes for tracking the transfer of iron-sulfur cluster and other metal cofactors in biosynthetic reaction pathways.* J Am Chem Soc, 2015. **137**(1): p. 390-8.

79. Vranish, J.N., D. Das, and D.P. Barondeau, *Real-Time Kinetic Probes Support Monothiol Glutaredoxins As Intermediate Carriers in Fe-S Cluster Biosynthetic Pathways.* ACS Chem Biol, 2016. **11**(11): p. 3114-3121.

80. Fox, N.G., M. Chakrabarti, S.P. McCormick, P.A. Lindahl, and D.P. Barondeau, *The Human Iron-Sulfur Assembly Complex Catalyzes the Synthesis of [2Fe-2S] Clusters on ISCU2 That Can Be Transferred to Acceptor Molecules.* Biochemistry, 2015. **54**(25): p. 3871-9.

81. Fox, N.G., D. Das, M. Chakrabarti, P.A. Lindahl, and D.P. Barondeau, *Frataxin Accelerates [2Fe-2S] Cluster Formation on the Human Fe-S Assembly Complex.* Biochemistry, 2015. **54**(25): p. 3880-9.

82. Ferecatu, I., S. Goncalves, M.P. Golinelli-Cohen, M. Clemancey, A. Martelli, S. Riquier, E. Guittet, J.M. Latour, H. Puccio, J.C. Drapier, E. Lescop, and C. Bouton, *The diabetes drug target MitoNEET governs a novel trafficking pathway to rebuild an Fe-S cluster into cytosolic aconitase/iron regulatory protein 1.* J Biol Chem, 2014. **289**(41): p. 28070-86.

83. Nechushtai, R., A.R. Conlan, Y. Harir, L. Song, O. Yogev, Y. Eisenberg-Domovich, O. Livnah, D. Michaeli, R. Rosen, V. Ma, Y. Luo, J.A. Zuris, M.L. Paddock, Z.I. Cabantchik, P.A. Jennings, and R. Mittler, *Characterization of Arabidopsis NEET reveals an ancient role for NEET proteins in iron metabolism.* Plant Cell, 2012. **24**(5): p. 2139-54.

84. Yuan, H., X. Li, X. Zhang, R. Kang, and D. Tang, *CISD1 inhibits ferroptosis by protection against mitochondrial lipid peroxidation.* Biochem Biophys Res Commun, 2016. **478**(2): p. 838-44.

85. Taminelli, G.L., V. Sotomayor, A.G. Valdivieso, M.L. Teiber, M.C. Marin, and T.A. Santa-Coloma, *CISD1 codifies a mitochondrial protein upregulated by the CFTR channel.* Biochem Biophys Res Commun, 2008. **365**(4): p. 856-62.

86. Kusminski, C.M., W.L. Holland, K. Sun, J. Park, S.B. Spurgin, Y. Lin, G.R. Askew, J.A. Simcox, D.A. McClain, C. Li, and P.E. Scherer, *MitoNEET-driven alterations in adipocyte mitochondrial activity reveal a crucial adaptive process that preserves insulin sensitivity in obesity.* Nat Med, 2012. **18**(10): p. 1539-49.

87. Geldenhuys, W.J., T.C. Leeper, and R.T. Carroll, *mitoNEET as a novel drug target for mitochondrial dysfunction.* Drug Discov Today, 2014. **19**(10): p. 1601-6.

88. Sengupta, S., R. Nechushtai, P.A. Jennings, J.N. Onuchic, P.A. Padilla, R.K. Azad, and R. Mittler, *Phylogenetic analysis of the CDGSH iron-sulfur binding domain reveals its ancient origin.* Sci Rep, 2018. **8**(1): p. 4840.

89. Shoshan-Barmatz, V., V. De Pinto, M. Zweckstetter, Z. Raviv, N. Keinan, and N. Arbel, *VDAC, a multi-functional mitochondrial protein regulating cell life and death.* Mol Aspects Med, 2010. **31**(3): p. 227-85.

90. Fukada, K., F. Zhang, A. Vien, N.R. Cashman, and H. Zhu, *Mitochondrial proteomic analysis of a cell line model of familial amyotrophic lateral sclerosis.* Molecular & Cellular Proteomics, 2004. **3**(12): p. 1211-23.

91. Reddy, P.H., *Is the mitochondrial outermembrane protein VDAC1 therapeutic target for Alzheimer's disease?* Biochim Biophys Acta, 2013. **1832**(1): p. 67-75.

92. Smilansky, A., L. Dangoor, I. Nakdimon, D. Ben-Hail, D. Mizrachi, and V. Shoshan-Barmatz, *The Voltage-dependent Anion Channel 1 Mediates Amyloid beta Toxicity and Represents a Potential Target for Alzheimer Disease Therapy.* J Biol Chem, 2015. **290**(52): p. 30670-83.

93. Shoshan-Barmatz, V., E. Nahon-Crystal, A. Shteinfer-Kuzmine, and R. Gupta, *VDAC1, mitochondrial dysfunction, and Alzheimer's disease.* Pharmacol Res, 2018. **131**: p. 87-101.

94. Manczak, M., T. Sheiko, W.J. Craigen, and P.H. Reddy, *Reduced VDAC1 protects against Alzheimer's disease, mitochondria, and synaptic deficiencies.* Journal of Alzheimers Disease, 2013. **37**(4): p. 679-90.

95. Tikunov, A., C.B. Johnson, P. Pediaditakis, N. Markevich, J.M. Macdonald, J.J. Lemasters, and E. Holmuhamedov, *Closure of VDAC causes oxidative stress and accelerates the Ca(2+)-induced mitochondrial permeability transition in rat liver mitochondria.* Archives of Biochemistry and Biophysics, 2010. **495**(2): p. 174-81.

96. Fang, D. and E.N. Maldonado, *VDAC Regulation: A Mitochondrial Target to Stop Cell Proliferation.* Adv Cancer Res, 2018. **138**: p. 41-69.

97. Gatliff, J., D. East, J. Crosby, R. Abeti, R. Harvey, W. Craigen, P. Parker, and M. Campanella, *TSPO interacts with VDAC1 and triggers a ROS-mediated inhibition of mitochondrial quality control.* Autophagy, 2014. **10**(12): p. 2279-96.

98. Maldonado, E.N., K.L. Sheldon, D.N. DeHart, J. Patnaik, Y. Manevich, D.M. Townsend, S.M. Bezrukov, T.K. Rostovtseva, and J.J. Lemasters, *Voltage-dependent anion channels modulate mitochondrial metabolism in cancer cells: regulation by free tubulin and erastin.* J Biol Chem, 2013. **288**(17): p. 11920-9.

99. Messina, A., S. Reina, F. Guarino, and V. De Pinto, *VDAC isoforms in mammals.* Biochim Biophys Acta, 2012. **1818**(6): p. 1466-76.

100. Sampson, M.J., R.S. Lovell, and W.J. Craigen, *The murine voltage-dependent anion channel gene family. Conserved structure and function.* J Biol Chem, 1997. **272**(30): p. 18966-73.

101. Wan, C., B. Borgeson, S. Phanse, F. Tu, K. Drew, G. Clark, X. Xiong, O. Kagan, J. Kwan, A. Bezginov, K. Chessman, S. Pal, G. Cromar, O. Papoulas, Z. Ni, D.R. Boutz, S. Stoilova, P.C. Havugimana, X. Guo, R.H. Malty, M. Sarov, J. Greenblatt, M. Babu, W.B. Derry, E.R. Tillier, J.B. Wallingford, J. Parkinson, E.M. Marcotte, and A. Emili, *Panorama of ancient metazoan macromolecular complexes.* Nature, 2015. **525**(7569): p. 339-44.

102. Guruharsha, K.G., J.F. Rual, B. Zhai, J. Mintseris, P. Vaidya, N. Vaidya, C. Beekman, C. Wong, D.Y. Rhee, O. Cenaj, E. McKillip, S. Shah, M. Stapleton, K.H. Wan, C. Yu, B. Parsa, J.W. Carlson, X. Chen, B. Kapadia, K. VijayRaghavan, S.P. Gygi, S.E. Celniker, R.A. Obar, and S. Artavanis-Tsakonas, *A protein complex network of Drosophila melanogaster.* Cell, 2011. **147**(3): p. 690-703.

103. Schein, S.J., M. Colombini, and A. Finkelstein, *Reconstitution in planar lipid bilayers of a voltage-dependent anion-selective channel obtained from paramecium mitochondria.* J Membr Biol, 1976. **30**(2): p. 99-120.

104. De Pinto, V., F. Guarino, A. Guarnera, A. Messina, S. Reina, F.M. Tomasello, V. Palermo, and C. Mazzoni, *Characterization of human VDAC isoforms: a peculiar function for VDAC3?* Biochim Biophys Acta, 2010. **1797**(6-7): p. 1268-75.

105. Bak, D.W., J.A. Zuris, M.L. Paddock, P.A. Jennings, and S.J. Elliott, *Redox characterization of the FeS protein MitoNEET and impact of thiazolidinedione drug binding.* Biochemistry, 2009. **48**(43): p. 10193-5.

106. Wang, Y.M., A.P. Landry, and H.G. Ding, *The mitochondrial outer membrane protein mitoNEET is a redox enzyme catalyzing electron transfer from FMNH2 to oxygen or ubiquinone.* Journal of Biological Chemistry, 2017. **292**(24): p. 10061-10067.

107. Bak, D.W. and S.J. Elliott, *Alternative FeS cluster ligands: tuning redox potentials and chemistry.* Curr Opin Chem Biol, 2014. **19**: p. 50-8.

108. Rostovtseva, T.K. and S.M. Bezrukov, *VDAC regulation: role of cytosolic proteins and mitochondrial lipids.* J Bioenerg Biomembr, 2008. **40**(3): p. 163-70.

109. Rostovtseva, T.K. and S.M. Bezrukov, *VDAC inhibition by tubulin and its physiological implications.* Biochim Biophys Acta, 2012. **1818**(6): p. 1526-35.

110. Azoulay-Zohar, H., A. Israelson, S. Abu-Hamad, and V. Shoshan-Barmatz, *In self-defence: hexokinase promotes voltage-dependent anion channel closure and prevents mitochondria-mediated apoptotic cell death.* Biochem J, 2004. **377**(Pt 2): p. 347-55.

111. Colombini, M., *A candidate for the permeability pathway of the outer mitochondrial membrane.* Nature, 1979. **279**(5714): p. 643-5.

112. Tsutsui, Y. and P.L. Wintrode, *Hydrogen/deuterium exchange-mass spectrometry: a powerful tool for probing protein structure, dynamics and interactions.* Curr Med Chem, 2007. **14**(22): p. 2344-58.

113. Gaggini, M., M. Morelli, E. Buzzigoli, R.A. DeFronzo, E. Bugianesi, and A. Gastaldelli, *Non-alcoholic fatty liver disease (NAFLD) and its connection with insulin resistance, dyslipidemia, atherosclerosis and coronary heart disease.* Nutrients, 2013. **5**(5): p. 1544-60.

114. Lieber, C.S., *Alcoholic fatty liver: its pathogenesis and mechanism of progression to inflammation and fibrosis.* Alcohol, 2004. **34**(1): p. 9-19.

115. Zima, T., L. Fialova, O. Mestek, M. Janebova, J. Crkovska, I. Malbohan, S. Stipek, L. Mikulikova, and P. Popov, *Oxidative stress, metabolism of ethanol and alcohol-related diseases.* Journal of Biomedical Science, 2001. **8**(1): p. 59-70.

116. Evans, J.L., I.D. Goldfine, B.A. Maddux, and G.M. Grodsky, *Are oxidative stress-activated signaling pathways mediators of insulin resistance and beta-cell dysfunction?* Diabetes, 2003. **52**(1): p. 1-8.

117. Hu, X., A. Jogasuria, J. Wang, C. Kim, Y. Han, H. Shen, J. Wu, and M. You, *MitoNEET Deficiency Alleviates Experimental Alcoholic Steatohepatitis in Mice by Stimulating Endocrine Adiponectin-Fgf15 Axis.* J Biol Chem, 2016. **291**(43): p. 22482-22495.

118. Holmuhamedov, E. and J.J. Lemasters, *Ethanol exposure decreases mitochondrial outer membrane permeability in cultured rat hepatocytes.* Arch Biochem Biophys, 2009. **481**(2): p. 226-33.

119. Habener, A., A. Chowdhury, F. Echtermeyer, R. Lichtinghagen, G. Theilmeier, and C. Herzog, *MitoNEET Protects HL-1 Cardiomyocytes from Oxidative Stress Mediated Apoptosis in an In Vitro Model of Hypoxia and Reoxygenation.* PLoS One, 2016. **11**(5): p. e0156054.

120. Mons, C., T. Botzanowski, A. Nikolaev, P. Hellwig, S. Cianferani, E. Lescop, C. Bouton, and M.P. Golinelli-Cohen, *The H2O2-Resistant Fe-S Redox Switch MitoNEET Acts as a pH Sensor To Repair Stress-Damaged Fe-S Protein.* Biochemistry, 2018. **57**(38): p. 5616-5628.

121. Golinelli-Cohen, M.P., E. Lescop, C. Mons, S. Goncalves, M. Clemancey, J. Santolini, E. Guittet, G. Blondin, J.M. Latour, and C. Bouton, *Redox Control of the Human Iron-Sulfur Repair Protein MitoNEET Activity via Its Iron-Sulfur Cluster.* J Biol Chem, 2016. **291**(14): p. 7583-93.

122. Conlan, A.R., M.L. Paddock, C. Homer, H.L. Axelrod, A.E. Cohen, E.C. Abresch, J.A. Zuris, R. Nechushtai, and P.A. Jennings, *Mutation of the His ligand in mitoNEET stabilizes the 2Fe-2S cluster despite conformational heterogeneity in the ligand environment.* Acta Crystallogr D Biol Crystallogr, 2011. **67**(Pt 6): p. 516-23.

123. Chen, X.Y., H.H. Ren, D. Wang, Y. Chen, C.J. Qu, Z.H. Pan, X.N. Liu, W.J. Hao, W.J. Xu, K.J. Wang, D.F. Li, and Q.S. Zheng, *Isoliquiritigenin Induces Mitochondrial Dysfunction and Apoptosis by Inhibiting mitoNEET in a Reactive Oxygen Species-Dependent Manner in A375 Human Melanoma Cells.* Oxid Med Cell Longev, 2019. **2019**: p. 9817576.

124. Landry, A.P., Z. Cheng, and H. Ding, *Reduction of mitochondrial protein mitoNEET [2Fe-2S] clusters by human glutathione reductase.* Free Radic Biol Med, 2015. **81**: p. 119-27.

125. Landry, A.P. and H. Ding, *Redox control of human mitochondrial outer membrane protein MitoNEET [2Fe-2S] clusters by biological thiols and hydrogen peroxide.* J Biol Chem, 2014. **289**(7): p. 4307-15.

126. Wang, Y., A.P. Landry, and H. Ding, *The mitochondrial outer membrane protein mitoNEET is a redox enzyme catalyzing electron transfer from FMNH2 to oxygen or ubiquinone.* J Biol Chem, 2017. **292**(24): p. 10061-10067.

127. Turrens, J.F., *Mitochondrial formation of reactive oxygen species.* J Physiol, 2003. **552**(Pt 2): p. 335-44.

128. Murphy, M.P., *How mitochondria produce reactive oxygen species.* Biochem J, 2009. **417**(1): p. 1-13.

129. Phaniendra, A., D.B. Jestadi, and L. Periyasamy, *Free radicals: properties, sources, targets, and their implication in various diseases.* Indian J Clin Biochem, 2015. **30**(1): p. 11-26.

130. Pham-Huy, L.A., H. He, and C. Pham-Huy, *Free radicals, antioxidants in disease and health.* Int J Biomed Sci, 2008. **4**(2): p. 89-96.

131. Malia, T.J. and G. Wagner, *NMR structural investigation of the mitochondrial outer membrane protein VDAC and its interaction with antiapoptotic Bcl-xL.* Biochemistry, 2007. **46**(2): p. 514-25.

132. Nasr, M.L., D. Baptista, M. Strauss, Z.J. Sun, S. Grigoriu, S. Huser, A. Pluckthun, F. Hagn, T. Walz, J.M. Hogle, and G. Wagner, *Covalently circularized nanodiscs for studying membrane proteins and viral entry.* Nat Methods, 2017. **14**(1): p. 49-52.

133. Ben-Hail, D. and V. Shoshan-Barmatz, *Purification of VDAC1 from rat liver mitochondria.* Cold Spring Harb Protoc, 2014. **2014**(1): p. 94-9.

134. Altschul, S.F., W. Gish, W. Miller, E.W. Myers, and D.J. Lipman, *Basic local alignment search tool.* J Mol Biol, 1990. **215**(3): p. 403-10.

135. Baxter, E.L., J.A. Zuris, C. Wang, P.L. Vo, H.L. Axelrod, A.E. Cohen, M.L. Paddock, R. Nechushtai, J.N. Onuchic, and P.A. Jennings, *Allosteric control in a metalloprotein dramatically alters function.* Proc Natl Acad Sci U S A, 2013. **110**(3): p. 948-53.

136. Aubol, B.E., K.L. Hailey, L. Fattet, P.A. Jennings, and J.A. Adams, *Redirecting SR Protein Nuclear Trafficking through an Allosteric Platform.* J Mol Biol, 2017. **429**(14): p. 2178-2191.

137. Fisher, K.M., E. Haglund, J.K. Noel, K.L. Hailey, J.N. Onuchic, and P.A. Jennings, *Geometrical Frustration in Interleukin-33 Decouples the Dynamics of the Functional Element from the Folding Transition State Ensemble.* PLoS One, 2015. **10**(12): p. e0144067.

138. Hailey, K.L., D.T. Capraro, S. Barkho, and P.A. Jennings, *Allosteric switching of agonist/antagonist activity by a single point mutation in the interluekin-1 receptor antagonist, IL-1Ra.* J Mol Biol, 2013. **425**(13): p. 2382-92.

139. Hailey, K.L., S. Li, M.D. Andersen, M. Roy, V.L. Woods, Jr., and P.A. Jennings, *Pro-interleukin (IL)-1beta shares a core region of stability as compared with mature IL-1beta while maintaining a distinctly different configurational landscape: a comparative hydrogen/deuterium exchange mass spectrometry study.* J Biol Chem, 2009. **284**(38): p. 26137-48.

140. Keshwani, M.M., K.L. Hailey, B.E. Aubol, L. Fattet, M.L. McGlone, P.A. Jennings, and J.A. Adams, *Nuclear protein kinase CLK1 uses a non-*

traditional docking mechanism to select physiological substrates. Biochem J, 2015. **472**(3): p. 329-38.

141. Plocinik, R.M., S. Li, T. Liu, K.L. Hailey, J. Whitesides, C.T. Ma, X.D. Fu, G. Gosh, V.L. Woods, Jr., P.A. Jennings, and J.A. Adams, *Regulating SR protein phosphorylation through regions outside the kinase domain of SRPK1.* J Mol Biol, 2011. **410**(1): p. 131-45.

142. Barkho, S., L.C. Pierce, M.L. McGlone, S. Li, V.L. Woods, Jr., R.C. Walker, J.A. Adams, and P.A. Jennings, *Distal loop flexibility of a regulatory domain modulates dynamics and activity of C-terminal SRC kinase (csk).* PLoS Comput Biol, 2013. **9**(9): p. e1003188.

143. Bai, F., F. Morcos, R.R. Cheng, H. Jiang, and J.N. Onuchic, *Elucidating the druggable interface of protein-protein interactions using fragment docking and coevolutionary analysis.* Proc Natl Acad Sci U S A, 2016. **113**(50): p. E8051-E8058.

144. Yang, J., R. Yan, A. Roy, D. Xu, J. Poisson, and Y. Zhang, *The I-TASSER Suite: protein structure and function prediction.* Nat Meth, 2015. **12**(1): p. 7-8.

145. Perrier-Cornet, A., J.C. Ianotto, F. Mingant, M. Perrot, E. Lippert, and H. Galinat, *Decreased turnover aspirin resistance by bidaily aspirin intake and efficient cytoreduction in myeloproliferative neoplasms.* Platelets, 2017: p. 1-6.

146. Finn, R.D., J. Clements, W. Arndt, B.L. Miller, T.J. Wheeler, F. Schreiber, A. Bateman, and S.R. Eddy, *HMMER web server: 2015 update.* Nucleic Acids Research, 2015. **43**(Web Server issue): p. W30-W38.

147. Johnson, D.C., D.R. Dean, A.D. Smith, and M.K. Johnson, *Structure, function, and formation of biological iron-sulfur clusters.* Annu Rev Biochem, 2005. **74**: p. 247-81.

148. Zhang, C., *Essential functions of iron-requiring proteins in DNA replication, repair and cell cycle control.* Protein Cell, 2014. **5**(10): p. 750-60.

149. Fenton, H.J.H., *LXXIII.-Oxidation of tartaric acid in presence of iron.* Journal of the Chemical Society, Transactions, 1894. **65**(0): p. 899-910.

150. Valko, M., D. Leibfritz, J. Moncol, M.T. Cronin, M. Mazur, and J. Telser, *Free radicals and antioxidants in normal physiological functions and human disease.* Int J Biochem Cell Biol, 2007. **39**(1): p. 44-84.

151. Dixon, S.J. and B.R. Stockwell, *The role of iron and reactive oxygen species in cell death.* Nat Chem Biol, 2014. **10**(1): p. 9-17.

152. Winterbourn, C.C., *Toxicity of iron and hydrogen peroxide: the Fenton reaction.* Toxicol Lett, 1995. **82-83**: p. 969-74.

153. Maio, N. and T.A. Rouault, *Iron-sulfur cluster biogenesis in mammalian cells: New insights into the molecular mechanisms of cluster delivery.* Biochim Biophys Acta, 2015. **1853**(6): p. 1493-512.

154. Paul, V.D. and R. Lill, *Biogenesis of cytosolic and nuclear iron-sulfur proteins and their role in genome stability.* Biochim Biophys Acta, 2015. **1853**(6): p. 1528-39.

155. Braymer, J.J. and R. Lill, *Iron-sulfur cluster biogenesis and trafficking in mitochondria.* J Biol Chem, 2017. **292**(31): p. 12754-12763.

156. Lill, R., R. Dutkiewicz, S.A. Freibert, T. Heidenreich, J. Mascarenhas, D.J. Netz, V.D. Paul, A.J. Pierik, N. Richter, M. Stumpfig, V. Srinivasan, O. Stehling, and U. Muhlenhoff, *The role of mitochondria and the CIA machinery in the maturation of cytosolic and nuclear iron-sulfur proteins.* Eur J Cell Biol, 2015. **94**(7-9): p. 280-91.

157. Sharma, A.K., L.J. Pallesen, R.J. Spang, and W.E. Walden, *Cytosolic iron-sulfur cluster assembly (CIA) system: factors, mechanism, and relevance to cellular iron regulation.* J Biol Chem, 2010. **285**(35): p. 26745-51.

158. Netz, D.J., J. Mascarenhas, O. Stehling, A.J. Pierik, and R. Lill, *Maturation of cytosolic and nuclear iron-sulfur proteins.* Trends Cell Biol, 2014. **24**(5): p. 303-12.

159. Rouault, T.A., *Mammalian iron-sulphur proteins: novel insights into biogenesis and function.* Nat Rev Mol Cell Biol, 2015. **16**(1): p. 45-55.

160. Banci, L., F. Camponeschi, S. Ciofi-Baffoni, and R. Muzzioli, *Elucidating the Molecular Function of Human BOLA2 in GRX3-Dependent Anamorsin Maturation Pathway.* J Am Chem Soc, 2015. **137**(51): p. 16133-43.

161. Laleve, A., C. Vallieres, M.P. Golinelli-Cohen, C. Bouton, Z. Song, G. Pawlik, S.M. Tindall, S.V. Avery, J. Clain, and B. Meunier, *The antimalarial drug primaquine targets Fe-S cluster proteins and yeast respiratory growth.* Redox Biol, 2016. **7**: p. 21-29.

162. Choby, J.E., L.A. Mike, A.A. Mashruwala, B.F. Dutter, P.M. Dunman, G.A. Sulikowski, J.M. Boyd, and E.P. Skaar, *A Small-Molecule Inhibitor*

of Iron-Sulfur Cluster Assembly Uncovers a Link between Virulence Regulation and Metabolism in Staphylococcus aureus. Cell Chem Biol, 2016. **23**(11): p. 1351-1361.

163. Bak, D.W., J.A. Zuris, M.L. Paddock, P.A. Jennings, and S.J. Elliott, *Redox Characterization of the FeS Protein MitoNEET and Impact of Thiazolidinedione Drug Binding.* Biochemistry, 2009. **48**(43): p. 10193-10195.

164. Bak, D.W., J.A. Zuris, M.L. Paddock, P.A. Jennings, and S.J. Elliott, *Redox Characterization of the FeS Protein MitoNEET and Impact of Thiazolidinedione Drug Binding (vol 48, pg 10193, 2009).* Biochemistry, 2010. **49**(26): p. 5620-5620.

165. Banci, L., I. Bertini, V. Calderone, S. Ciofi-Baffoni, A. Giachetti, D. Jaiswal, M. Mikolajczyk, M. Piccioli, and J. Winkelmann, *Molecular view of an electron transfer process essential for iron-sulfur protein biogenesis.* Proc Natl Acad Sci U S A, 2013. **110**(18): p. 7136-41.

166. Netz, D.J., M. Stumpfig, C. Dore, U. Muhlenhoff, A.J. Pierik, and R. Lill, *Tah18 transfers electrons to Dre2 in cytosolic iron-sulfur protein biogenesis.* Nat Chem Biol, 2010. **6**(10): p. 758-65.

167. Zhang, Y., E.R. Lyver, E. Nakamaru-Ogiso, H. Yoon, B. Amutha, D.W. Lee, E. Bi, T. Ohnishi, F. Daldal, D. Pain, and A. Dancis, *Dre2, a conserved eukaryotic Fe/S cluster protein, functions in cytosolic Fe/S protein biogenesis.* Mol Cell Biol, 2008. **28**(18): p. 5569-82.

168. Saito, Y., H. Shibayama, H. Tanaka, A. Tanimura, I. Matsumura, and Y. Kanakura, *PICOT is a molecule which binds to anamorsin.* Biochemical and Biophysical Research Communications, 2011. **408**(2): p. 329-333.

169. Li, H., D.T. Mapolelo, S. Randeniya, M.K. Johnson, and C.E. Outten, *Human glutaredoxin 3 forms [2Fe-2S]-bridged complexes with human BolA2.* Biochemistry, 2012. **51**(8): p. 1687-96.

170. Frey, A.G., D.J. Palenchar, J.D. Wildemann, and C.C. Philpott, *A Glutaredoxin.BolA Complex Serves as an Iron-Sulfur Cluster Chaperone for the Cytosolic Cluster Assembly Machinery.* J Biol Chem, 2016. **291**(43): p. 22344-22356.

171. Qi, W., J. Li, and J.A. Cowan, *A structural model for glutathione-complexed iron-sulfur cluster as a substrate for ABCB7-type transporters.* Chem Commun (Camb), 2014. **50**(29): p. 3795-8.

172. Li, J., S.A. Pearson, K.D. Fenk, and J.A. Cowan, *Glutathione-coordinated [2Fe-2S] cluster is stabilized by intramolecular salt bridges.* J Biol Inorg Chem, 2015. **20**(8): p. 1221-7.

173. Srinivasan, V., A.J. Pierik, and R. Lill, *Crystal structures of nucleotide-free and glutathione-bound mitochondrial ABC transporter Atm1.* Science, 2014. **343**(6175): p. 1137-40.

174. Schaedler, T.A., J.D. Thornton, I. Kruse, M. Schwarzlander, A.J. Meyer, H.W. van Veen, and J. Balk, *A conserved mitochondrial ATP-binding cassette transporter exports glutathione polysulfide for cytosolic metal cofactor assembly.* J Biol Chem, 2014. **289**(34): p. 23264-74.

175. Wachnowsky, C., I. Fidai, and J.A. Cowan, *Cytosolic iron-sulfur cluster transfer-a proposed kinetic pathway for reconstitution of glutaredoxin 3.* FEBS Lett, 2016. **590**(24): p. 4531-4540.

176. Kumar, C., A. Igbaria, B. D'Autreaux, A.G. Planson, C. Junot, E. Godat, A.K. Bachhawat, A. Delaunay-Moisan, and M.B. Toledano, *Glutathione revisited: a vital function in iron metabolism and ancillary role in thiol-redox control.* EMBO J, 2011. **30**(10): p. 2044-56.

177. Haenen, G.R. and A. Bast, *Glutathione revisited: a better scavenger than previously thought.* Front Pharmacol, 2014. **5**: p. 260.

178. Sen, S., B. Rao, C. Wachnowsky, and J.A. Cowan, *Cluster exchange reactivity of [2Fe-2S] cluster-bridged complexes of BOLA3 with monothiol glutaredoxins.* Metallomics, 2018. **10**(9): p. 1282-1290.

179. Pizzorno, J., *Glutathione!* Integr Med (Encinitas), 2014. **13**(1): p. 8-12.

180. Schafer, F.Q. and G.R. Buettner, *Redox environment of the cell as viewed through the redox state of the glutathione disulfide/glutathione couple.* Free Radic Biol Med, 2001. **30**(11): p. 1191-212.

181. Bak, D.W., T.J. Bechtel, J.A. Falco, and E. Weerapana, *Cysteine reactivity across the subcellular universe.* Curr Opin Chem Biol, 2019. **48**: p. 96-105.

182. Ribas, V., C. Garcia-Ruiz, and J.C. Fernandez-Checa, *Glutathione and mitochondria.* Front Pharmacol, 2014. **5**: p. 151.

183. Bachhawat, A.K. and A. Kaur, *Glutathione Degradation.* Antioxid Redox Signal, 2017. **27**(15): p. 1200-1216.

184. Mari, M., A. Morales, A. Colell, C. Garcia-Ruiz, and J.C. Fernandez-Checa, *Mitochondrial glutathione, a key survival antioxidant.* Antioxid Redox Signal, 2009. **11**(11): p. 2685-700.

185. Ballatori, N., S.M. Krance, S. Notenboom, S. Shi, K. Tieu, and C.L. Hammond, *Glutathione dysregulation and the etiology and progression of human diseases.* Biological Chemistry, 2009. **390**(3): p. 191-214.

186. Krezel, A. and W. Bal, *Coordination chemistry of glutathione.* Acta Biochimica Polonica, 1999. **46**(3): p. 567-80.

187. Qi, W., J. Li, C.Y. Chain, G.A. Pasquevich, A.F. Pasquevich, and J.A. Cowan, *Glutathione-complexed iron-sulfur clusters. Reaction intermediates and evidence for a template effect promoting assembly and stability.* Chem Commun (Camb), 2013. **49**(56): p. 6313-5.

188. Wang, L., B. Ouyang, Y. Li, Y. Feng, J.P. Jacquot, N. Rouhier, and B. Xia, *Glutathione regulates the transfer of iron-sulfur cluster from monothiol and dithiol glutaredoxins to apo ferredoxin.* Protein Cell, 2012. **3**(9): p. 714-21.

189. Fidai, I., C. Wachnowsky, and J.A. Cowan, *Glutathione-complexed [2Fe-2S] clusters function in Fe-S cluster storage and trafficking.* J Biol Inorg Chem, 2016. **21**(7): p. 887-901.

190. Sipos, K., H. Lange, Z. Fekete, P. Ullmann, R. Lill, and G. Kispal, *Maturation of cytosolic iron-sulfur proteins requires glutathione.* J Biol Chem, 2002. **277**(30): p. 26944-9.

191. Banci, L., D. Brancaccio, S. Ciofi-Baffoni, R. Del Conte, R. Gadepalli, M. Mikolajczyk, S. Neri, M. Piccioli, and J. Winkelmann, *[2Fe-2S] cluster transfer in iron-sulfur protein biogenesis.* Proc Natl Acad Sci U S A, 2014. **111**(17): p. 6203-8.

192. Li, J. and J.A. Cowan, *Glutathione-coordinated [2Fe-2S] cluster: a viable physiological substrate for mitochondrial ABCB7 transport.* Chem Commun (Camb), 2015. **51**(12): p. 2253-5.

193. Gonzalez-Cabo, P., A. Bolinches-Amoros, J. Cabello, S. Ros, S. Moreno, H.A. Baylis, F. Palau, and R.P. Vazquez-Manrique, *Disruption of the ATP-binding cassette B7 (ABTM-1/ABCB7) induces oxidative stress and premature cell death in Caenorhabditis elegans.* J Biol Chem, 2011. **286**(24): p. 21304-14.

194. Kispal, G., P. Csere, B. Guiard, and R. Lill, *The ABC transporter Atm1p is required for mitochondrial iron homeostasis.* FEBS Lett, 1997. **418**(3): p. 346-50.

195. Cavadini, P., G. Biasiotto, M. Poli, S. Levi, R. Verardi, I. Zanella, M. Derosas, R. Ingrassia, M. Corrado, and P. Arosio, *RNA silencing of the mitochondrial ABCB7 transporter in HeLa cells causes an iron-deficient phenotype with mitochondrial iron overload.* Blood, 2007. **109**(8): p. 3552-9.

196. Mittler, R., M. Darash-Yahana, Y.S. Sohn, F. Bai, L. Song, I.Z. Cabantchik, P.A. Jennings, J.N. Onuchic, and R. Nechushtai, *NEET Proteins: A New Link Between Iron Metabolism, Reactive Oxygen Species, and Cancer.* Antioxid Redox Signal, 2019. **30**(8): p. 1083-1095.

197. Netz, D.J., H.M. Genau, B.D. Weiler, E. Bill, A.J. Pierik, and R. Lill, *The conserved protein Dre2 uses essential [2Fe-2S] and [4Fe-4S] clusters for its function in cytosolic iron-sulfur protein assembly.* Biochem J, 2016. **473**(14): p. 2073-85.

198. Salem, A.F., D. Whitaker-Menezes, A. Howell, F. Sotgia, and M.P. Lisanti, *Mitochondrial biogenesis in epithelial cancer cells promotes breast cancer tumor growth and confers autophagy resistance.* Cell Cycle, 2012. **11**(22): p. 4174-80.

199. Calabrese, G., B. Morgan, and J. Riemer, *Mitochondrial Glutathione: Regulation and Functions.* Antioxid Redox Signal, 2017. **27**(15): p. 1162-1177.

200. Siontorou, C.G., G.P. Nikoleli, D.P. Nikolelis, and S.K. Karapetis, *Artificial Lipid Membranes: Past, Present, and Future.* Membranes (Basel), 2017. **7**(3).

201. Evanly Vo, H.C.W., and Juris P.Germanas, *Preparation and Characterization of [2Ga-2S] Anabaena 7120 Ferredoxin, the First Gallium-Sulfur Cluster-Containing Protein.* Journal of the American Chemical Society, 1997. **119**: p. 1934-1940.

202. Xu, X., S. Scanu, J.S. Chung, M. Hirasawa, D.B. Knaff, and M. Ubbink, *Structural and functional characterization of the ga-substituted ferredoxin from Synechocystis sp. PCC6803, a mimic of the native protein.* Biochemistry, 2010. **49**(36): p. 7790-7.

203. Xu, X., S.K. Kim, P. Schurmann, M. Hirasawa, J.N. Tripathy, J. Smith, D.B. Knaff, and M. Ubbink, *Ferredoxin/ferredoxin-thioredoxin reductase*

complex: Complete NMR mapping of the interaction site on ferredoxin by gallium substitution. FEBS Lett, 2006. **580**(28-29): p. 6714-20.

204. Pochapsky, T.C., M. Kuti, and S. Kazanis, *The solution structure of a gallium-substituted putidaredoxin mutant: GaPdx C85S.* J Biomol NMR, 1998. **12**(3): p. 407-15.

205. Bak, D.W. and S.J. Elliott, *Conserved hydrogen bonding networks of MitoNEET tune Fe-S cluster binding and structural stability.* Biochemistry, 2013. **52**(27): p. 4687-96.

206. Barile, E. and M. Pellecchia, *NMR-based approaches for the identification and optimization of inhibitors of protein-protein interactions.* Chem Rev, 2014. **114**(9): p. 4749-63.

207. Fielding, L., *NMR methods for the determination of protein-ligand dissociation constants.* Curr Top Med Chem, 2003. **3**(1): p. 39-53.

208. Sugiki, T., K. Furuita, T. Fujiwara, and C. Kojima, *Current NMR Techniques for Structure-Based Drug Discovery.* Molecules, 2018. **23**(1).